Recent progress on core-shell structured BaTiO3@polymer/fluorinated polymers nanocomposites for high energy storage: Synthesis, dielectric properties and applications

Fatima Ezzahra Bouharras, Mustapha Raihane, Bruno Ameduri

Recent Progress on Core-Shell Structured $BaTiO_3$@polymer/Fluorinated Polymers Nanocomposites for High Energy Storage: Synthesis, Dielectric properties and Applications

Fatima Ezzahra BOUHARRAS, [a.b] Mustapha RAIHANE, [a*] Bruno AMEDURI [b*]

[a] Laboratory of Organometallic and Macromolecular Chemistry-Composite Materials (LCO2MC). Faculty of Sciences and Techniques, Cadi-Ayyad University, Av. Abdelkrim Khattabi, BP 549, 40000 Marrakesh. Morocco

[b] ICGM, Univ Montpellier, ENSCM, CNRS, Montpellier, France

Abstract

This review aims at updating various studies to design $BaTiO_3$@polymer/Fluoropolymer nanocomposites, to study their properties and performances and to supply their applications. Dielectric nanocomposite materials with high energy density exhibit promising performances for energy storage applications. Major efforts have been performed to combine the efficient properties and high dielectric constant of ceramics with the flexibility and easy processing of polymers. Actually, the dielectric properties of the nanocomposite are influenced by the dielectric features of both ceramic and polymer. Thus, the choice of the two components become crucial in turning the desired properties. Another important factor is the modification strategy to get such nanocomposites, where the major routes are the "grafting from", "grafting onto" and melt process while most fluoropolymers studied are polyvinylidene fluoride (PVDF), VDF containing-copolymers and terpolymers and poly(acrylates) bearing fluoroalkyl side groups. Additionally, fluorinated silanes have also been involved in sol-gel chemistry to decorate $BaTiO_3$ surface, as well as tetrafluorophthalic acid or fluorinated dopamine did. This review also summaries the current state of high energy density nanocomposites based on $BaTiO_3$ as a ceramic nanofiller and fluoropolymer as matrix.

Keywords: barium titanate; dielectric constant; fluoropolymers; grafting; PVDF; capacitors.

List of abbreviations and acronyms

ATRP: Atom transfer radical polymerization

BT: barium titanate

C2: phthalic acid

CSPE: Composite solid polymer electrolyte

CTFE: Chlorotrifluoroethylene

CFE: Chlorofluoroethylene

F3C2: 4-(trifluoromethyl)phthalic acid

F4C: 2,3,4,5-tetrafluorobenzoic acid

F4C2: tetrafluorophthalic acid

P5F: poly{2,5-bis[(2,3,4,5,6-pentafluoro) oxycarbonyl]styrene}

P7F or PM7F: poly{2,5-bis[(2,3,5,6-tetrafluoro-4-trifluoromethyl)oxycarbonyl]styrene}

PAC : Sodium polyacrylate

PGMA : poly(glycidyl methacrylate)

PHEMA : poly(2-hydroxylethyl methacrylate)

PHFDA : poly(1H,1H,2H,2H-heptadecafluorodecyl acrylate)

PMMA : poly(methyl methacrylate)

PTFEMA : Poly(2,2,2,trifluoroethyl methacrylate)

PTFMPCS or P3F: poly{2,5-bis[(4- trifluoromethoxyphenyl)oxycarbonyl]styrene}

RAFT: Reversible addition fragmentation chain transfer agent

SPE: Solid polymer electrolyte

TrFE: Trifluoroethylene

VDF: Vinylidene fluoride

ε: Dielectric permittivity

I. Introduction

A nanocomposite is a multiphase material in which one of the components has at least one dimension of a nanometric scale. These nanocomposite materials can be classified according to their matrix group to ceramic, metal or polymer matrix nanocomposite [1]. For the last category that is of interests in the present review, the system consists on polymer matrix containing nanofillers dispersed in it, which results in outstanding properties, resulting in nanocomposite with high potentials [2,3].

In the recent years, dielectric nanocomposites with high energy density have received a great interest because of their wide range use in several applications such as electronic industry [4–9]. Generally, the energy density of a dielectric material can be illustrated as $U = \frac{1}{2}\ \varepsilon_0\ \varepsilon_r\ E^2$ where ε_0, ε_r and E are the permittivity of the free space (8.854×10^{-14} F/cm), relative permittivity and electric breakdown strength, respectively. Thus, obtaining high energy densities can be achieved either by increasing the relative permittivity and/or the electric breakdown strength of the material. Great efforts have been made to achieve both high dielectric permittivity and high breakdown strength. In fact, high permittivities could be obtained with ceramic nanoparticles and the most studied one is $BaTiO_3$ (~3000) [10–15], while high breakdown strength could be achieved with polymers like PVDF and VDF-copolymers (5000 KV/cm) [16–18]. By combining both these materials, a high energy density nanocomposite could be obtained. So far, a large number of polymers have been used in the synthesis of dielectric nanocomposites by introducing $BaTiO_3$ nanoparticles into fluoropolymer matrices (*e.g.*, PVDF [19–21], and VDF copolymers such as poly(vinylidene fluoride-*co*-trifluoroethylene) poly(VDF-*co*-TrFE) [22], poly(vinylidene fluoride-*co*-chlorotrifluoroethylene) poly(VDF-*co*-CTFE),[23] poly(vinylidene fluoride-*ter*-trifluoroethylene-*ter*-chlorofluoroethylene)) or non-fluoropolymer matrices (*e.g.*, poly(methyl methacrylate) (PMMA)[24] or poly(glycidyl methacrylate) (PGMA) [25]). Actually, PVDF and VDF copolymers have received particular attention due to the fact that they present the highest dielectric constants among all polymeric materials (6-12) thanks to the strong C-F dipole moment [26–28].

Apart from the polymeric matrix and the ceramic nanofiller, the interface between the different components plays a major role in the dielectric properties. Thus, it

is considered as a third phase in the nanocomposite system [29]. Todd *et al*. [30] developed a model called the "interphase power law" in order to study the complex permittivity of the composite system. To do so, this model uses the permittivities and the volume fractions of the filler, polymer and the interface region. The suggested model provides insight into the role of the interface and its effect on dielectric permittivity. Tanaka *et al*. [31] proposed a model to understand the dielectric properties of a nanocomposite material (Fig. 1). They considered that the interface of a spherical inorganic nanoparticle embedded into a polymer matrix consists on three layers:

(i) The bonded layer (~ 1 nm): this layer corresponds to a transition layer where the polymer and the nanoparticles are bonded by coupling agent such as a silane.

(ii) The bound layer (several nm): called also the interfacial layer, where the polymer chains are strongly bounded and/or interacted to both the bond layer and the nanoparticle surface.

(iii) The loose layer (several tens of nm): this region has a poor interaction with the second layer.

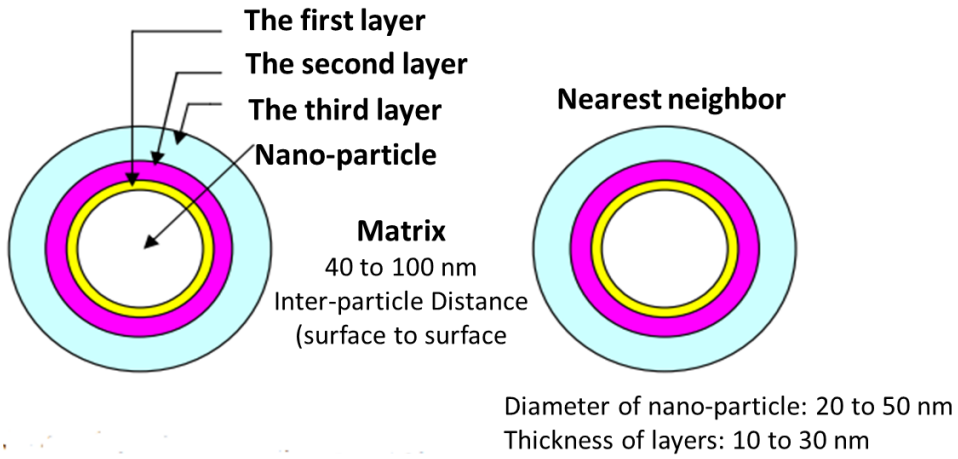

Fig. 1. Multi-core model for nano-particle – polymer interfaces. Reproduced with permission from [31]. Copyright 2005 IEEE Xplore Digital library.

Thus, the interfacial region between the nanoparticles and the polymer must be considered since it contributes in the dielectric properties of the nanocomposite. Therefore, in addition to the choice of the nanoparticle and the polymer matrix, the

selection of an appropriate pre-treatment of nanoparticles is crucial to obtain high energy density nanocomposites.

This review summarizes the recent work established on nanocomposites based on barium titanate (BT) as a filler and fluoropolymer as a matrix. After reminding the synthesis and properties of BT and fluoropolymers in the two first parts, the different strategies used to produce such nanocomposites are summarized in a third one. The fourth section highlights the importance of the surface treatment of nanoparticles by fluorinated agents or polymers, and then reports surveys on the design of nanocomposites made by one core of BT and double shell of polymer named as "core@double shell" system. The fifth part will cover the applications followed by the conclusion and perspectives.

II. $BaTiO_3$ ceramic fillers

II.1. Structure and crystallization

Barium titanate (BT) is one of the best ferroelectric ceramic and a good candidate for a wide range of applications due to its excellent dielectric, ferroelectric and piezoelectric properties [32,33]. It is also a dielectric material that belongs to the group having a structure of perovskite material of chemical formula $A(II)B(IV)O_3$, whose crystalline structure is a face centered cube [34]. The divalent ions occupy the top corner of the cell while the tetravalent ions are placed at the center of the cube whereas O^{2-} ions are located at the center of each face (Fig. 2a). However, as the temperature decreased, crystallographic changes in $BaTiO_3$ occur and it goes through successive phase transitions: it undergoes a paraelectric to ferroelectric transition to a tetragonal structure at 120 °C (Curie temperature, Tc), it is orthorhombic between -90 and 5 °C and, finally, it is rhombohedral below -90 °C (Fig. 2b) [35,36].

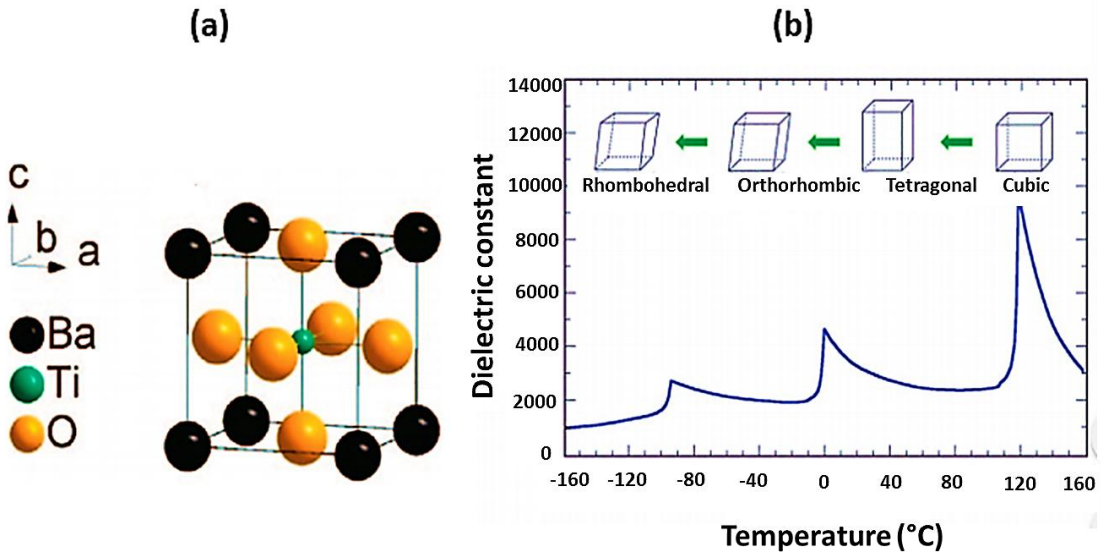

Fig. 2. (a) Unit cell of $BaTiO_3$. Reproduced with permission from [32]. Copyright 2008 American Chemical Society, and (b) Barium titanate dielectric constant as a function of temperature. Reproduced with permission from [37]. Copyright 2012 IEE Xplore Digital Library.

II.2. Synthesis of Barium titanate

$BaTiO_3$ presents a wide range of applications in the field of electronics thanks to its high dielectric permittivity [38–41]. In order to achieve the desired properties and practical applications, the quality of the $BaTiO_3$ powders is very important, which depends strongly on their synthesis method. Several routes to prepare BT have been reported by different authors, mentioned below.

II.2.1. Hydro/solvothermal synthesis

The hydro- or solvothermal method is a wet chemical preparation of $BaTiO_3$ powder that involves solutions, gels or suspensions subjected to temperatures and pressures ranging from room temperature to 1000 °C and from atmospheric pressure to 100 MPa, respectively [42–44]. The chemical synthesis utilizes the reaction of $Ba(OH)_2$ and a titanium source, according to reaction 1.

$$Ba(OH)_2 + TiO_2 \rightarrow BaTiO_3 + H_2O \qquad (1)$$

The synthesis process is carried out in stainless steel autoclave without any agitation, under heating and pressure. The final material exhibits different properties depending on the experimental conditions. As an example, Hao *et al*. [45] synthesized monodispersed $BaTiO_3$ and studied the effect of different parameters on the growth-up mechanism of $BaTiO_3$ nanocrystals. Temperature, considered as the most important factor that influences the reaction, was studied and it was found that the increase of temperature leads to a decrease of grain size of $BaTiO_3$ nanopowders. However, the opposite effect was observed with the concentration. The grain size of nanopowders was found to decrease by decreasing the concentration, as it was shown by SEM (Fig. 3).

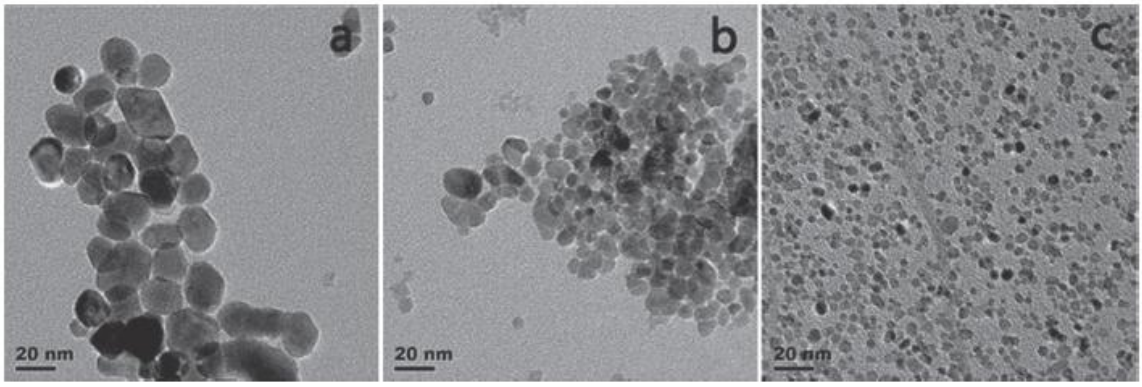

Fig. 3. TEM images of the $BaTiO_3$ nanoparticles synthesized at 180 °C for 12 h at the concentration of (a) 3 mol/L, (b) 1.5 mol/L, (c) 0.75 mol/L. Reproduced with permission of [45]. Copyright 2013 The Ceramic Society of Japan.

II.2.2. Solid state synthesis

The solid state is considered as the most conventional synthesis method that can be achieved from reaction between TiO_2 and $BaCO_3$ (equation 2). To get $BaTiO_3$, the reactants are first mixed in order to reduce agglomerate and promote their homogeneity, then, are subjected to high temperatures in the region of 1000 °C [46–48].

$$BaCO_3 + TiO_2 \rightarrow BaTiO_3 + CO_2 \qquad (2)$$

However, this method produces relatively coarse and agglomerated particles, which is not suitable for most applications. In order to get fine-grained powders, alternative processing methods have been developed with chemical routes using non-oxide precursors [49,50].

II.2.3. Sol-gel synthesis

Barium titanate could be also synthesized using sol-gel method to yield a crystalline material at much lower temperatures than usually required for solid-state reactions [51]. This method involves the use of hydrolysis to form gels from metal oxides before subjecting them on a post processing to obtain high purity $BaTiO_3$ [52–54]. As shown in Table 1, different starting materials could be used to obtain $BaTiO_3$. Mazdiyasni *et al*. [55] used barium isopropoxyde derived from high purity Ba metal, while Flaschen *et al*. [56] involved $Ba(OH)_2$. However, it is found that high purity Ba (99.99 %) could be achieved by using barium isopropoxyde as a starting material [52].

Table 1. Comparison of Starting Materials for the Synthesis of Barium Titanate. Reproduced with permission of [57]. Copyright 1988 American Ceramic Society.

Starting materials	Comments
$BaCO_3$ and TiO_2	High-temperature process; lower purity; cheaper raw materials
$Ba(OH)_2$ and $Ti(OC_3H_7)_4$	Ba alkoxide not required
BaO-derived precursor and $Ti(OC_3H_7)_4$	Reaction chemistry uncertain; effect of impurities needs to be studied
Ba-derived $Ba(OC_3H_7)_4$ and $Ti(OC_3H_7)_4$	Ultrafine, stoichiometric and high-purity powders are obtained; expensive reagents needed.

II.3. Dielectric properties

The properties of ferroelectric materials are closely related to their crystalline structure, which can be closely related to their size [58–60]. Indeed, the permittivity of the ferroelectric ceramic is also strongly dependent on the size of the grains. Zhao *et al* . [61] reported the effect of grain size of $BaTiO_3$ on its dielectric permittivity. Fig. 4 shows the variation of the dielectric permittivity of $BaTiO_3$ particles at different sizes. At 1200 nm, the profile is similar to the bulk material with a curie temperature (Tc) of about 120 °C, associated with a sharp transition from ferroelectric to paraelectric phase and ε_{max} up to 5000. When the particle size decreases to 300 nm, the Tc decreases with a

wider phase transition and a ε_{max} around 3500. Finally, at 50 nm, no phase transition was observed and ε_{max} goes below 1000.

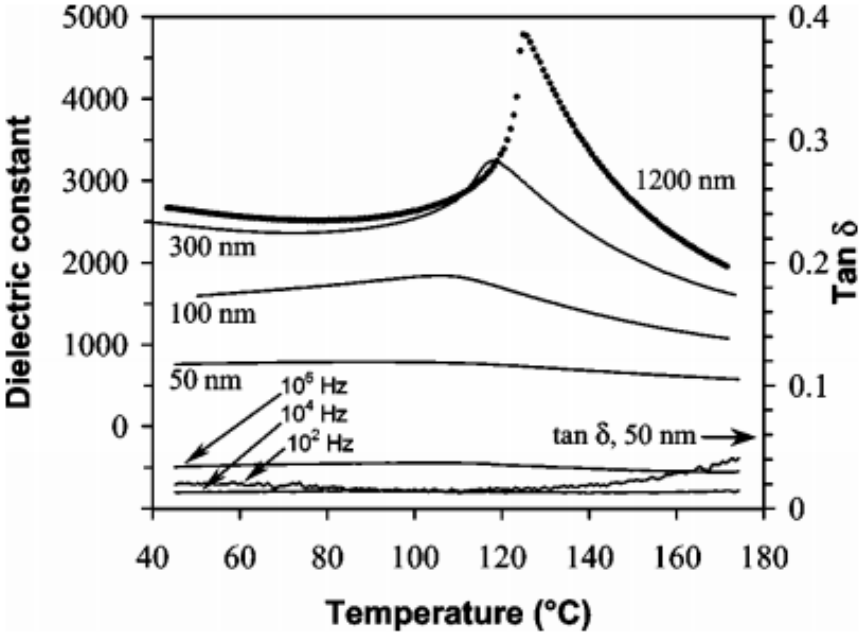

Fig. 4. Relative dielectric constant and tan δ at 10^4 Hz as a function of temperature of $BaTiO_3$ using different sizes (50-1200 nm). Reproduced with permission of [61]. Copyright 2004 American Physical Society.

Another factor that influences the dielectric permittivity of $BaTiO_3$ is the porosity. The effect of this parameter on dielectric properties was studied by Hsiang *et al.* [62] In fact, previous models have been reported (*e.g.*, Niesel's equation [63] and Maxwell relationship [64]), assuming that the dielectric constant of a matrix phase ($BaTiO_3$) for porous ceramics to be constant while the effect of pores on dielectric constant can be neglected. Fig. 5 exhibits the dielectric constant of $BaTiO_3$ ceramics for different porosities. It was concluded that for porosity below 10 %, the experimental results were consistent with the values obtained from theoretical models. However, when the porosity was greater than 10 %, a deviation between the experimental and theoretical values was found [62].

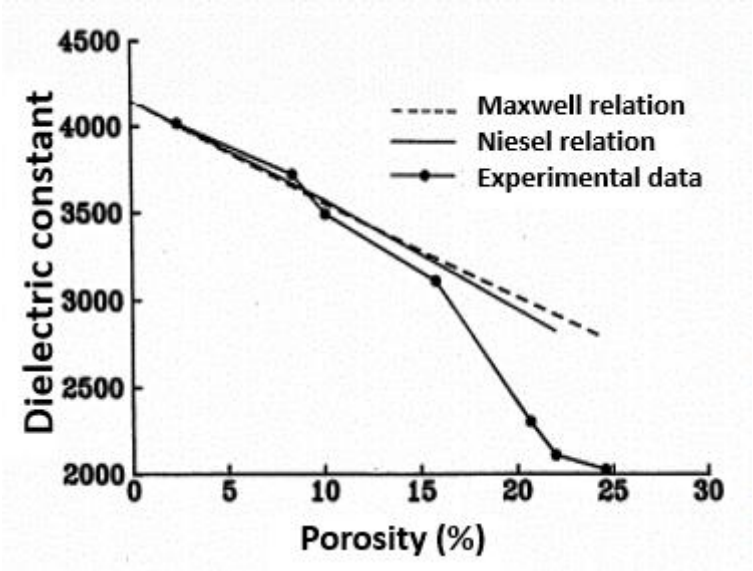

Fig. 5. Values of dielectric constant of $BaTiO_3$ at room temperature for different porosities. Reproduced with permission of [62]. Copyright 1995 Japan Society of Applied Physics.

However, when the ceramic filler is added to a polymer matrix, the dielectric permittivity will depend on the dielectric properties of both phases. In fact, various models have been developed to predict the dielectric permittivity of composite material [65–67]. Maxwell-Garnet Equation is valid for a composite system with spherical particles and low filler loading. It can be expressed by equation (3):

$$\varepsilon_{eff} = \left[1 + \frac{3\varphi_f(\varepsilon_{f-}\varepsilon_m)}{\varphi_m(\varepsilon_f - \varepsilon_m) + 3\varepsilon_m}\right] \qquad (3)$$

where ε_{eff} is the effective permittivity of the composite material, ε_f and ε_m correspond to the permittivities of the filler and polymer, respectively, whereas φ_f and φ_m stand for the volume fractions of filler and matrix, respectively. In fact, this model neglects the effect of the interphase between the filler and polymer matrix and this assumption will be valid for a micro-scale composite [67]. However, for nanocomposites materials, the effect of the interphase could not be longer negligible and must be taken into account.

Vo and Shi [68] proposed a model to describe the effect of the interphase region on the dielectric permittivity of the nanocomposite, taking into account the dielectric permittivities and volume fractions of polymer, nanofiller and interphase. The used

relationship to model the effective permittivity for nanocomposite materials containing three components (matrix, interphase region, and filler) can be supplied by equation (4):

$$\varepsilon_c = \frac{h + 2l}{h - l} \tag{4}$$

where:

$$h = A - 2B - C \tag{5}$$

and

$$l = \frac{\varepsilon_3 - 1}{\varepsilon_3 + 2} A - \frac{(2\varepsilon_3 + 1)}{(\varepsilon_3 + 2)(2\varepsilon_3 + \varepsilon_2)} m \left(\frac{b^3}{c^3}\right) \tag{6}$$

with:

$$A = 1 + 2\frac{(\varepsilon_3 - \varepsilon_2)(\varepsilon_2 - \varepsilon_1)}{(2\varepsilon_3 + \varepsilon_2)(2\varepsilon_2 + \varepsilon_1)} \left(\frac{a^3}{b^3}\right) \tag{7}$$

$$B = \frac{(\varepsilon_3 - 1)(\varepsilon_3 - \varepsilon_2)}{(\varepsilon_3 + 2)(2\varepsilon_3 + \varepsilon_2)} \left(\frac{b^3}{c^3}\right) \tag{8}$$

$$C = \frac{(\varepsilon_3 - 1)(\varepsilon_3 + 2\varepsilon_2)(\varepsilon_2 - 1)}{(\varepsilon_3 + 2)(2\varepsilon_3 + \varepsilon_2)(2\varepsilon_2 + \varepsilon_1)} \left(\frac{a^3}{c^3}\right) \tag{9}$$

$$m = (\varepsilon_3 - \varepsilon_2)\frac{(\varepsilon_3 + 2\varepsilon_2)(\varepsilon_2 - \varepsilon_1)}{(2\varepsilon_3 + \varepsilon_1)}\left(\frac{a^3}{b^3}\right) \tag{10}$$

$$\frac{a^3}{b^3} = \frac{(1 + k\varphi_F)}{(1 + k)} \tag{11}$$

$$\frac{b^3}{c^3} = \varphi_F \left[1 + k\frac{(1 - \varphi_F)}{(1 + k\varphi_F)}\right] \tag{12}$$

$$\frac{a^3}{c^3} = \varphi_F \tag{13}$$

$\varepsilon_{1,}\ \varepsilon_2\ and\ \varepsilon_3$ stand for the dielectric permittivities of the ceramic nanoparticles, interphase and polymer matrix, respectively. φ_F represents the volume fraction of ceramic nanofillers, while k is the interphase volume constant, that reflects the matrix/filler interaction strength, where a value of zero designates an insignificant filler-

matrix interaction, while positive values indicate the presence of strong interactions [68].

III. Strategies of the design of core-shell $BaTiO_3$@polymer/Fluorinated polymer nanocomposites

The role of the polymer matrix is to receive the nanoscale reinforcements to provide the strength in the structure, to improve the properties, and to give the desired shape to the nanocomposite. Thus, these polymer shells will have a great effect on the physical properties of the nanocomposites including its dielectric permittivity. The best case is that the polymer shells exhibit high dielectric permittivity and a good compatibility with the nanofiller, resulting in significantly enhanced energy density of the resulting nanocomposites. Actually, the most studied polymer matrices are fluorinated polymers that display dielectric constants of about 10 at 1 kHz (Table 2) [69–72]. Although having many benefits, the final properties of the nanocomposite will not only depend on the constituting materials but also on the processing methods. Actually, different strategies are used to prepare polymer-based $BaTiO_3$ nanocomposite, as shown in Scheme 1.

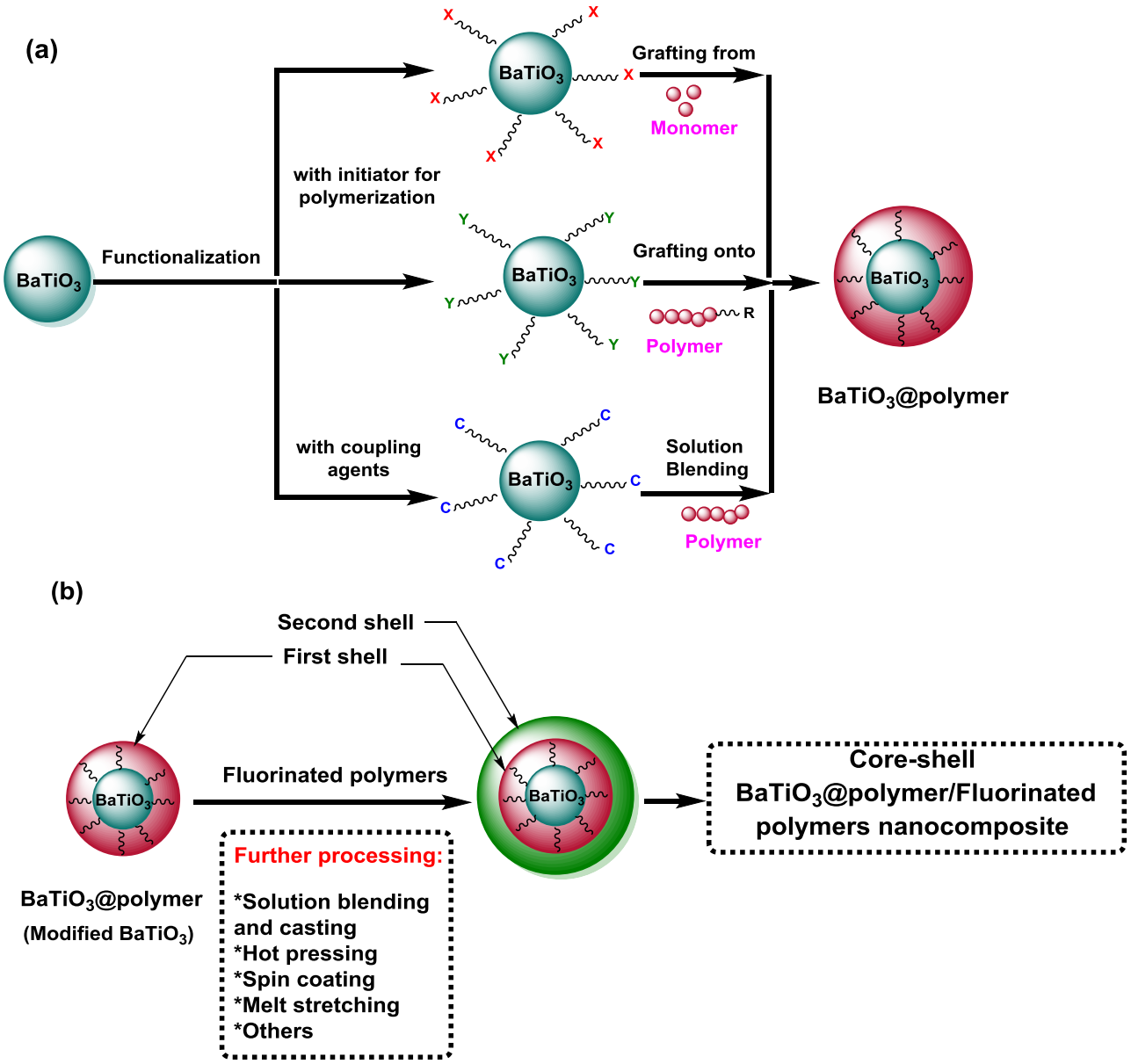

Scheme 1. Schematic illustration of (a) the surface modification of $BaTiO_3$ and (b) the synthesis process of $BaTiO_3$ based polymer nanocomposites, where X stands for -Br (Atom transfer radical polymerization, ATRP); –SC(S)Z (Reversible addition fragmentation chain transfer agent polymerization, RAFT), Y stands for alkyne, R stands for Azide (click chemistry), while C is assigned to coupling agent (*e,g*; silane agent, dopamine, phosphonic acid…) .

Generally, there are different synthetic strategies to get such nanocomposites, including hot pressing [73] , spin coating [74] and melt stretching [75,76] (Scheme 1-b). However, before combining the inorganic fillers with the organic polymer matrix,

surface functionalization of the ceramic must be conducted in a first place. Actually, this surface modification is a crucial step in the synthesis process by allowing good compatibility and dispersion of ceramic nanofiller into polymer matrix (Scheme 1-a). Thus, the first step aims to chemically modify $BaTiO_3$ surface using the "grafting from", "grafting onto" or blending process. The first strategy relies on the formation of the nanocomposites by means of controlled radical polymerization or reversible deactivation radical polymerization (RDRP) of monomers on initiator-functionalized nanoparticle surfaces. The second one consists of the formation of nanocomposites by grafting the pre-prepared polymer chains onto the nanoparticles surface via a reaction between the polymer end-groups and the functional groups on the nanoparticle surfaces. The last technique considers the formation of the nanocomposite by a simple casting or blending using the prepared polymer. These processes yield $BaTiO_3$ surface modified with polymer labeled as $BaTiO_3$@polymer.

In order to further improve the final properties of the prepared nanocomposites, the core-double shell approach could be used. It consists of a simple blending of $BaTiO_3$@polymer with a second polymer shell yielding a nanocomposite labeled as core-double shell system. The final nanocomposites could be then achieved by further processing such as hot pressing, spin coating and melt stretching (Scheme 1-b).

The most relevant routes reported in the literature for the design of core-shell $BaTiO_3$@polymer/Fluorinated polymers nanocomposites (Scheme 1-b) are solution blending or solution mixing between modified $BaTiO_3$ core ($BaTiO_3$@polymer) and fluorinated polymers as the shell. The materials obtained by casting were molded by hot pressing to prepare the sample films for mechanical, dielectric, and thermal properties.

However, melt-stretching and hot-pressing have also been used for the preparation of core-shell nanocomposites. In fact, Ghallabi *et al.* [77] reported the development of three-phase composites with carbon nanotube (MWCNT) and $BaTiO_3$ nanoparticles .0embedded into PVDF ($BaTiO_3$@(MWCNT) /PVDF nanocomposites) using Haake blending mixer and pressed by hot-molding technique. Ferri *et al.* [75] also reported the characterization of the nanoscale piezoelectric and ferroelectric behavior of stretched $BaTiO_3$/PVDF nanocomposites by means of the piezoelectric force microscopy (PFM) technique. First, $BaTiO_3$ was functionalized with nitrodopamine

(NTD) leading to $BaTiO_3$@NTD modified structures. Then, the nanocomposites with functionalized nanoparticles and PVDF (labelled $BaTiO_3$@NTD/PVDF) were elaborated by blending solution in DMAc solvent. The material obtained by casting was then melt-compounded using a twin-screw micro-extruder and compression molded into a film of 100 μm thickness. The samples were stretched at a draw temperature of 90 °C up to a strain ε=100 % to promote the PVDF polar β crystal phase and thus enabled the polymer to display a piezoelectric response. Indeed, You *et al.* [76] reported another route of nanocomposites preparation by coupling in-*situ* polymerization and hot-stretching techniques. First, the polyaniline (PANI) functionalized barium titanate labelled $BaTiO_3$@PANI nanoparticles were prepared by *in-situ* polymerization of aniline monomer in the presence of $BaTiO_3$. Then, polyarylene Ether Nitrile (PEN)-based nanocomposite films with 40 wt% pure BT and $BaTiO_3$@PANI functionalized nanoparticles were prepared.

Table 2. Dielectric properties of different polymers. Reproduced with permission of [78]. Copyright 2016 American Chemical Society.

Polymers	***Dielectric constant (1 kHz)***	***Loss tangent (1 kHz)***	***Dielectric strength (kV/cm)***
LDPE	2.3	0.003	309
high-density polyethylene (HDPE)	2.3	0.0002−0.0007	223
BOPP	2.2	0.0002	7500
Polystyrene	2.4−2.7	0.008	2000
poly(ethylene terephthalate) (PET)	3.6	0.01	2750−3000
PMMA	4.5	0.05	2500
polyvinyl chloride (PVC)	3.4	0.018	400
polyetheretherketone (PEEK)	4.0	0.009 (100 kHz)	
poly(phthalazinone ether ketone)	3.5	0.0063	4700
polycarbonate (PC)	3.0	0.0015 (1000 kV/cm)	2520
Epoxy	4.5	0.015	250−450
PVDF	10-12	0.04	1500−5000
P(VDF-TrFE) [79]	11	0.08	770
P(VDF-TrFE-CFE) [79,80]	21-55	0.09-0.1	59-660

PTFE	2	0.0001	880−1760
PDMS	2.6	0.01	660
Polyimide	3.5	0.04	2380
Polyurethane	4.6	0.02	200
polyvinyl alcohol	12	0.3	1000
Aromatic polyurea(poly(diaminodiphenylmethane diphenylmethane diisocyanate) [P(MDA/MDI)]	4.2	0.005	8000

IV. Structure and properties of core-shell $BaTiO_3$@polymer/Fluorinated polymer nanocomposites

IV.1. Fluoropolymer matrix

Because of their widespread use in many applications, fluoropolymers present a number of interesting properties including high thermal stability, hydrophybicity, improved chemical inertness and low surface tension [81–84]. Recently, many fluorinated polymers and copolymers have been widely used to the synthesis of $BaTiO_3$ based nanocomposites, including PVDF and VDF copolymers (Table 3) [20,27,85–90].

Table 3. Chemical structures of the most used fluoropolymers in dielectric nanocomposites.

Polymer	Chemical structure
Poly(vinylidene fluoride): PVDF	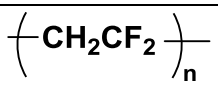
Poly(vinylidene fluoride-*co*-hexafluoropropylene) Poly(VDF-*co*-HFP)	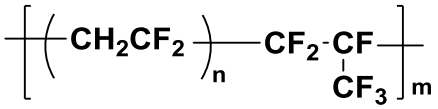
Poly(vinylidene fluoride-*ter*-trifluoroethylene-*ter*-chlorotrifluoroethylene): poly(VDF-*ter*-TrFE-*ter*-CTFE)	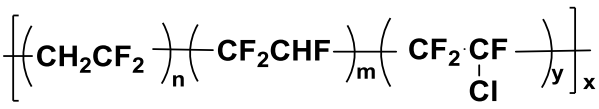

Polyvinylidene fluoride is a semi-crystalline polymer, which contains 59.4 wt % of fluorine and 3 wt % hydrogen atoms [26]. It presents a complex structure that may

exist in five different crystalline phases and the most investigated ones are: α, β and γ phases (Fig. 6) [91]. Although each phase exhibits various properties, β phase was found to be the most interesting polymorph of PVDF for technological applications thanks to its piezoelectric, pyroelectric and ferroelectric properties that originate from the orientation of the strong dipole in $–CH_2-CF_2$ units along the polymeric chains [26].

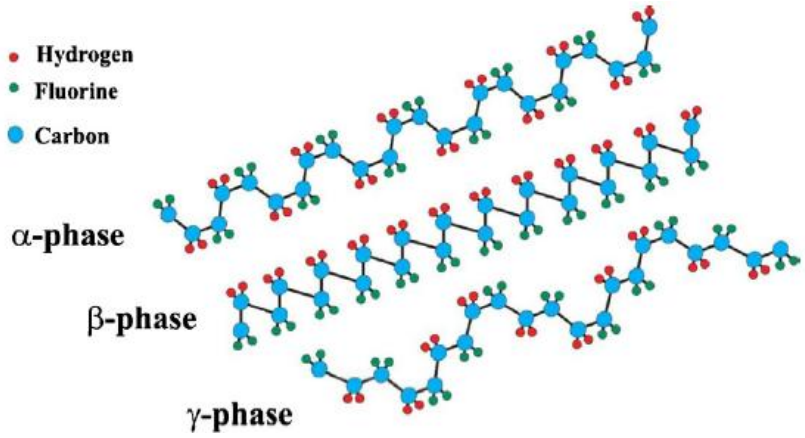

Fig. 6. Schematic illustration of three crystalline phases of PVDF. Reproduced with permission of [91]. Copyright 2014 Elsevier.

In order to improve the properties of PVDF and expand its field of applications, several works have been reported on the use of VDF copolymers [26,72,92] or even mixed with ceramics to form nanocomposite systems [93,94]. For example, poly(vinylidene fluoride-co-hexafluoropropene) poly(VDF-*co*-HFP), has been mostly used in Li-ion batteries as polymer electrolyte or even in production of membranes [95–97]. This interest arises from the fact that this copolymer is chemically inert and exhibits a lower crystallinity compared to that of PVDF [98]. Claude *et al*. [18] prepared poly(VDF-*ter*-TrFE-*ter*-CTFE) terpolymer from the radical copolymerization of VDF and CTFE followed by the reductive dechlorination of CTFE units.

Table 4. Structural Characteristics of the prepared VDF- based ferroelectric co- and terpolymers. Reproduced with permission of [18]. Copyright 2008 American Chemical Society.

	Composition (mol %)					
Polymer	**VDF**	**TrFE**	**CTFE**	χ_c **(%)**	T_m **(°C)**	ε_r
1	73.6	0	26.4	7.2		14.1
2	73.6	3.9	22.5	14.4	37.8	16.4

3	73.6	9.2	17.2	17.1	72.5	24.1
4	73.6	11.9	14.5	18.0	86.7	24.0
5	73.6	18.3	8.1	24.2	121.0	14.7
6	73.6	19.3	7.1	28.6	127.0	14.2
7	73.6	26.4	0	35.4	163.0	10.4

χ_c, T_m *and* ε_r *stand for crystallinity, melting temperature and relative permittivity, respectively.*

Table 4 shows that the introduction of 3.9 mol % of TrFE and 22.5 mol % of CTFE into the PVDF matrix decreases the crystallinity and melting temperature from 50-70% and 155-198 °C for PVDF to 14.4 % and 38 for poly(VDF-*ter*-TrFE-*ter*-CTFE) terpolymer. Moreover, the highest permittivities were found in polymers 3 and 4 (Table 4) which indicate the effect and also the importance of molecular composition of terpolymers on the final properties of the system. Soulestin *et al.* [92] reviewed the synthesis and properties of poly(VDF-*ter*-TrFE-*ter*-Monomer) terpolymers. The influence of polymerization strategies and types of termonomers used on the final properties were also discussed. It was concluded that CTFE and CFE are among the most used comonomers since they affect efficiently the crystalline lattice of poly(VDF-*co*-TrFE) terpolymers. Moreover, this terpolymer is considered to be one of the most promising materials thanks to its higher polarization, which is one of the most important features of ferroelectric polymers. Cho *et al.* [99] reported the formation of the β-phase in a poly(VDF-*ter*-TrFE-*ter*-CTFE) film (PVDF:TrFE:CTFE = 62:31:7 in mol%) by solution annealing process at room temperature, by crystallizing the polymer below the curie temperature (Fig. 7). This method led to polymeric films with enhanced ferroelectricity compared to a thermally annealed one.

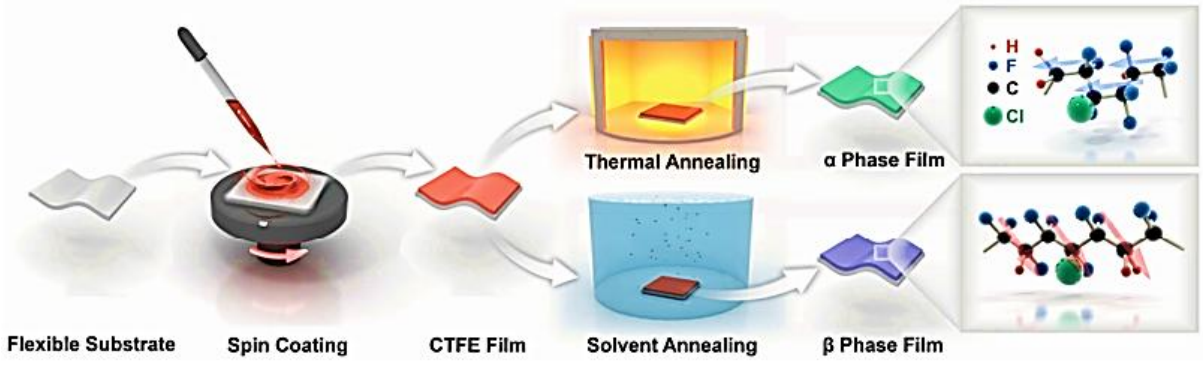

Fig. 7. Illustration of the formation of the α and β phases formed using thermal and solvent annealing, respectively. Annealing at a temperature below the curie

temperature, using solvent annealing, forms a β-phase dominant film whereas a thermal annealing above the phase transition temperature forms an α-phase dominant film. Reproduced with permission of [99]. Copyright 2016 Wiley.

IV.2. Surface modification of $BaTiO_3$

Barium titanate nanoparticles are often used as ceramic fillers for polymer matrix composites because they are one of the most commercially available high dielectric constant-materials. However, since untreated $BaTiO_3$ nanoparticles tend to form agglomerates, the good dispersion of the nanoparticle fillers into the polymer matrix and the compatibility between them are always the important factors conditioning the performances of the nanocomposites. Thereby, the surface functionalization is a crucial feature.

IV-2-1. Modification of $BaTiO_3$ with fluorinated agent

So far, several strategies have been proposed to prevent aggregation of $BaTiO_3$ nanoparticles inserted into the polymer matrix, including surface hydroxylation [100], phosphonic acid [74,101], dopamine [102,103] and coupling agents [104–106]. In order to highlight the importance of the hydroxylation step, Zhou *et al.* [100] reported a comparison between the dielectric properties of a nanocomposite based on a PVDF polymer matrix and raw (c-BT) or hydroxylated (h-BT) $BaTiO_3$ nanoparticles. The results showed that nanocomposites made by hydroxylated nanoparticles display a low temperature and frequency dependence. This suggests that the strong interactions between h-BT fillers and PVDF matrix is the main reason for improving dielectric properties. Dalle Vacche *et al*. [106] studied the effect of surface modification of $BaTiO_3$ with (3-aminopropyl) triethoxysilane (APTES) as a silane coupling agent on properties of poly(VDF-*co*-TrFE)/$BaTiO_3$ composites. The modified particles were well-dispersed in the polymer matrix than that of the unmodified ones leading to reduced aggregate and enhancing the compatibility with the poly(VDF-*co*-TrFE) matrix. In another work, Kim *et al*. [107] reported that surface modification of $BaTiO_3$ with phosphonic acid formed well-ordered nanoparticles into poly(VDF-*co*-HFP) matrix leading to high dielectric constant ($\varepsilon = 43$) and high breakdown strength (210 V μm^{-1}).

However, in order to get better interfacial interactions between the nanofiller and the fluoropolymer, fluorinated modifiers are more preferred as they contain fluorine atoms in their end chains. To study the influence on the compatibility with fluorine polymers, Ehrhardt *et al*. [108] used n-octyl phosphonic acid (OPA) and pentafluorobenzylphosphonic acid (PFBPA) to modify the surface of $BaTiO_3$. The phosphonic acid coated $BaTiO_3$ were then dispersed in solutions of poly(VDF-*co*-HFP) copolymer to form nanocomposites by spin coating technique.

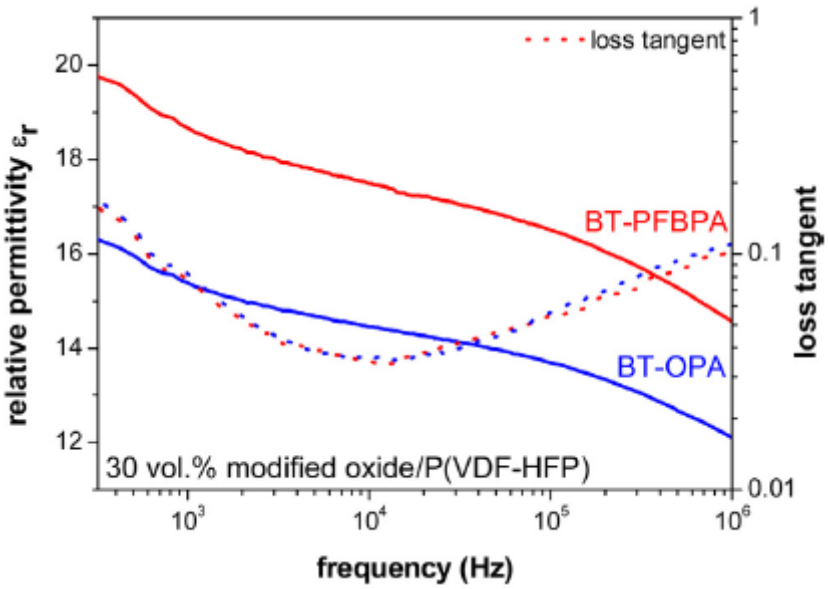

Fig. 8. Relative permittivity of BT/Poly(VDF-*co*-HFP) composite films prepared with 30 vol.% $BaTiO_3$ coated with pentafluorobenzyl phosphonic acid (BT-PFBPA) and octylphosphonic acid (BT-OPA). Reproduced with permission of [108]. Copyright 2013 Elsevier.

Results show that the phosphonic acid with a fluorinated organic host gives rise to a slightly increased of relative permittivity of the resulting composite materials compared to the one containing n-octyl phosphonic acid (Fig. 8). This suggests that pentafluorobenzylphosphonic acid provides a better chemical compatibility with poly(VDF-*co*-HFP).

PFBPA was used in another survey to modify $BaTiO_3$ surface. For example, Kim *et al*. [74] utilized pentafluorobenzylphosphonic acid (PFBPA) to functionalize $BaTiO_3$

surface before adding poly(VDF-*co*-HFP), to form nanocomposite by spin coating the dispersions on aluminum coated glass substrate (Fig. 9).

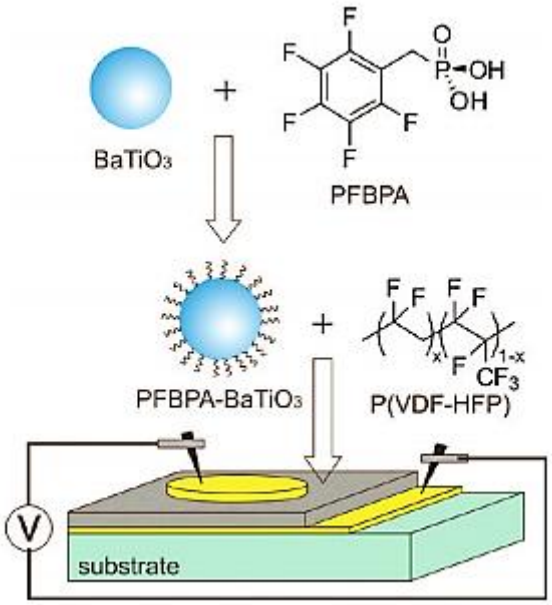

Fig. 9. Illustration of surface modification of $BaTiO_3$ with PFBPA. Reproduced with permission of [74]. Copyright 2009 American Chemical Society.

Authors reported the surface modification of $BaTiO_3$ with PFBPA formed homogenous dispersion into the polymeric matrix and therefore uniform nanocomposite thin films.

Zhang *et al*. [109] used (1H,1H,2H,2H-perfluorooctyltrimethoxysilane) to introduce a short perfluoroalkyl chain onto the surface of $BaTiO_3$ nanofibers by chemical reaction between the HO- groups of the oxydized surface of BT and methoxy groups of the fluorinated silane. Then, the modified nanoparticles were incorporated into PVDF by solution blending (Scheme 2). The results indicate that the fluorosilane modified $BaTiO_3$ nanofiber results in a strong interchain interaction with PVDF matrix and improved the interface compatibility between the functionalized filler and the fluoropolymer.

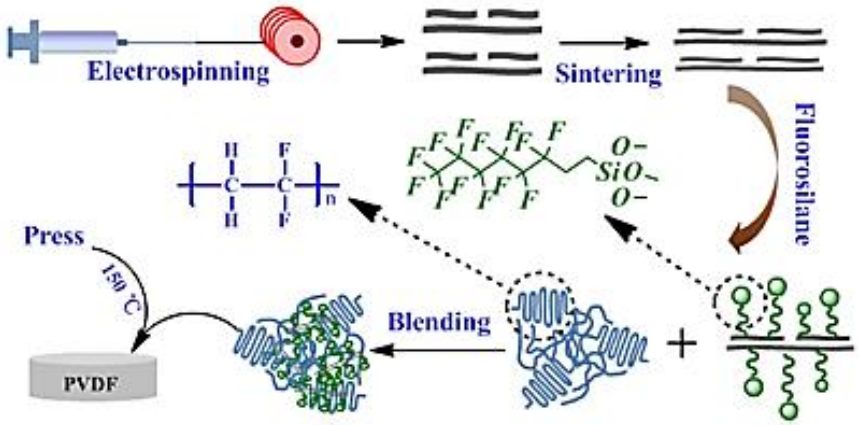

Scheme 2. Schematic illustration of the preparation of PVDF/BT nanocomposite. Reproduced with permission of [109]. Copyright 2014 Elsevier

In another work, Yu *et al.* [110] reported the preparation of PVDF/BT nanocomposites. The nanoparticles were firstly modified with tetrafluorophtalic acid, then incorporated into PVDF matrix by a solution casting method. Fig. 10 displays the surface modification process of BT with tetrafluorophtalic acid and the effects on the modification on the PVDF/BT nanocomposite. The fluorinated acid reacts with the hydroxyl groups already present onto the surface of BT using its alkoxy chains. Thanks to its fluorinated aryl groups, the modified BT exhibits good compatibility with PVDF, improves the dispersion of BT and introduces more space charges in the polymer which results in generation of passivation layers, and thereby enhancing the breakdown strength of the nanocomposite.

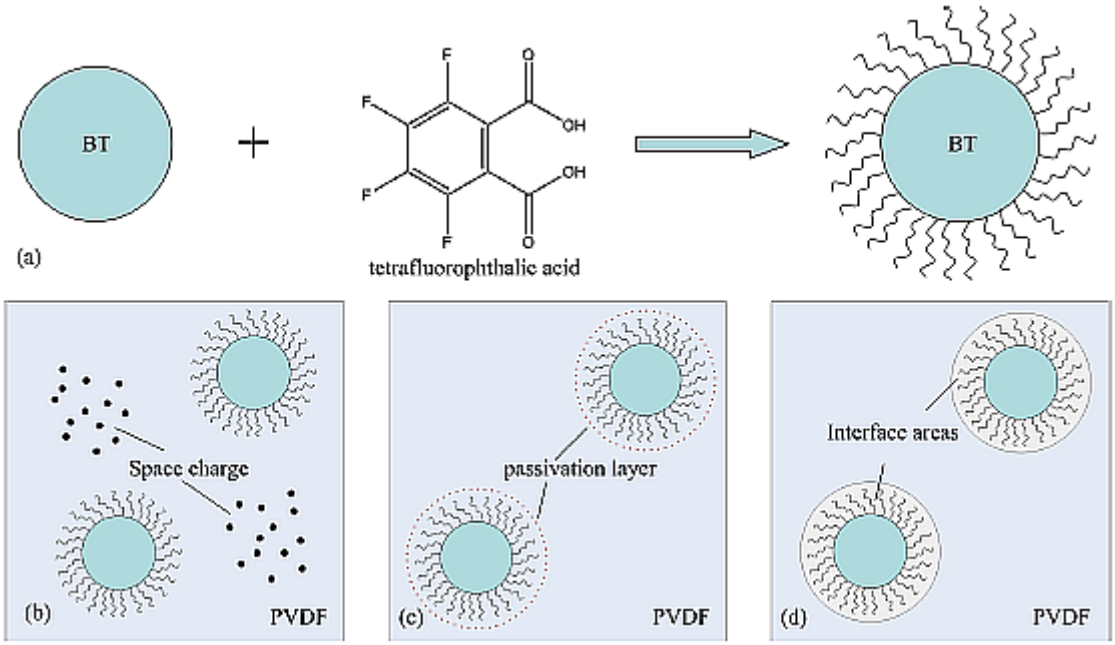

Fig. 10. Schematic of surface modification processing of BT nanoparticles (a) and the effects of surface modified BT nanoparticles in BT/PVDF nanocomposites (b), (c), and (d). Reproduced with permission of [110]. Copyright 2013 American Institute of Physics.

Wang *et al*. [111] prepared BT/poly(VDF-*co*-HFP) nanocomposites by a solution casting method. The $BaTiO_3$ nanoparticles were first functionalized with fluoro-polydopamine via a spontaneous self-polymerization upon the surface of $BaTiO_3$ nanowires (Fig. 11), then, a desired amount of modified BT was inserted into poly(VDF-*co*-HFP) matrix. It was found that by anchoring a long fluorinated chain upon the dopamine, the resulting fluoro-dopamine modified BT presented homogenous distribution in the polymer matrix, suggesting an excellent compatibility with the fluoropolymer matrix. Moreover, the fluoro-dopamine shell layers improved the dispersion of nanowires and thus increases the affinity with the polymer matrix, resulting in enhanced dielectric permittivity and breakdown strength.

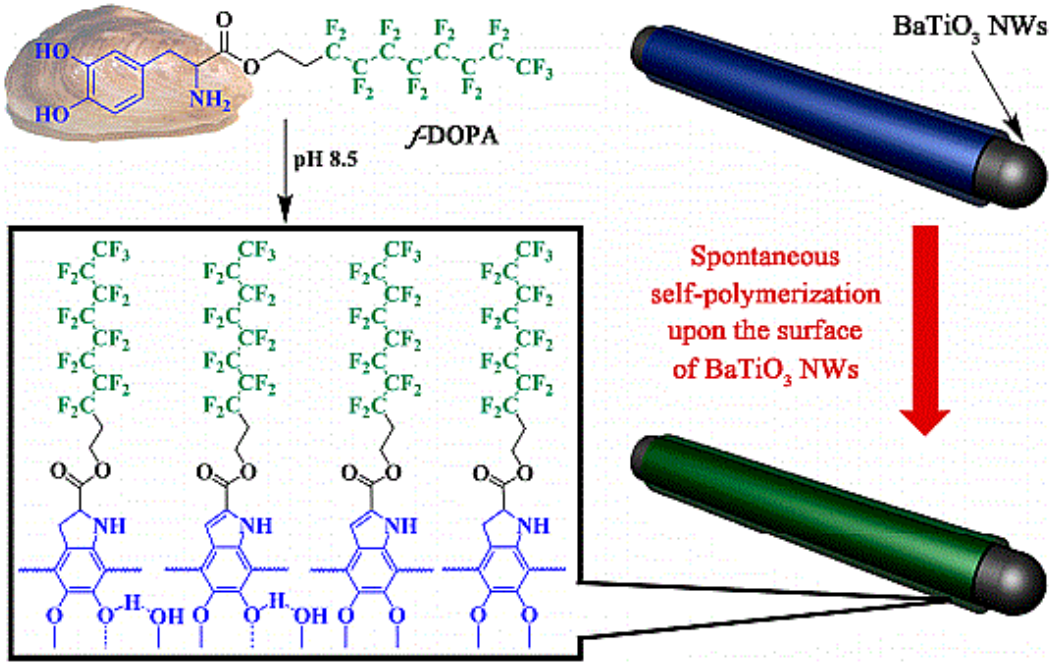

Fig. 11. Schematic illustration of the preparation process for fluorinated-DOPA@$BaTiO_3$ NWs. Inset is a photograph of a mussel. Reproduced with permission of [111]. Copyright 2017 American Chemical Society.

IV-2-2. Modification of $BaTiO_3$ with polymer prepared by "Grafting from" route

IV-2-2-1. PMMA@BT

Wang *et al.* proceeded to $BaTiO_3$ functionalization with PMMA using ATRP polymerization [112]. The nanoparticles were first coated with tetrameric metallophthalocyanine (TMPc), from which PMMA brushes are grafted. In order to make a comparison, composites without the TMPc interfacial layer were also synthesized. The particle size and size distribution of the resulting nanocomposite were studied (Fig. 12). It was found that by increasing the feed ratio of MMA from 5.2 to 18 wt %, the hydrodynamic diameter (Dh) for BTO@TMPc-PMMA particles increased from 109 nm to 186 nm, proving the succefull grafting of PMMA onto coated $BaTiO_3$.

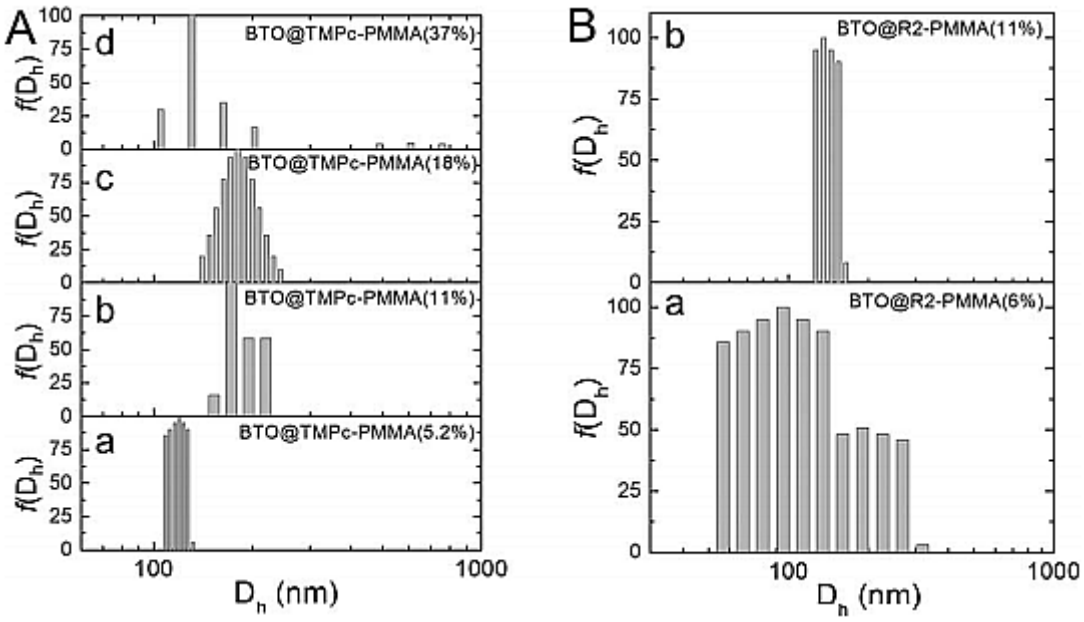

Fig. 12. DLS hydrodynamic diameter (D_h) distribution for (A) BTO@TMPc-PMMA and (B) BTO@R2c-PMMA nanoparticles in DMF. The maximum light scattering intensity is normalized to 100%. Reproduced with permission of [112]. Copyright 2014 Wiley.

IV-2-2-2. PTFEMA or PMMA@BT

Zhang *et al.* [113] prepared a core shell structured nanocomposites with different shell composition and shell thickness by grafting the polymer onto BT surface using ATRP polymerization. Methyl methacrylate (MMA) and 2,2,2-trifluoroethyl methacrylate (TFEMA) were used and two different amounts of these monomers were adopted (Table 5).

Table 5. Summary of grafted polymer contents measured by TGA under nitrogen atmosphere. Reproduced with permission of [113]. Copyright 2017 Elsevier.

Samples	Feed ratio of monomer to BT-Br (w/w)	Weight loss of grafted polymer (%)
BT-Br	--	1.5
BT@PMMA1	1:1	7.0
BT@PMMA2	2:1	9.5
BT@PTFEMA1	1:1	3.0
BT@PTFEMA2	2:1	3.5

The different analyses performed on the nanocomposites evidenced the successful grafting of both PMMA and PTFEMA onto BT surface. TGA results showed that by increasing monomer feed ratio, the grafted mass of the two polymers increased, which indicate that the grafted polymer content can be controlled by varying the monomer: initiator molar ratio (for example, by increasing the feed ratio of monomer: initiator from 1:1 to 2:1, the weight loss of PMMA increases from 5.5 % to 8.0 %). Moreover, Fig. 13 exhibits the shell thickness of the polymer covering BT surface increases by increasing the monomer feed ratios from 7 nm to 12 nm for PMMA and from 4.5 nm to 5.5 nm for PTFEMA.

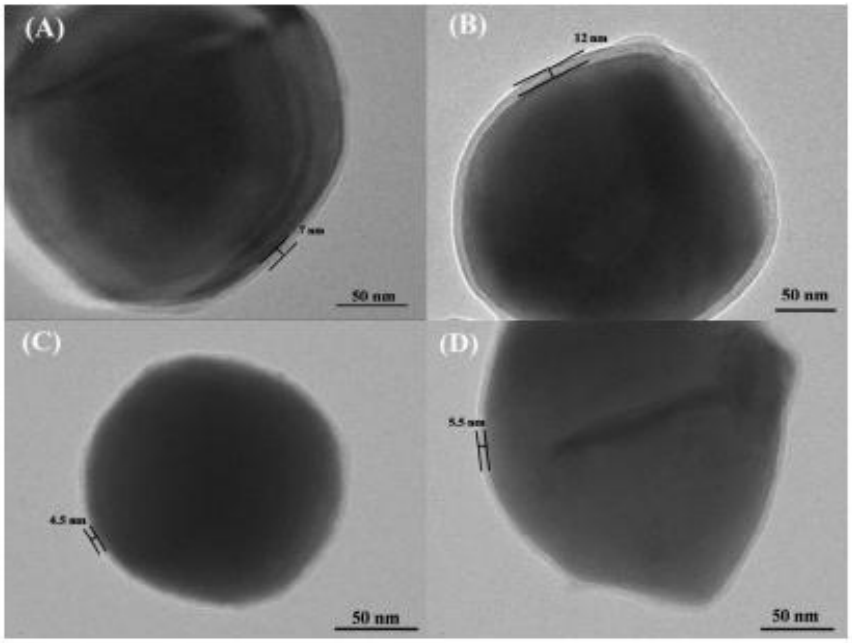

Fig. 13. TEM images of the BT@polymer nanoparticles: (A) BT@PMMA1, (B) BT@PMMA2, (C) BT@PTFEMA1 and (D) BT@PTFEMA2. Reproduced with permission of [113]. Copyright 2017 Elsevier.

IV-2-2-3. PPFOMA@BT

Zhang *et al*. [114] prepared a core shell nanocomposite by grafting 1H,1H,2H,2H-perfluorooctyl methacrylate (PPFOMA) onto BT using ATRP polymerization. First, nanoparticles were treated by hydroxylation, silylation and amidation to anchor the ATRP initiator, then PPFOMA polymer chain was grafted from

the initiating sites (Scheme 3). At high PPFOMA feed ratios, the nanoparticles could be suspended in the solvent overnight without precipitation. This suggests that the functionalization of BT nanoparticles with PPFOMA polymer chains leads to a better dispersion of the composite particles. In addition, the dielectric properties of nanocomposites were studied. The dielectric constant (ε) increased significantly by increasing the $BaTiO_3$ fraction in the nanocomposite and reached 7.4 (for a fraction of 71 wt% in $BaTiO_3$), which is 3 times higher than that of PPFOMA (ε=2.6).

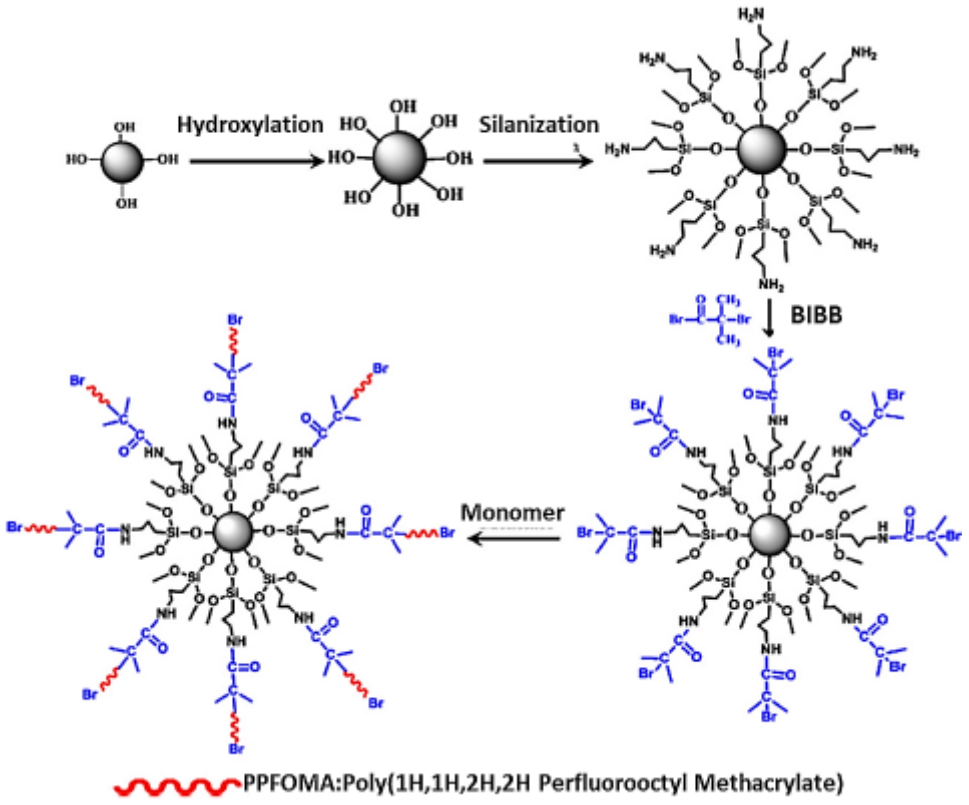

Scheme 3. Preparation of PPFOMA@$BaTiO_3$ by SI-ATRP of 1H,1H,2H,2H-perfluorooctyl methacrylate (PPFOMA). Reproduced with permission of [114]. Copyright 2013 Elsevier.

IV-2-2-4. PtBA@BT

Du *et al.* [115] used poly(*tert*-butyl acrylate) (P*t*BA) to functionalize BT surface by ATRP polymerization (Fig. 14). The first step dealt with the hydroxylation of BT surface by hydrogen peroxide in order to create –OH groups on their surface. The second and third steps consisted of the grafting of silane and bromine agents to obtain

ATRP initiating sites, respectively. The last step was the polymerization of *t*BA from functionalized nanoparticles. Theses authors reported that the P*t*BA functionalized nanoparticles reduce the surface energy of the nanoparticles and avoid aggregation leading to a better dispersion and homogenous nanocomposites.

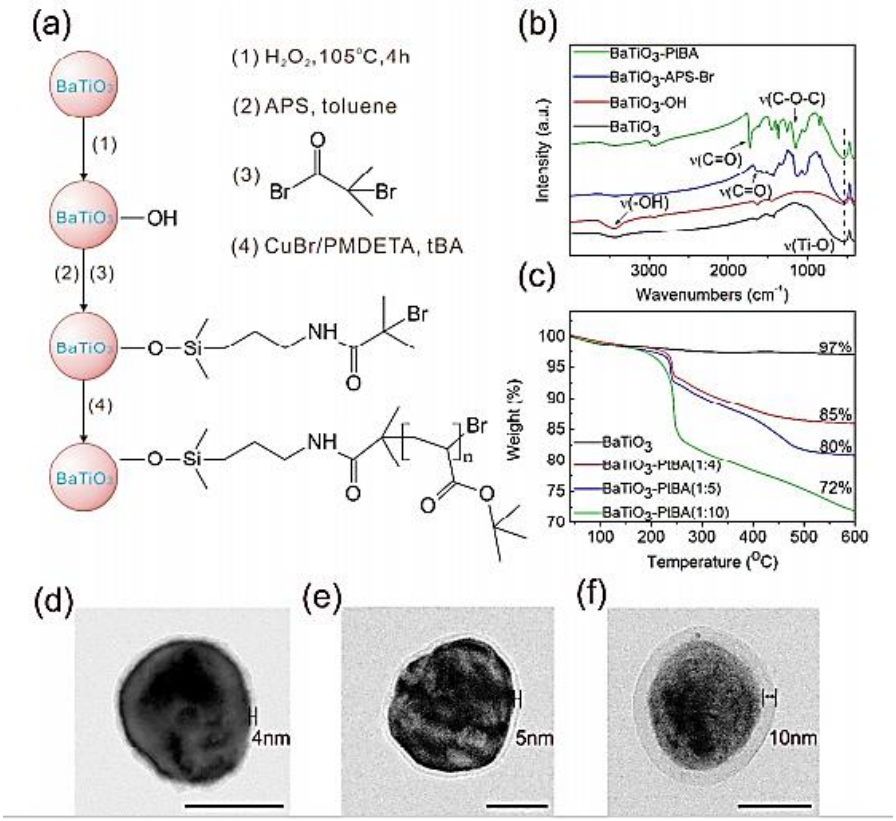

Fig. 14. Preparation process and characterizations of the nanoparticles with core-shell structure. a) Schematic diagram illustrating the preparation process of the $BaTiO_3$-P*t*BA by ATRP of *tert*-butyl acrylate. b) FT-IR spectra of the $BaTiO_3$ at various stages of treatment. c) TGA thermogramms for pure $BaTiO_3$ and $BaTiO_3$-PtBA with different polymer shell thicknesses. d-f) TEM images of the core-shell structured $BaTiO_3$-PtBA nanoparticles (scale bar 50 nm). Reproduced with permission of [115]. Copyright 2018 American Chemical Society.

IV-2-2-5. PGMA@BT

Ejaz *et al.* [25] prepared core-shell nanocomposites via ATRP polymerization through two steps: i) immobilization of initiator sites onto $BaTiO_3$ surface and ii) ATRP polymerization of glycidyl methacrylate (GMA). The dielectric permittivity of PGMA and PGMA@BT nanocomposite decreases as the frequency increases from 100 Hz to 1

MHz (Fig. 15). At room temperature, the nanocomposite displays a very high permittivity (54 at 1 kHz) which is 10 times higher than that of PGMA (5.3 at 1 kHz). This enhanced permittivity is related to the good dispersion of the ceramic fillers into the polymer matrix.

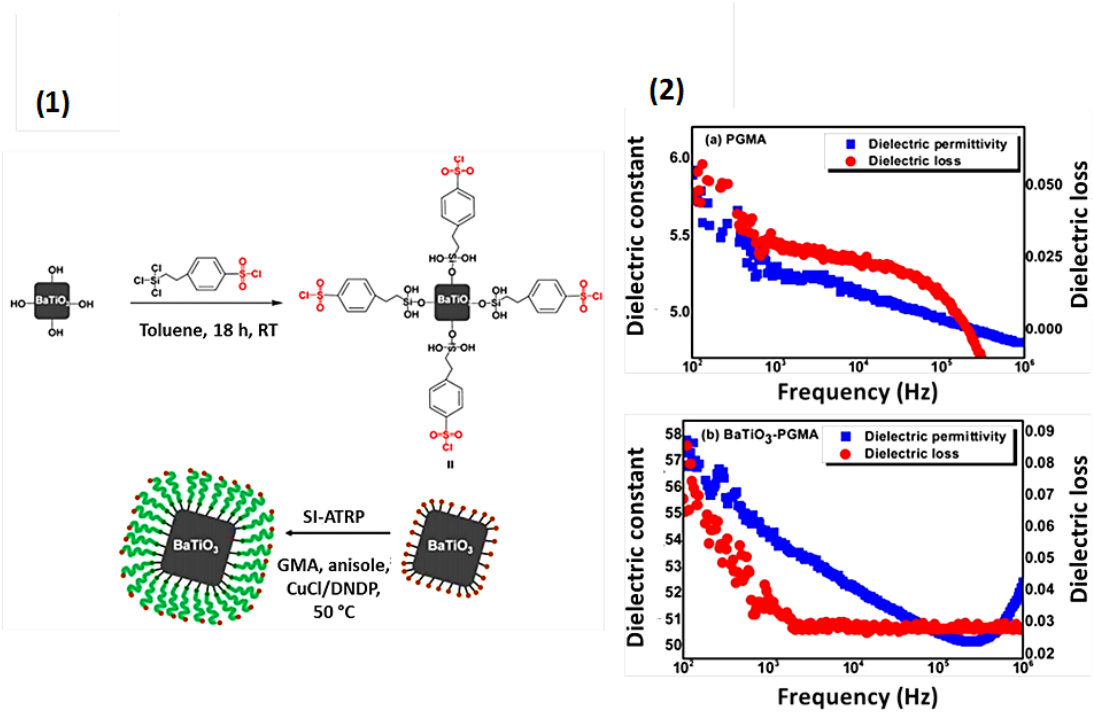

Fig. 15. (1) Synthesis of $BaTiO_3$-PGMA core-shell nanocomposites by SI-ATRP of glycidyl methacrylate (GMA) from $BaTiO_3$ nanoparticles. (2) Frequency dependent dielectric properties at 100 -1 MHz: (a) PGMA and (b) $BaTiO_3$-PGMA nanocomposite. Reproduced with permission of [25]. Copyright 2015 Wiley.

IV-2-2-6. PHEMA-b-PHEMA@BT or PHEMA-b-PANa@BT

Huang *et al*. [116] prepared a well- defined core@shell structured nanocomposites by ATRP polymerization of (meth)acrylates. Since the resulting polymer in ATRP is still "living" after polymerization, it can reinitiate the polymerization of a second monomer to further yield block copolymers. Thus, a double shell polymer was grafted onto the first core@shell (Scheme 4). Three types of (meth)acrylate monomers were used: poly(methyl methacrylate) (PMMA), poly(2-hydroxyethylmethacrylate) (PHEMA) and poly(sodium acrylate) (PANa).

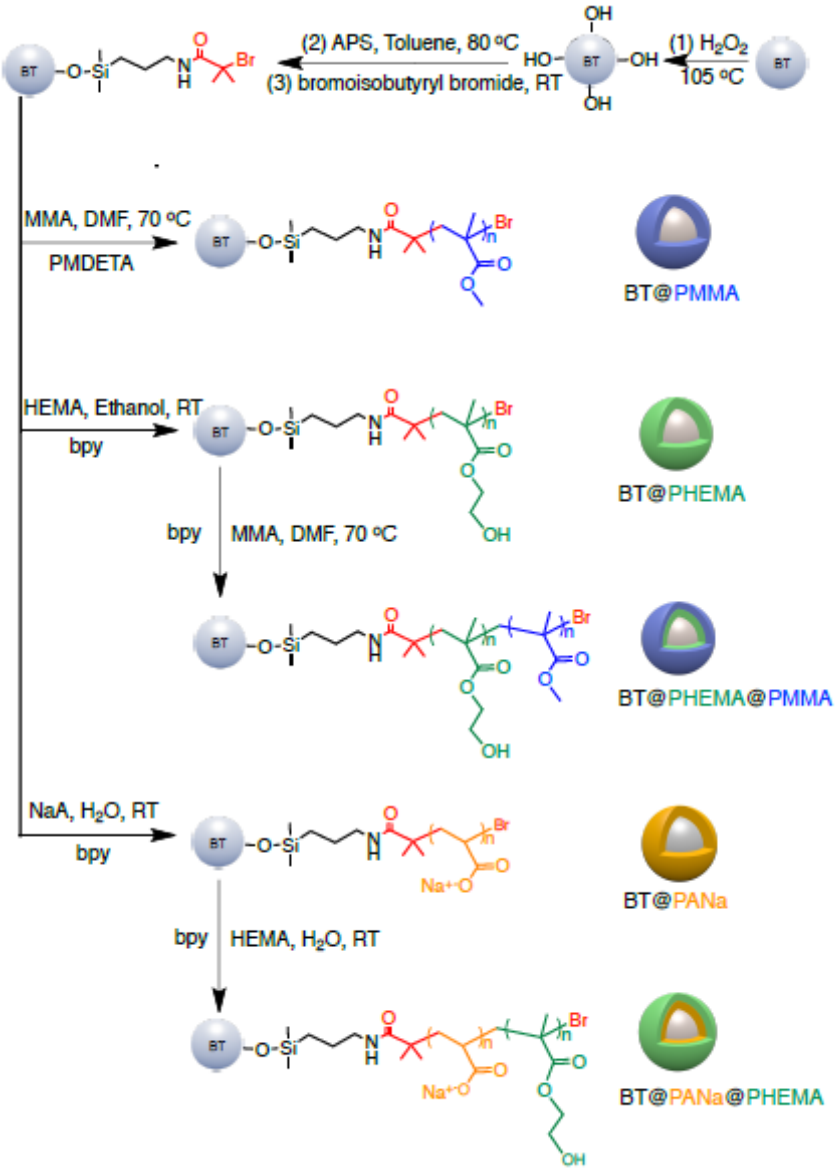

Scheme 4. Diagram illustrating the preparation processes of BT@shell structured nanocomposites. Reproduced with permission of [116]. Copyright 2016 American Chemical Society.

The first shell was chosen to display both high dielectric permittivity and electrical conductivity to provide high polarization, while the second one was selected to be more insulating to maintain a large resistivity and low loss. Fig. 16 exhibits the measured DC conductivity of neat polymers and core@shell structured BT nanocomposites. It can be clearly seen that the PHEMA exhibits a higher conductivity than that of PMMA. This high value comes from the fact that PHEMA presents highly polar –OH groups making it more sensible to impurities like water or ions, which

increase its conductivity. Indeed, BT@PHEMA@PMMA is close to that of BT@PMMA, while that of PMMA/PHEMA mixture presents a conductivity close to that of PHEMA. This could indicate the successful grafting of the polymer shell, and the more conductive PHEMA shell being well-isolated by the less conductive PMMA.

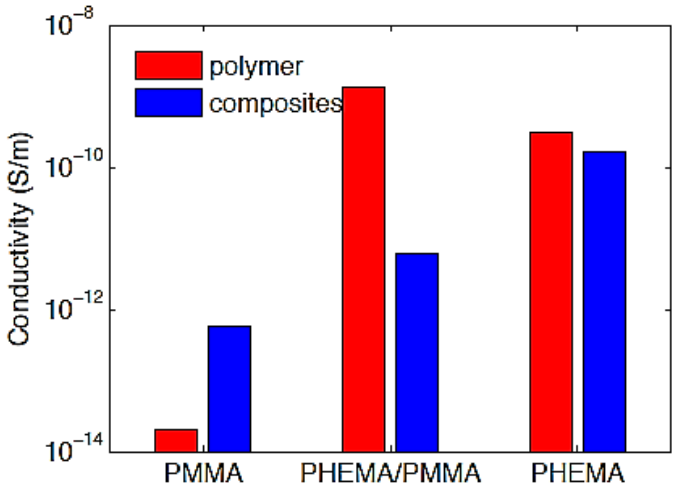

Fig. 16. The measured dc conductivity of neat polymers and BT@shell structured nanocomposites under a dc voltage of 10 V. Reproduced with permission of [116]. Copyright 2016 American Chemical Society.

IV-2-2-7. PMMA@BT/ PGMA@BT/PHEMA@BT

Zhu *et al*. [73] prepared three kinds of polymer nanocomposites using core@shell structured polymer@BT nanoparticles. $BaTiO_3$ nanofillers were functionalized with PMMA, PGMA and PHEMA by RAFT polymerization, where the polymer shells were controlled (reaction time) to have the same shell thickness.

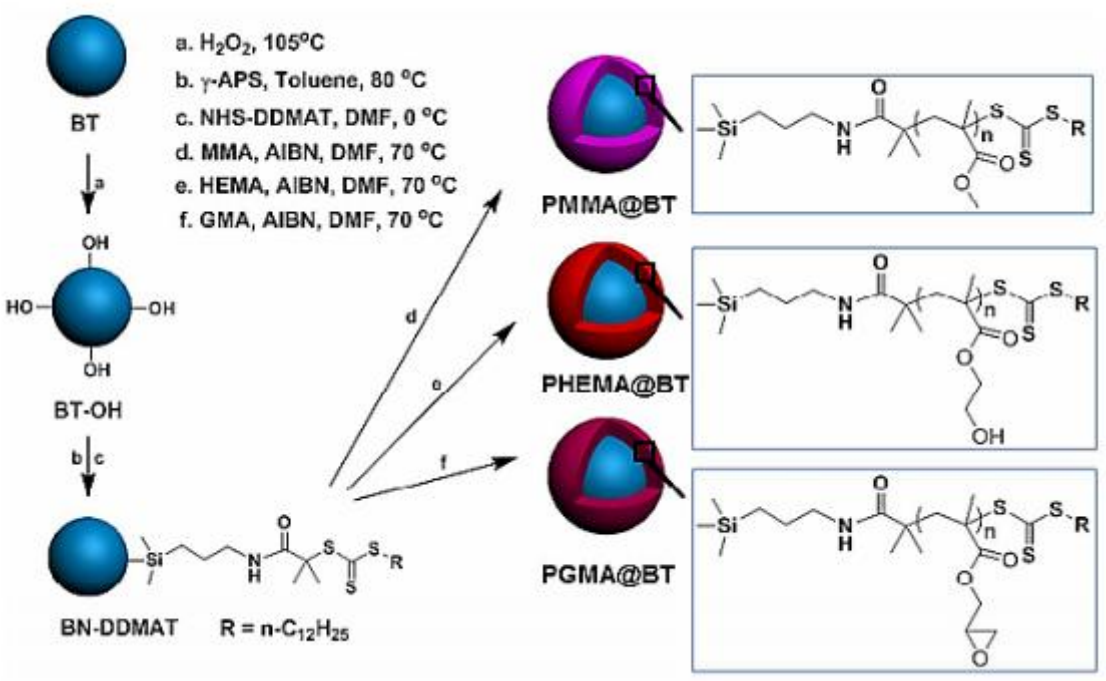

Scheme 5. Preparation process of the polymer@BT nanoparticles by surface initiated RAFT polymerization of various monomer (methyl methacrylate, glycidyl methacrylate and 2- hydroxyethyl methacrylate). Reproduced with permission of [73]. Copyright 2014 American Chemical Society.

Fig. 17 exhibits the TEM images of the polymer functionalized nanoparticles. The BT nanofillers are homogenously encapsulated by a thin layer of polymer, the thickness of which varies from 2-3 nm.

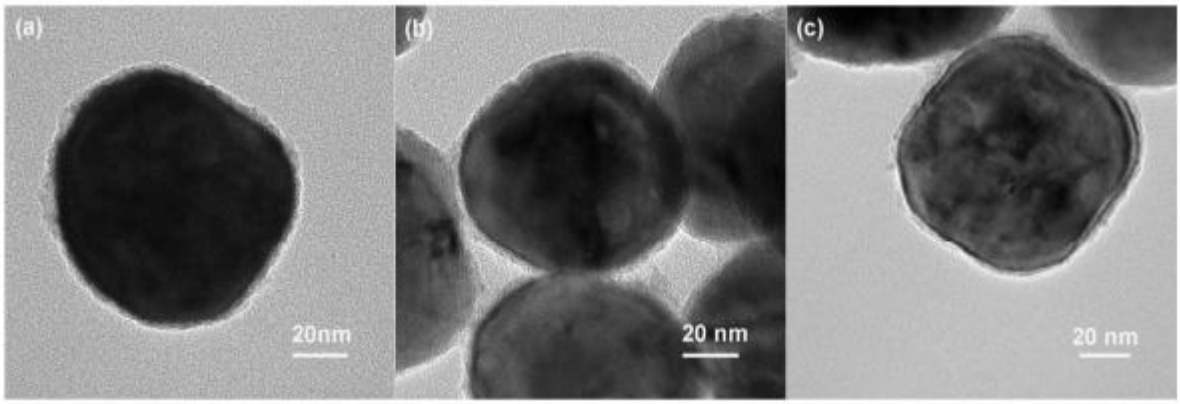

Fig. 17. TEM images of the synthesized of poly(methacrylate)@BT nanocomposites using different polymer shells by RAFT polymerization (a) PMMA, (b)

PHEMA and (c) PGMA. Reproduced with permission of [73]. Copyright 2014 American Chemical Society.

IV-2-2-8. PHFDA@BT and PTFEA@BT

Yang *et al.* [27] used two types of fluoroalkyl acrylates, 1H,1H,2H,2-Heptadecafluorodecyl acrylate (HFDA) and 2,2,2-trifluoroethyl acrylate (TFEMA) to functionalize BT surface by RAFT polymerization. These monomers were used to reduce the surface energy of BT nanoparticles and improved their compatibility with the polymer host matrix. The different analyses performed on the functionalized nanoparticles indicate the successful grafting of the two fluopolymers and the higher grafting density of PTFEMA@BT (0.031 chains/nm^2) compared to that of PHFDA@BT (0.021 chains/nm^2) (Table 6). This could be explained by the fact that the long fluoroalkyl groups of PHFDA leading to more larger steric hindrance.

Table 6. Characteristics of the Fluoro-Polymer@$BaTiO_3$ Hybrid Nanoparticles. Reproduced with permission of [27]. Copyright 2013 American Chemical Society.

Sample	***BT-PHFDA1***	***BT-PHFDA2***	***BT-PTFEA1***	***BT-PTFEA2***
Weight loss of nanopartilces (%) [a]	3.45	6.69	3.83	7.09
Mn *of grafting polymer (g/mol)* [b]	4.1×10^3	7.5×10^3	3.4×10^3	5.9×10^3
Mw/Mn *of grafting polymer* [b]	1.23	1.18	1.21	1.16
Grafting density (chains/nm^2) [c]	0.021	0.014	0.031	0.026

[a] *Calculated from TGA results based on the weight loss of BT-EDMAT nanoparticles.* [b] *Obtained from GPC results.* [c] *Considering each particle with d=100 nm and density of 6.02 g/cm^3.*

IV-2-2-9. PTFMPCS@BT

Chen *et al.* [86] prepared core shell structured $BaTiO_3$@rigid-fluoropolymer nanoparticles from the RAFT polymerization of 2,5-bis{[4-trifluoro(methoxyphenyl)oxycarbonyl]styrene}. By varying the monomer: BT feed ratios, the resulting nanocomposites were denoted as BT-3F1, BT-3F2, and BT-3F3, in which BT-3F1 and BT-3F3 had the thinnest and the thickest polymer shells, respectively. Fig. 18 exhibits the TEM images of the functionalized nanoparticles where BT-3F0 refers to unmodified BT. After grafting the polymer from the functionalized nanoparticles, a stable and dense polymer shell was covering the surface of the nanoparticles. The shell thickness varied from 4 to 12 nm (Fig. 18), suggesting the successful modification of nanoparticles.

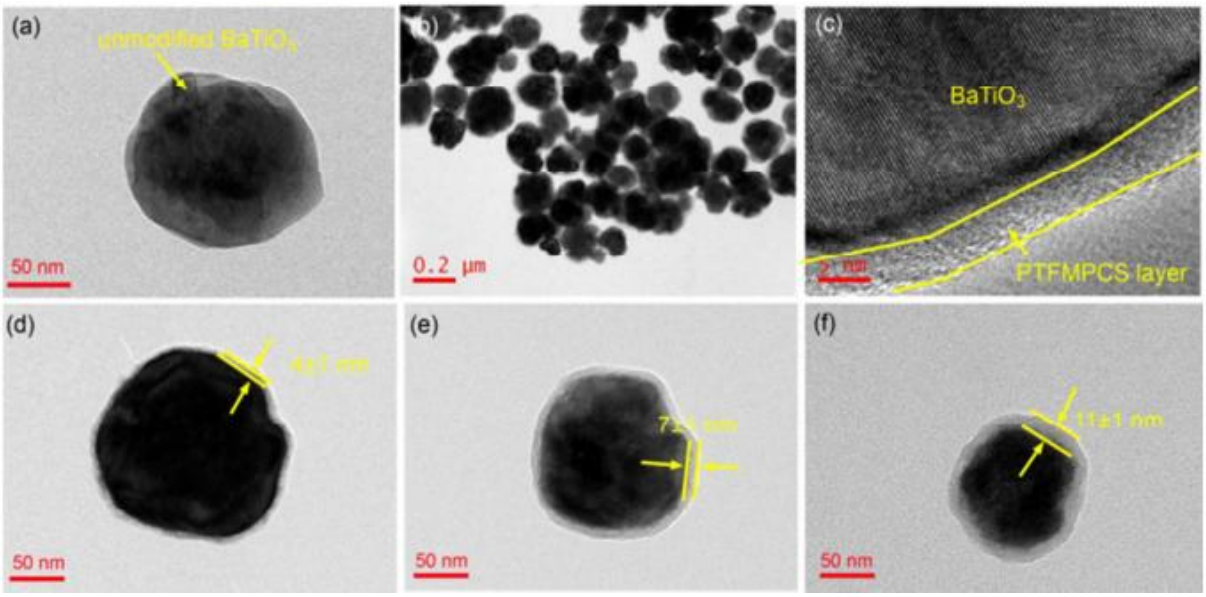

Fig. 18. TEM images of (a) BT-3F0, (b) (c) (d) BT-3F1, (e) BT-3F2, and (f) BT-3F3 functionalized BT nanoparticles via RAFT polymerization of 2,5-bis{[4-trifluoro(methoxyphenyl)oxycarbonyl]styrene}. Reproduced with permission of [86]. Copyright 2018 Royal Society of Chemistry.

IV-2-2-10. P3F, P5F or P7F@BT

Qian *et al.* [117] prepared three kinds of nanocomposites consisting of BT as nanofiller and fluorinated polymers as a matrix using RAFT polymerization (Scheme 6). The three monomers were first synthesized and denoted as poly{2,5-bis[(4-

trifluoro(methoxyphenyl)oxycarbonyl]styrene} (P-3F), poly{2,5-bis[(2,3,4,5,6-pentafluoro) oxycarbonyl]styrene} (P-5F), and poly{2,5-bis[(2,3,5,6-tetrafluoro-4-trifluoromethyl)oxycarbonyl]styrene} (P-7F).

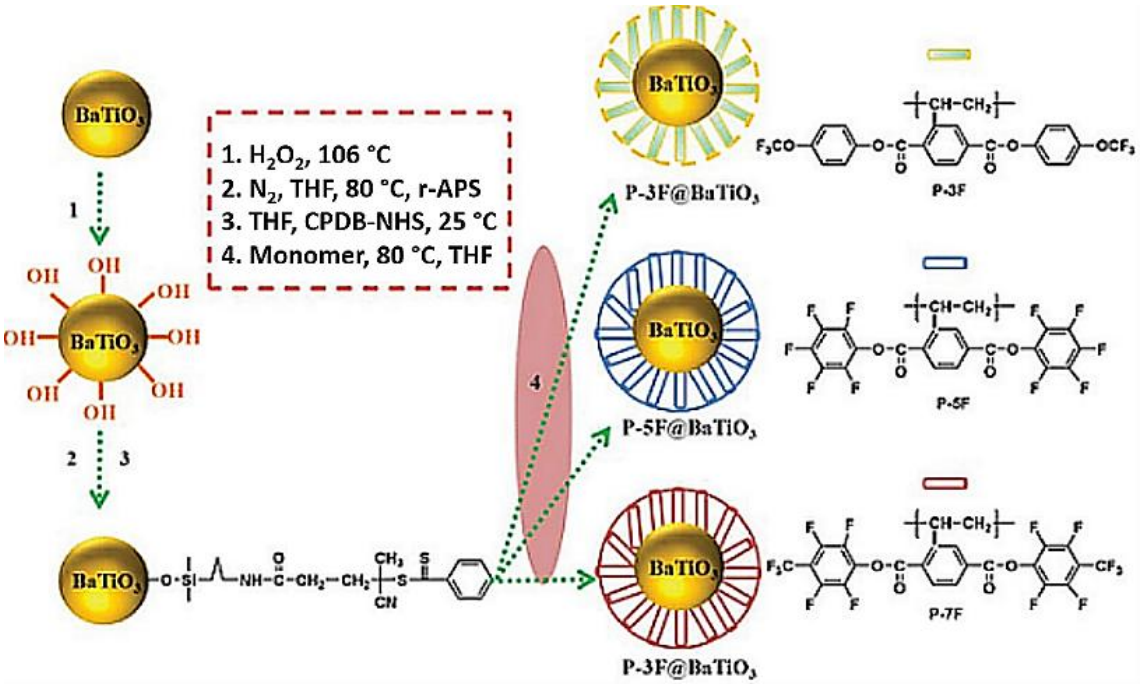

Scheme 6. Synthesis process of fluoropolymer@$BaTiO_3$ nanoparticles starting from $BaTiO_3$ surface functionalization then RAFT polymerization of three kinds of aromatic fluoromonomers. Reproduced with permission of [117]. Copyright 2018 Royal Society of Chemistry.

The functionalized nanoparticles were characterized to evidence the successful surface modification. Fig. 19-A exhibits the TEM images recorded for the nanocomposites and it clearly evidences the dense polymer shell covering the nanoparticles, where the thickness of which was around 7 nm. A mapping pattern images were also achieved on P-3F@BT nanocomposites where the different colors are attributed to Ba, Ti, O and F elements, which indicate that the fluoropolymers were successfully introduced onto the BT surface (Fig. 19-B).

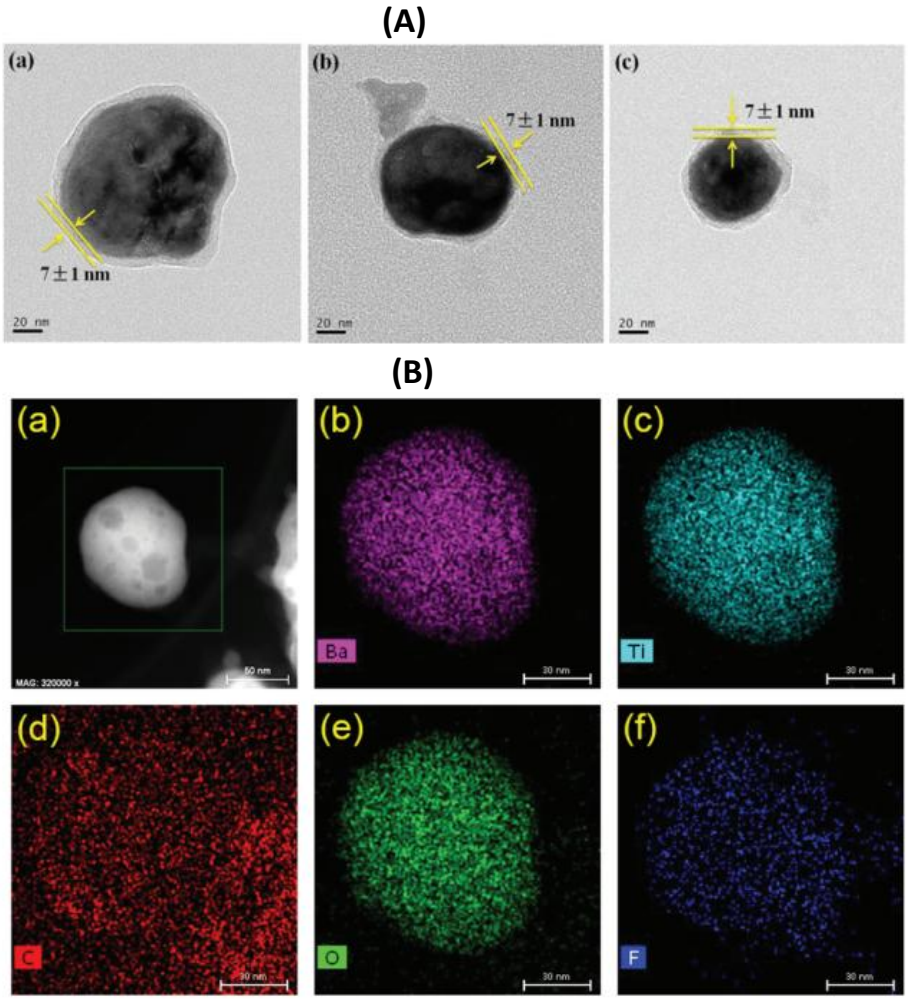

Fig. 19. (A) TEM images of (a) P-3F@ $BaTiO_3$, (b) P-5F@ $BaTiO_3$, and (c) P-7F@$BaTiO_3$ nanoparticles and (B) mapping pattern images of BT nanoparticles modified by P-3F. Reproduced with permission of [117]. Copyright 2018 Royal Society of Chemistry.

IV-2-2-11. PVDF@BT

Bouharras *et al.* [20] prepared a core shell structured nanocomposites using RAFT polymerization (Scheme 7). The first step consists in decorating the BT nanoparticles by xanthate functions, which further enabled to control the radical polymerization of VDF.

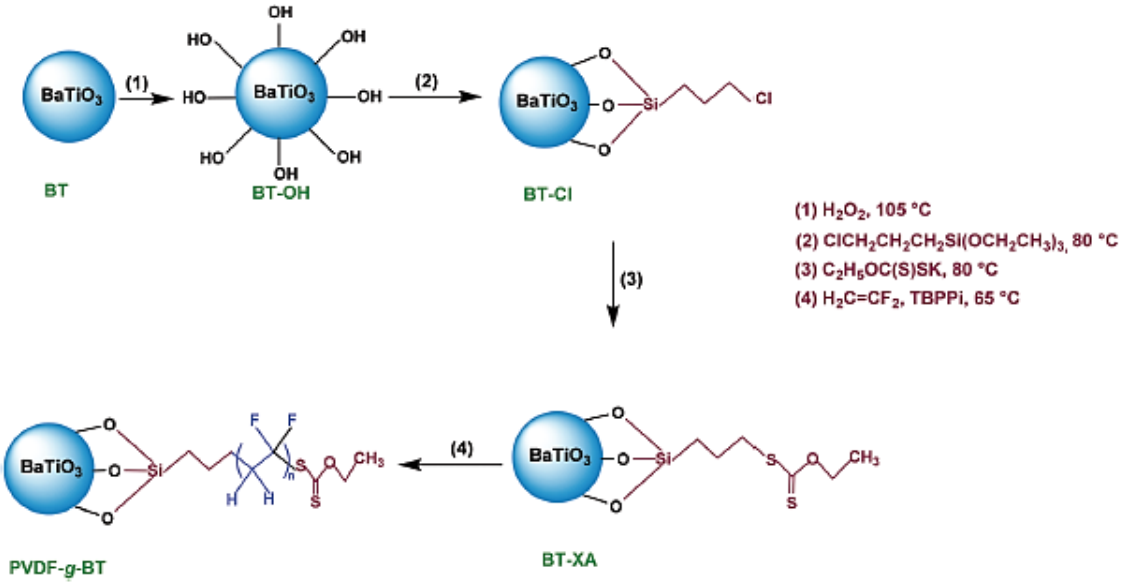

Scheme 7. Sketch illustrating the synthesis process of PVDF@$BaTiO_3$ nanocomposites by RAFT polymerization of VDF in the presence of $BaTiO_3$ nanoparticles bearing xanthates functions (TBPPi stands for *tert*-butyl peroxypivalate). Reproduced with permission of [20]. Copyright 2019 Royal Society of Chemistry.

Four different nanocomposites were synthesized by varying the feed amount of BT (concentration 3-20 wt %) and fully characterized.

Moreover, and for the first time, High Resolution Magic Angle Spinning (HRMAS) NMR was used for the first time to characterize such nanocomposites and enabled to determine the molar masses of PVDF grafted onto BT (Fig. 20). Results give evidences of the successful modification and grafting of PVDF, leading to nanocomposites with enhanced thermal stability.

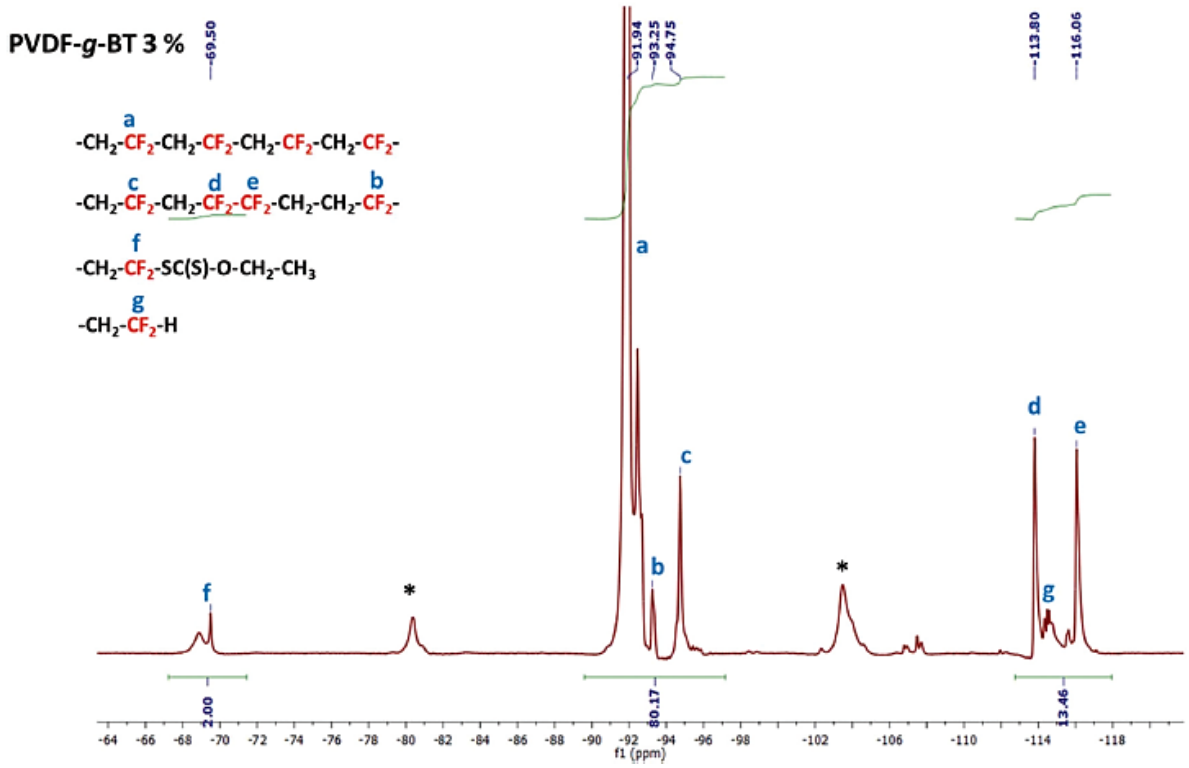

Fig. 20. Expansion of the -64 to -120 ppm region of the ^{19}F HRMAS spectrum recorded in d_6-DMSO of PVDF@$BaTiO_3$ nanocomposite filled with 3 wt % of $BaTiO_3$ (* stands for the spinning bands). Reproduced with permission of [20]. Copyright 2019 Royal Society of Chemistry.

The effect of BT loading on the properties was also studied. The results showed that the higher the BT content, the better the thermostability of the nanocomposites (Fig. 21). In fact, the starting degradation temperature was 91°C for the neat PVDF and reaches 391 °C after adding only 3 wt % of BT.

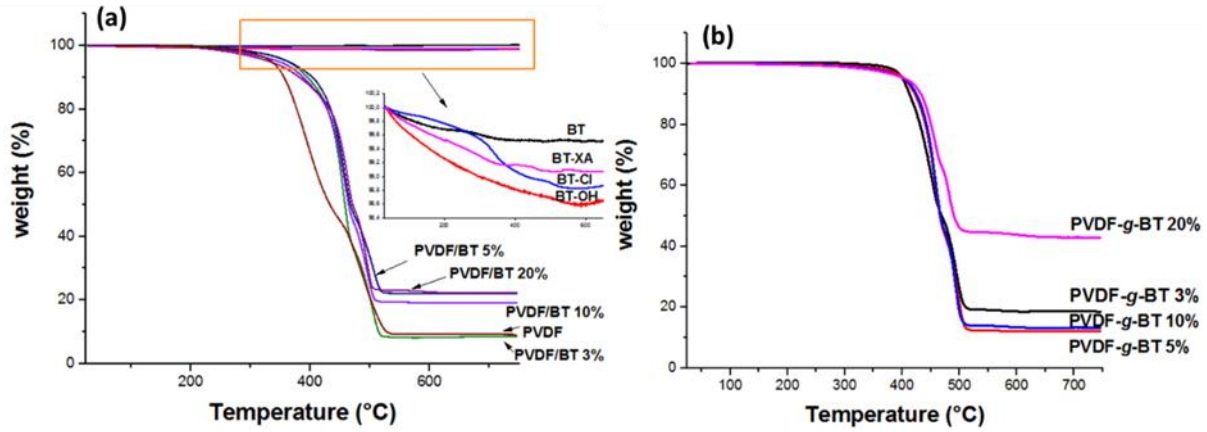

Fig. 21. TGA thermograms (under air) of (a) functionalized $BaTiO_3$ nanoparticles and PVDF@$BaTiO_3$ nanocomposites with different $BaTiO_3$ amount (3, 5, 10 and 20 wt %) after centrifugation but not purified and (b) TGA thermograms of $BaTiO_3$/PVDF nanocomposites after centrifugation but not purified and (b) TGA thermograms of $BaTiO_3$/PVDF nanocomposites after several purifications (PVDF@$BaTiO_3$). Reproduced with permission of [20]. Copyright 2019 Royal Society of Chemistry.

IV-2-2-12. PM7F@BT

Lv *et al.* [118] functionalized BT platelets with a fluoropolymer to improve their dispersion and compatibility in the nanocomposite. The fluoro-monomer (2,5-bis[(2,3,5,6-tetra fluoro-4-trifluoromethyl)oxycarbonyl]styrene, M7F) was first synthesized then grafted onto BT platelets surface by RAFT polymerization.

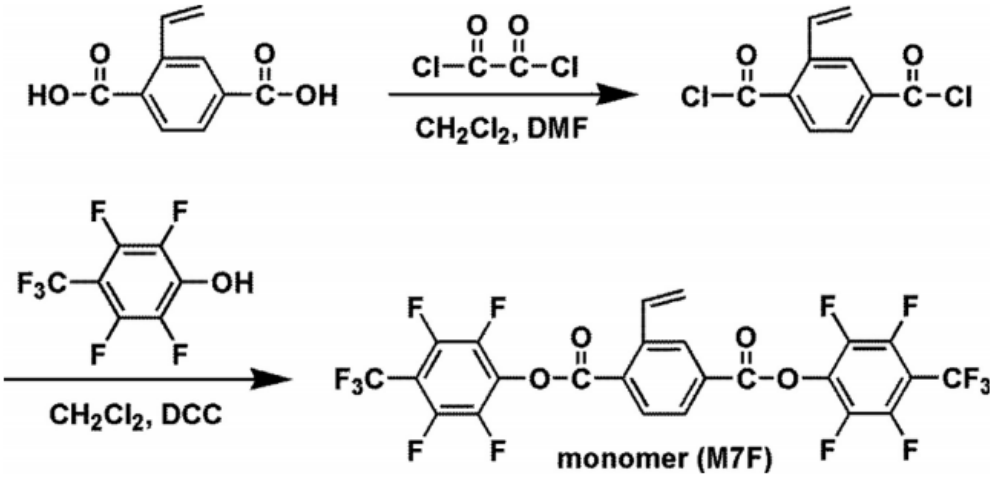

Scheme 8. Synthetic route to M7F styrene. Reproduced with permission of [118]. Copyright 2018 Elsevier.

It was found that the resulting platelets present a uniform morphology and the average thickness was about 1 μm. After immobilization of PM7F onto the functionalized platelets, different characterizations were performed and the results prove the successful grafting of this fluoropolymer onto the functionalized BT. Fig. 22 exhibits TEM images of PM7F@BT nanocomposite, where the polymer layer can be clearly seen and covering BT platelets with a thickness of 12.7 nm. Moreover, the structural unit in the molecular chain of this fluoropolymer contains 14 fluorine atoms, resulting in a decreased surface energy of BT platelets.

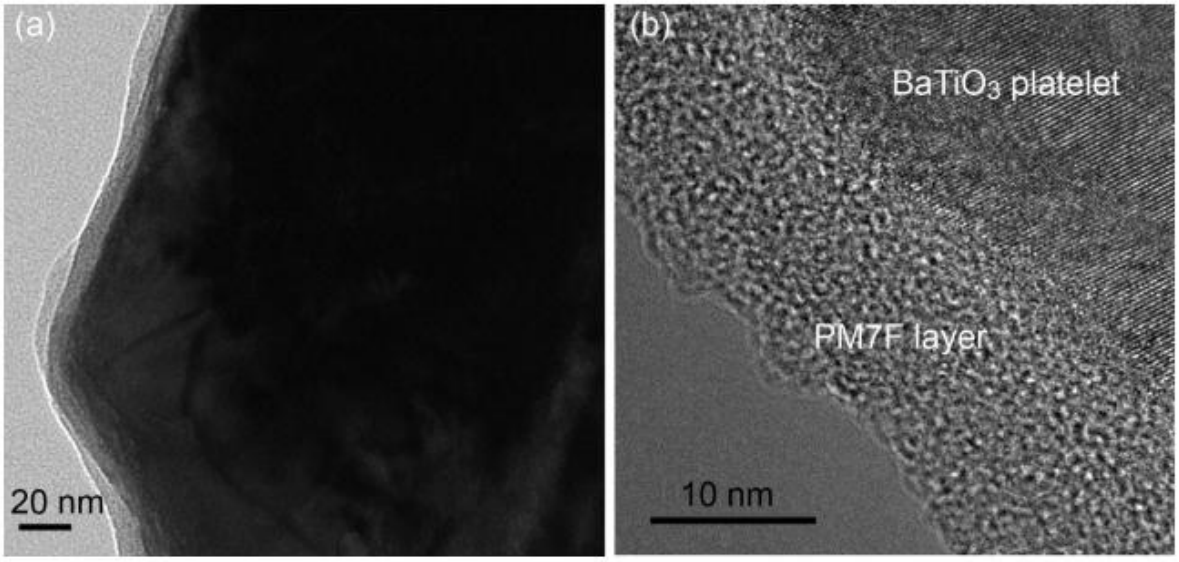

Fig. 22. (a) TEM image and (b) high-resolution TEM image of $BaTiO_3$-PM7F. Reproduced with permission of [118]. Copyright 2018 Elsevier.

IV-2-3. Modification of $BaTiO_3$ with polymer to prepared by "Grafting onto" route

IV-2-3-1. PS or PMMA@BT

Using the "grafting onto" technique, Yang *et al.* [119] reported another approach to functionalize BT nanoparticles with polymer in order to prepare nanocomposites made by either PS or PMMA. In a first step, RAFT polymerization enabled to synthesize thiol-terminated PS and PMMA. Then, three nanocomposites were obtained with different molar masses by means of thiol-ene click reaction between the functionalized nanoparticles by alkyl methacrylates and ω-thiol polymers (Fig. 23). Dielectric measurements revealed that the dielectric constant of the synthesized nanocomposites were significantly enhanced in comparison to the pure polymers (3.69 for PMMA and 2.74 for PS at 1 kHz).

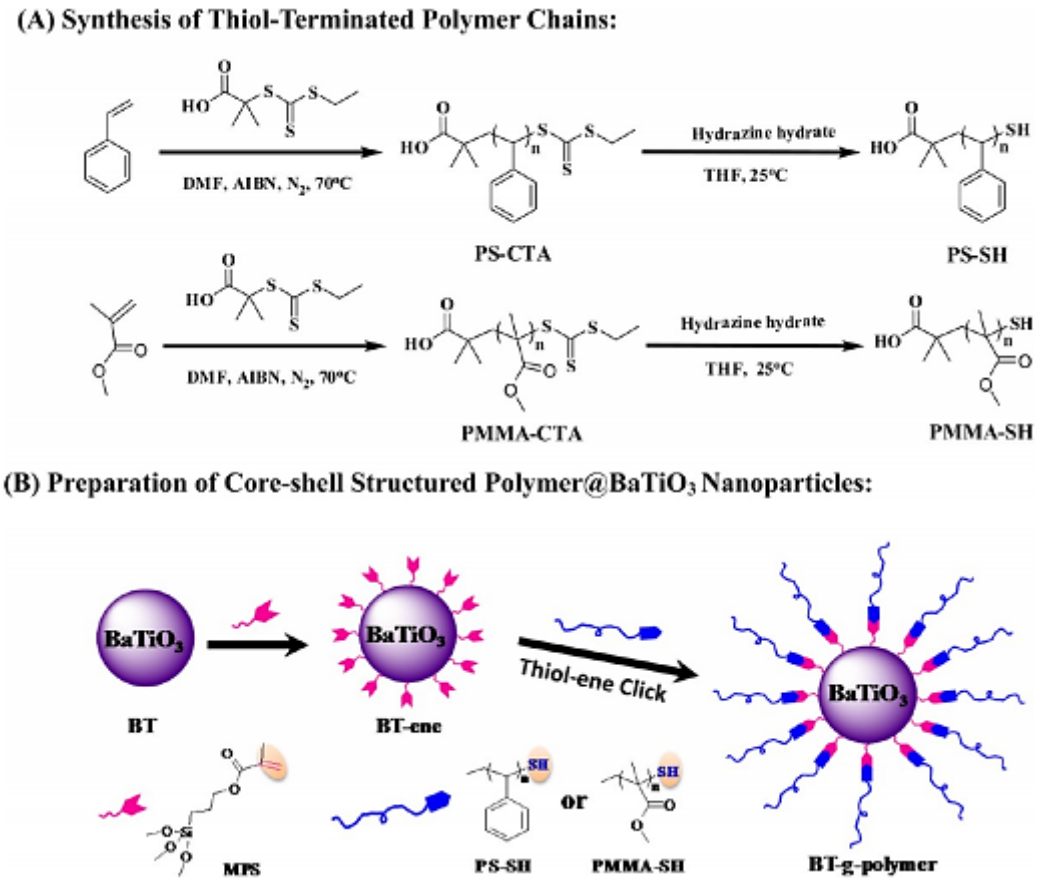

Fig. 23. Schematic Illustration for (A) Synthesis of thiol-terminated Polymer Chains via RAFT polymerization and (B) Preparation of Core−Shell Structured Polymer@$BaTiO_3$ Nanocomposites by Thiol−Ene Click Reaction with modified $BaTiO_3$. Reproduced with permission of [119]. Copyright 2014 American Chemical Society.

IV-2-3-2. PS or PVDF@BT

Ma *et al.* [85] used thiol-terminated PVDF (PVDF-SH) and polystyrene (PS-SH) to functionalize BT surface. PVDF-SH and PS-SH were synthesized in a two step process, starting from a RAFT polymerization, followed by the aminolysis as depicted in Fig. 24-a. The as prepared polymers were used to functionalize BT-ene nanoparticles using thiol-ene click reaction (Fig. 24-b).

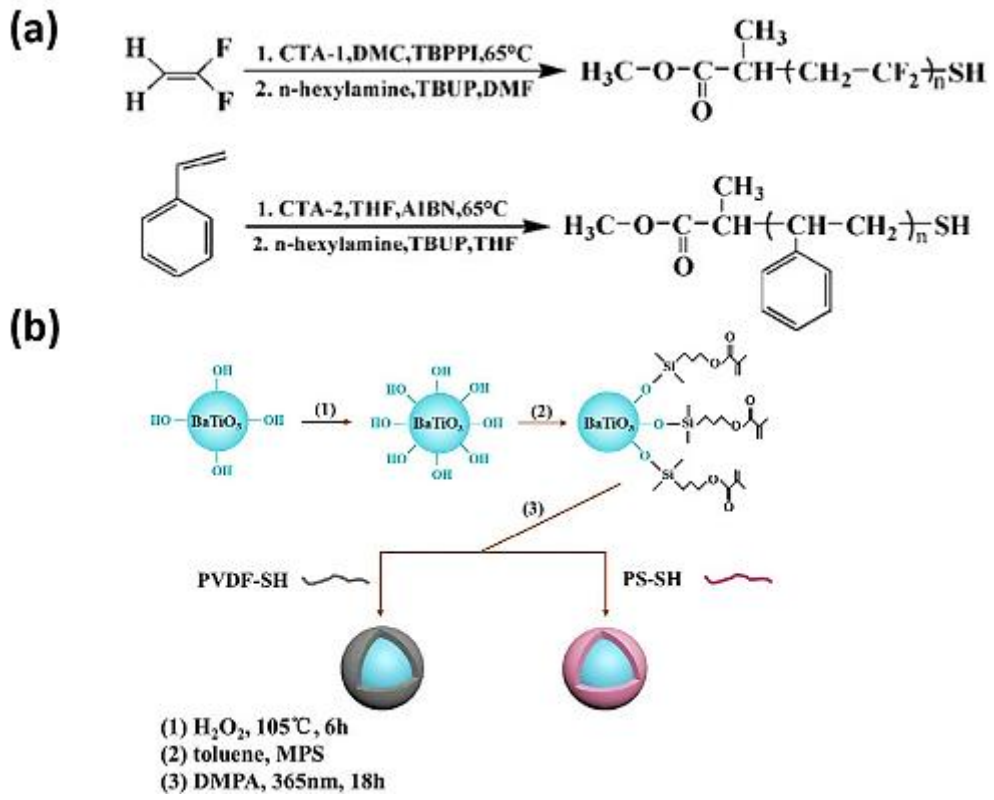

Fig. 24. (a) Synthesis process for the preparation of thiol-terminated polymers (CTA-1 refers to O-Ethyl-S-(1-methoxycarbonyl)ethyldithiocarbonate and CTA-2 stands for 2-([(dodecylsulfanyl)carbonothioyl]sulfanyl)-propanoic acid) and (b) Schematic diagram of the modification process of hybrid nanoparticles. Reproduced with permission of [85]. Copyright 2019 Elsevier.

The functionalized nanoparticles and the synthesized nanocomposites were fully characterized to give evidences on the successful surface modification and grafting of polymers. In addition, the TEM images of PS@BT and PVDF@BT nanocomposites highlight the nanoparticles surrounding by a thin polymer shell with a thickness of ~ 6 nm (Fig. 25).

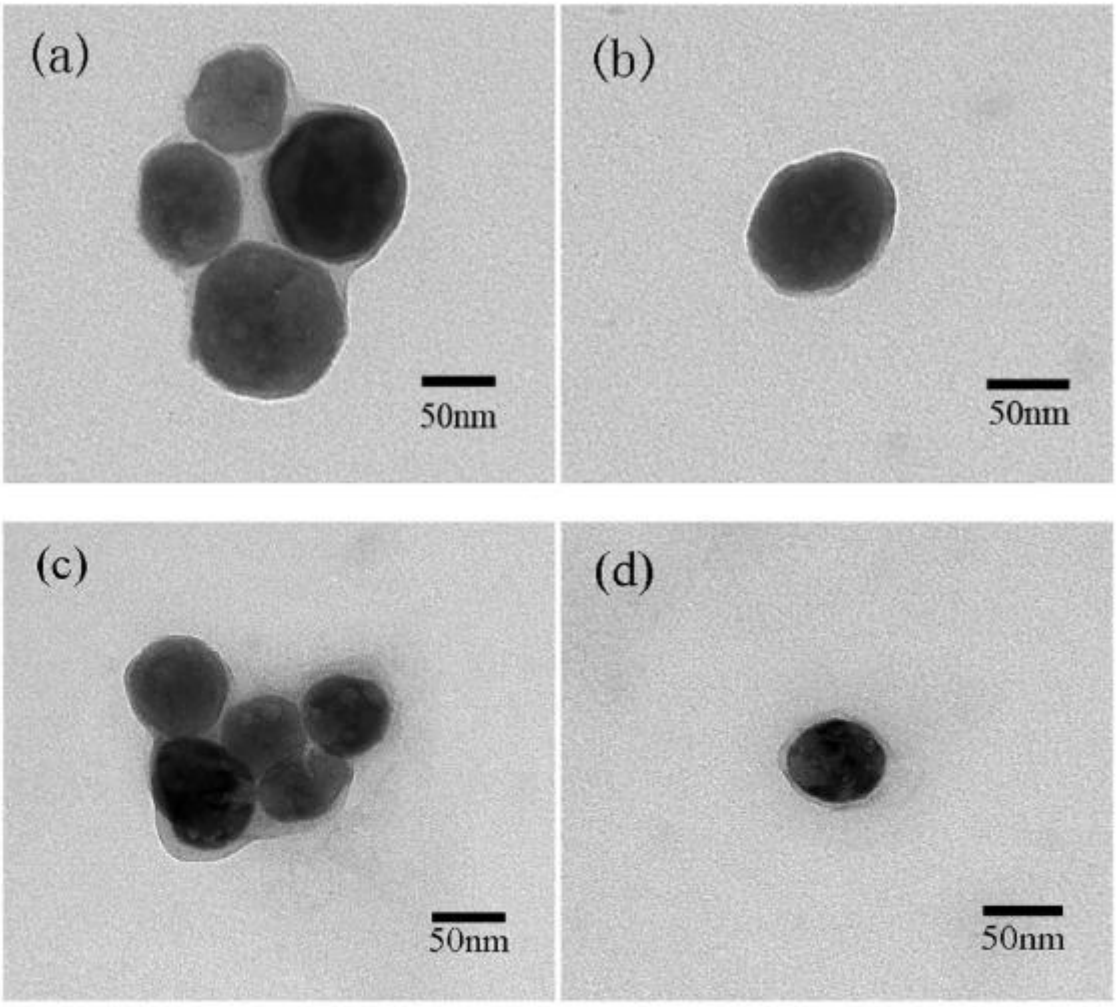

Fig. 25. TEM images of PVDF@BT (a, b) and PS@BT (c, d) nanocomposites synthesized by thiol-ene click reaction. Reproduced with permission of [85]. Copyright 2019 Elsevier.

IV-2-3-3. P(VDF-HFP-GMA)@BT

Xie *et al.* [88] modified BT surface using commercially available poly(VDF-*co*-HFP) functionalized with PGMA by ATRP polymerization. BT nanoparticles were first modified by amino-terminated silane molecules, then, the nanocomposites were prepared by a solution blending method leading to a covalent bond between the epoxy groups of GMA and amino groups at the surface of modified BT nanoparticles.

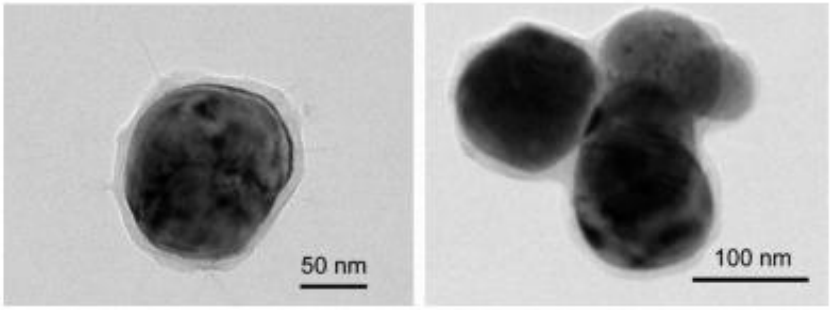

Fig. 26. TEM images of the washed PVDF-HFP-GMA grafted BT nanoparticles showing a PVDF-HFP-GMA layer of about 10 nm. Reproduced with permission of [88]. Copyright 2014 Royal Society of Chemistry.

To prove the successful grafting of the polymer chains onto the nanoparticles surfaces, the as-prepared nanocomposites were re-dissolved in DMF and washed several times in order to remove the free polymer chains. After purification, TEM analysis evidences that BT nanoparticles were coated by a polymer layer, ensuring the successful grafting of PVDF-HFP-GMA onto BT surface (Fig. 26).

IV.3. Design of core-shell $BaTiO_3$@polymer/Fluorinated polymer nanocomposites

Recent reviews have summarized the synthesis of $BaTiO_3$, its surface modification, and their introduction into polymer matrix to get dielectric nanocomposites [120,121]. A detailed review on ferroelectric polymers was also reported by Prateek *et al.* [78]; especially the use of PVDF and its VDF-based copolymer blends in dielectric composites materials for high energy capacitor applications. Regarding the importance of these fluoropolymers and their role in enhancing the final properties of the nanocomposite, further studies are moving toward the elaboration of nanocomposites consisting of a single core and a polymer double shell to get better properties. Herein, we discuss the system based on $BaTiO_3$ nanocomposites modified with a second shell based on a fluorinated polymer according to Scheme 1-b.

IV-3-1. PMMA@BT/poly(VDF-*co*-HFP)

Wang *et al.* [112] prepared three phase poly(VDF-*co*-HFP)/BTO@TMPc-PMMA nanocomposite films. First, BT nanoparticles were modified by ATRP polymerization of MMA (See section IV-2-2-1). Then, poly(VDF-*co*-HFP)/BTO@TMPc-PMMA nanocomposites were obtained by a simple mixing of poly(VDF-*co*-HFP) copolymer with the functionalized nanoparticles (Fig. 27).

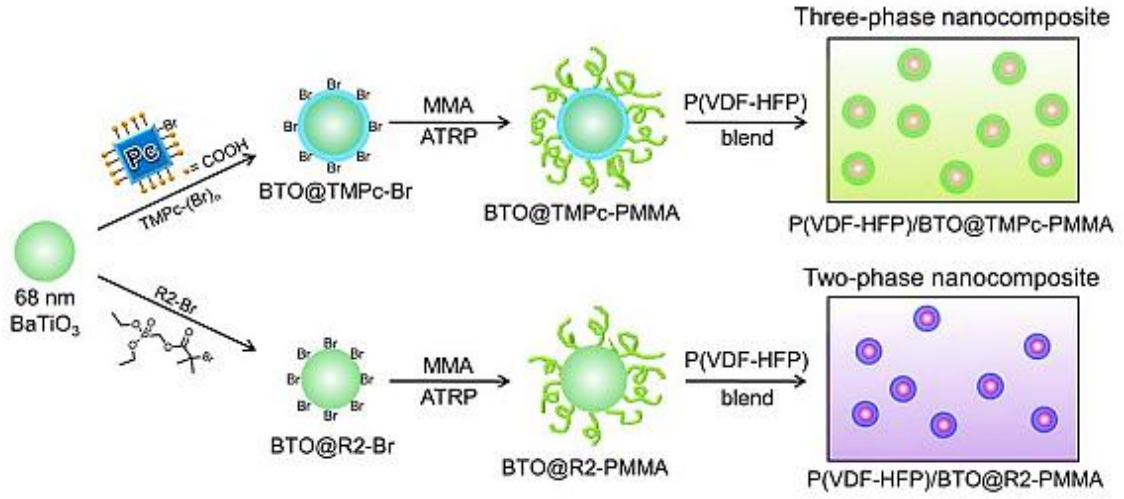

Fig. 27. Schematic illustration of the preparation of three- and two-phase poly(VDF-*co*-HFP)/$BaTiO_3$ nanocomposites, respectively. Reproduced with permission of [112]. Copyright 2014 Wiley.

Dielectric measurements on the synthesized nanocomposites indicated that the dielectric constant (ε_r) slightly decreased when the frequency increased (Fig. 28). In the case of the three-phase composite films, the introduction of the highly polarizable TMPc improved the permittivity significantly, in comparison with the two phase-composite films. Moreover, the dielectric loss (tan δ) was found to be relatively low (tan δ = 0.02 below 2 kHz) and overlapped with that of the neat poly(VDF-*co*-HFP) copolymer, which indicates that BT nanoparticles did not add additional loss to the system. However, the increase of tan δ at ca. 10^7 MHz could be attributed to the relaxation phenomenon of the amorphous poly(VDF-*co*-HFP).

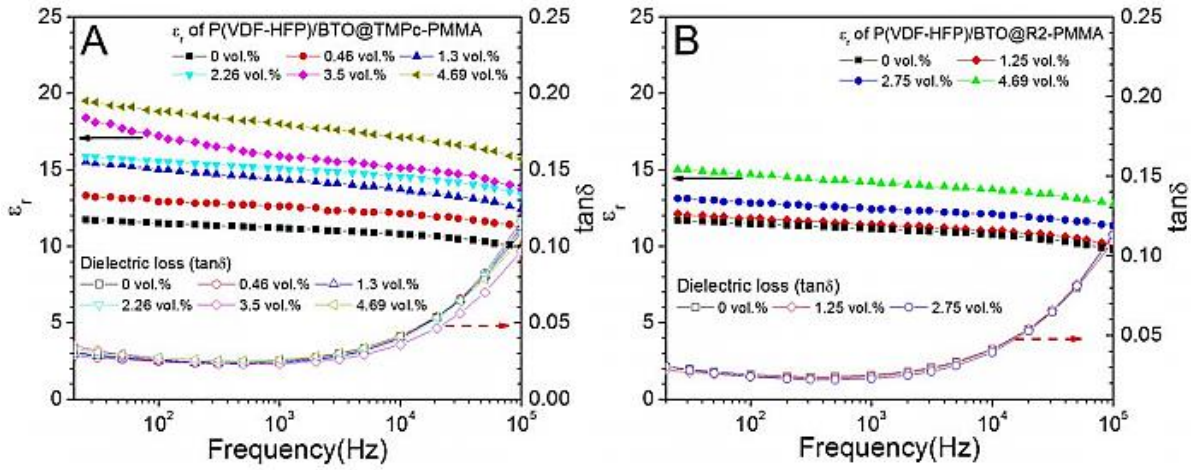

Fig. 28. Relative dielectric constant (ε_r) and dielectric loss (tan δ) as a function of frequency for (A) uniaxially stretched poly(VDF-*co*-HFP)/BTO@TMPc-PMMA and (B) uniaxially stretched poly(VDF-*co*-HFP)/BTO@R2-PMMA nanocomposite films, respectively. Reproduced with permission of [112]. Copyright 2014 Wiley.

IV-3-2. PTFEMA@BT or PMMA@BT/PVDF

Zhang *et al.* [113] prepared core shell structured BT nanoparticles with two different shell compositions and thicknesses (7 and 12 nm for PMMA@BT and 4.5 and 5.5 nm for PTFEMA@BT) by grafting PMMA and PTFEMA via ATRP polymerization (Section IV-2-2-2). Then, the resulting nanocomposites were incorporated into PVDF matrix by solution blending (Scheme 9).

Authors reported that higher dielectric constant and lower dielectric loss were achieved for both systems in comparison to those of pure PVDF. For example, after adding 80 wt % of PMMA@BT in the PVDF matrix, the dielectric permittivity increased from 6 to 30 at 100 Hz. Moreover, nanocomposites obtained by modification of BT with the fluorinated polymer (PTFEMA) led to lower dielectric loss (0.025 at 100 kHz) and high dielectric constant in comparison to those modified with PMMA (0.022 at 100 kHz). That was explained by the strong interchain forces between the two fluorinated shells matrix.

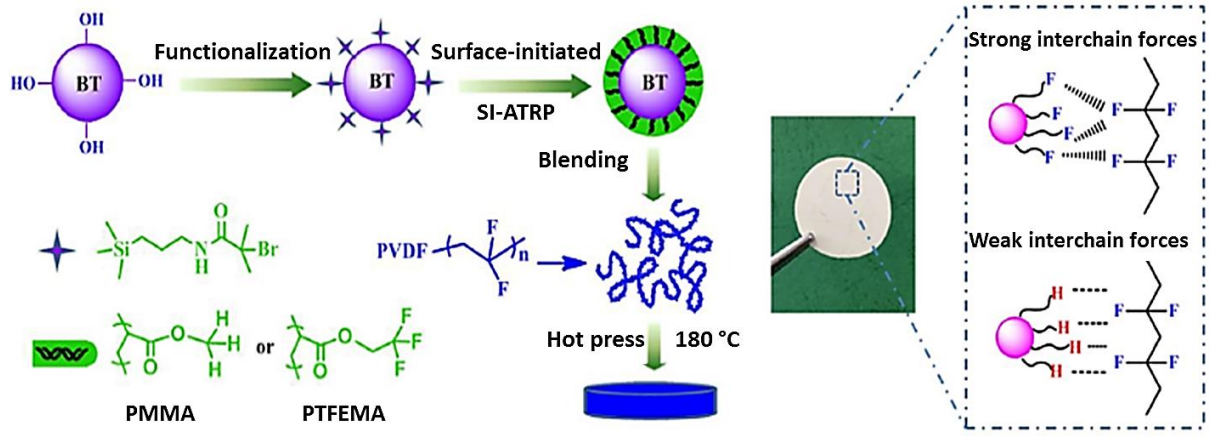

Scheme 9. Illustration for the preparation of BT@polymer/PVDF nanocomposite films. Reproduced with permission of [113]. Copyright 2017 Elsevier.

IV-3-3. Poly(*tert*-butyl-methacrylate) @BT/PVDF

Du *et al.* [115] used P*t*BA to functionalize BT surface by ATRP polymerization (See section IV-2-2-4). Then, the modified nanoparticles were mixed into a PVDF matrix. Results showed that the dielectric constant of the nanocomposites increased by increasing the P*t*BA@BT content from 8.5 for the pure PVDF to 15 for nanocomposite with 30 wt % of functionalized nanoparticles (Fig. 29).

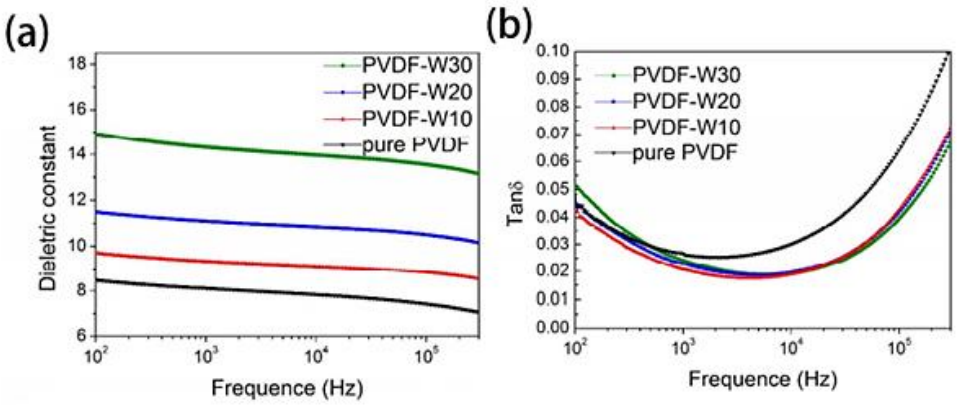

Fig. 29. Frequency dependence of room temperature a) dielectric constant and b) loss tangent for PVDF-based films. Reproduced with permission of [115]. Copyright 2018 American Chemical Society.

In order to be able to note the effect of P*t*BA polymer, films of PVDF based on non-functionalized BT were prepared. The dielectric measurements of PVDF/BT nanocomposites show low dielectric permittivities in comparison to those of P*t*BA@BT/PVDF (the dielectric constant at 100 Hz was 14.5 for PVDF/BT and was enhanced to 15 for PVDF-W30) (Fig. 30). This can be attributed to the fact that the non-treated nanoparticles tends to form aggregates and leads to poor dispersion in the polymer matrix which results in decreased performances.

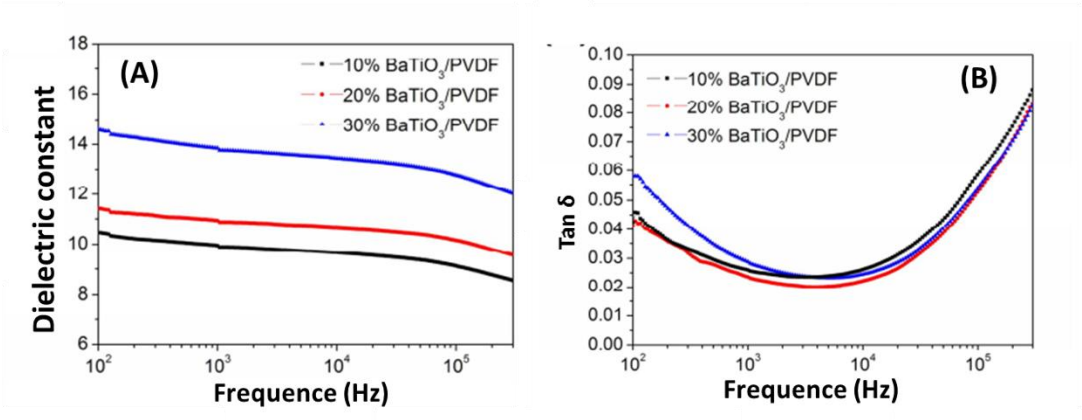

Fig. 30. Frequency dependence of room temperature (a) dielectric constant and (b) loss tangent for $BaTiO_3$/PVDF films. Reproduced with permission of [115]. Copyright 2018 American Chemical Society.

Moreover, the functionalization of BT nanofillers with P*t*BA not only avoids aggregation of the nanoparticles inside the PVDF matrix, but also preserves excellent mechanical properties of the polymer, which leads to good flexibility and integrated surface micromorphology.

IV-3-4. (PMMA or PHEMA or PGMA)@BT/PVDF

Zhu *et al.* [73] prepared three kinds of polymer nanocomposites using core shell structured polymer@BT nanoparticles as filler and PVDF as the polymer matrix.

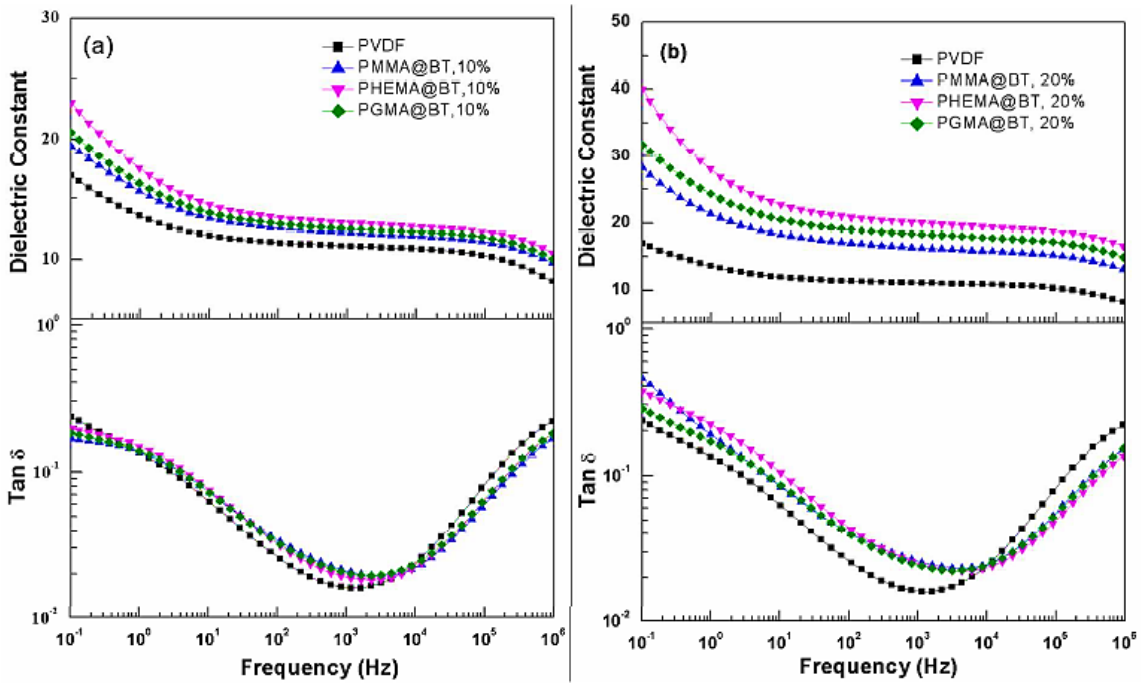

Fig. 31. Frequency dependence of dielectric constant and dielectric loss tangent of the polymer@BT based PVDF nanocomposites (a) 10 vol % BT and (b) 20 vol % BT. Reproduced with permission of [73]. Copyright 2014 American Chemical Society.

The first core shell nanocomposite was synthesized using RAFT polymerizations of MMA, GMA and HEMA from functionalized nanoparticles (See section IV-2-2-7). Then, a second shell of PVDF was introduced by a simple blending and hot pressing of the nanocomposite. Dielectric measurements revealed that, compared with the PVDF matrix, all the nanocomposites displayed enhanced dielectric constant and follows the order PHEMA@BT/PVDF (~21 at 10^2 Hz) > PGMA@BT/PVDF (~18 at 10^2 Hz) > PMMA@BT/PVDF (~16 at 10^2 Hz) (Fig. 31). This indicates that, at the same BT content, the dielectric constant of the resulting nanocomposite is determined by the dielectric constant of the interfacial region. Thus, nanocomposite processed from BT functionalized with PHEMA exhibits the highest permittivity due the large dipole moment of the pendant hydroxyethyl groups.

IV-3-5. PHFDA@BT or PTFEA@BT /poly(VDF-*co*-HFP)

Yang *et al.* [27] used two types of poly(fluoroacrylate) to functionalize BT surface by RAFT polymerization (See section IV-2-2-8) before introducing them into poly(VDF-*co*-HFP) polymer matrix using a solution blending method.

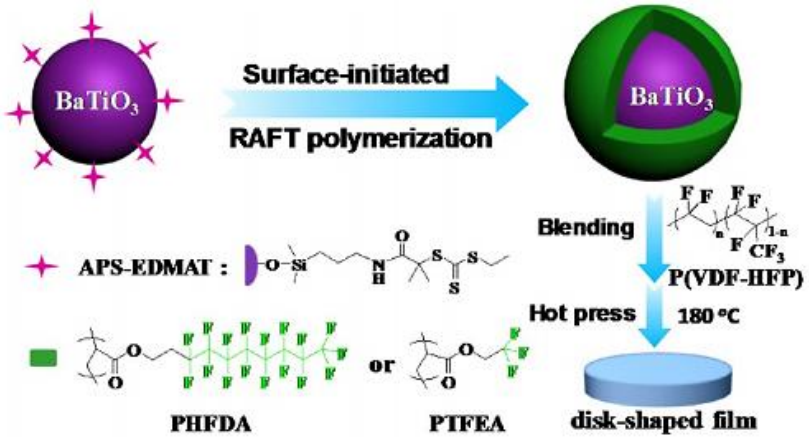

Scheme 10. Preparation of fluoro-polymer@$BaTiO_3$ nanoparticles and poly(VDF-*co*-HFP) nanocomposite films. Reproduced with permission of [27]. Copyright 2013 American chemical Society.

Actually, the functionalization of BT with poly(fluoroacrylate) not only led to enhanced energy storage capability of poly(VDF-*co*-HFP)/Fluoropolymer@BT nanocomposite in comparison with the pure copolymer, but also improved the dielectric properties. For instance, the energy density of the prepared nanocomposites was 5 times higher than that of the pure poly(VDF-*co*-HFP) under an electric field of 20 kV mm^{-1} , while the theoretical maximum energy density was 6.23 J cm^{-3}, which is 50% higher than that of the pure poly(VDF-*co*-HFP) (~4.10 J cm^{-3}).

IV-3-6. PTFMPCS@BT / poly(VDF-*ter*-TrFE- *ter*-CTFE)

Chen *et al*. [86] used a rigid poly(fluorostyrene) to functionalize BT surface by RAFT polymerization of 2,5-bis{(4-trifluoromethoxyphenyl)oxycarbonyl}styrene with three different shell thicknesses (where BT-3F0 stand for pristine BT and BT-3F1, BT-3F2 and BT-3F3 nanocomposites present shell thicknesses of 4, 7 and 11 nm, respectively) (See Section IV-2-2-9). The as prepared core shell structured nanoparticles were then incorporated into poly(VDF-*ter*-TrFE-*ter*-CTFE) *ter*-polymer matrix by varying their amount from 5 to 30 vol%. Morphological analysis showed the absence of pore and defects in the prepared nanocomposite films, which indicate that the functionalization of BT with fluoropolymer provides a strong interchain forces with the poly(VDF-*ter*-TrFE-*ter*-CTFE) host matrix. Fig. 32 exhibits the dielectric permittivity and dielectric loss of the BT@Fluoropolymer/poly(VDF-t*er*-TrFE-*ter*-

CTFE) nanocomposites films. For instance, the dielectric permittivity of poly(VDF-*ter*-TrFE-*ter*-CTFE) matrix was ~ 40 (at 1 kHz) and after introducing 30 vol% of BT-3F1 into poly(VDF-*ter*-TrFE-*ter*-CTFE) matrix, the dielectric permittivity increased from 40 to 80.6 (at 1 kHz). Moreover, by increasing the shell thickness of the nanoparticles (BT-3F3), and for the same filler loading, the dielectric permittivity decreased to ~ 60 (at 1 kHz). The results highlight that the dielectric behavior was significantly affected by the shell thickness and the permittivity of the nanocomposites films increased with the increase of BT@Fluoropolymer nanoparticles content.

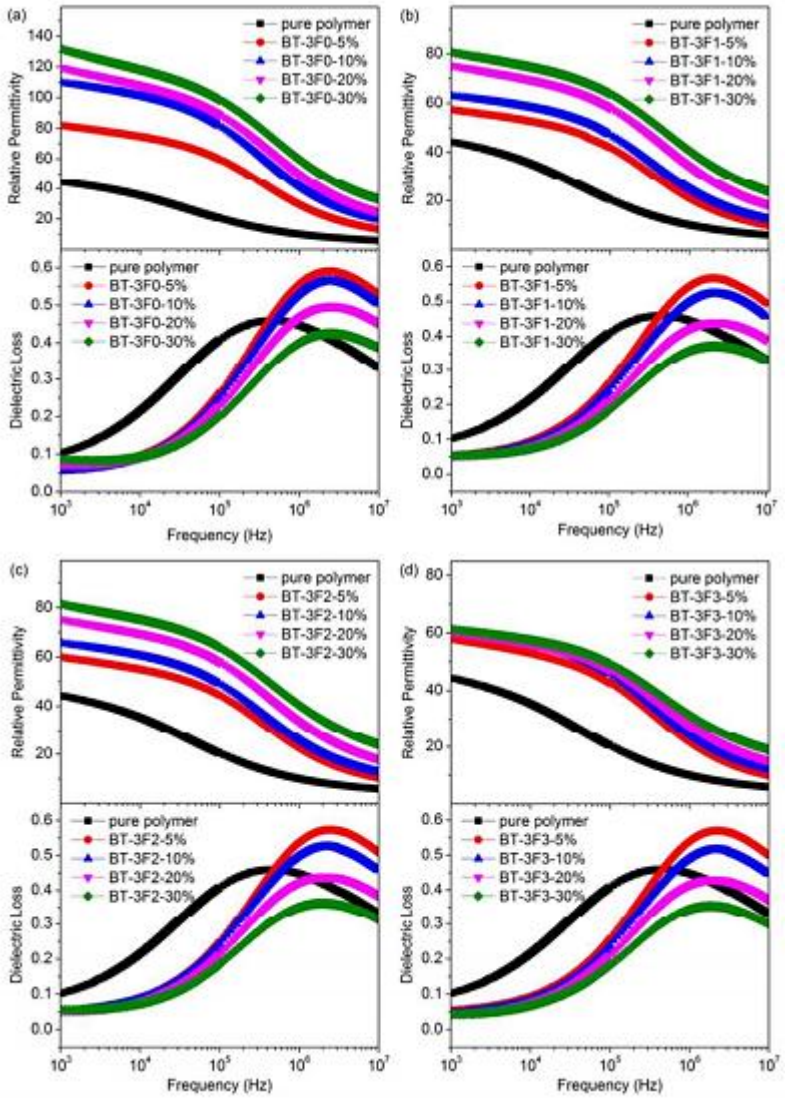

Fig. 32. Frequency dependence of permittivity and dielectric loss of the $BaTiO_3$@rigid-fluoro-polymer/poly(VDF-*ter*-TrFE-*ter*-CTFE) nanocomposites films

with (a) BT-3F0, (b) BT-3F1, (c) BT-3F2, and (d) BT-3F3. Reproduced with permission of [86]. Copyright 2018 Royal Society of Chemistry.

IV-3-7. PM7F@BT/ poly(VDF-*ter*-TrFE- *ter*-CTFE)

Lv *et al*. [118] modified BT surface using a fluoropolymer that contains 14 fluorine atoms by RAFT polymerization of {2,5-bis[(2,3,5,6-tetra fluoro-4-trifluoromethyl)oxycarbonyl]styrene} (Section IV-2-2-12). Then, the functionalized nanoparticles were introduced into poly(VDF-*ter*-TrFE-*ter*-CTFE) host matrix (Scheme 11).

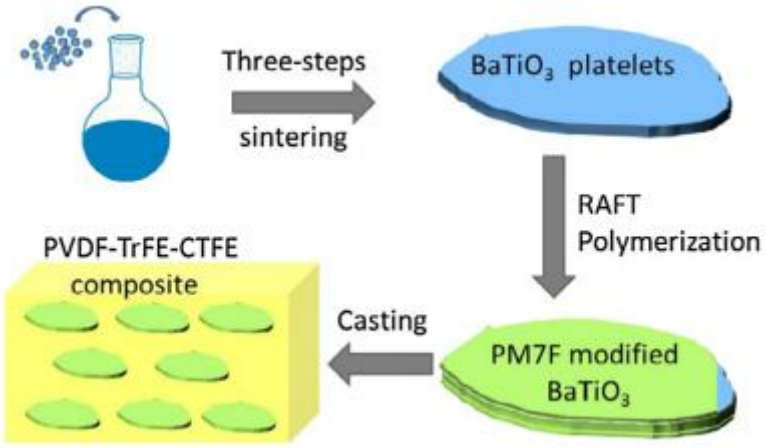

Scheme 11. Schematic illustration of $BaTiO_3$-PM7F/poly(VDF-*ter*-TrFE-*ter*-CTFE) nanocomposite films. Reproduced with permission of [118]. Copyright 2018 Elsevier.

Dielectric measurements revealed that the relative permittivity increased by increasing BT platelets volume fraction with a relatively small loading (Fig. 33). At 1 kHz, the permittivity of nanocomposite with only 5 vol% of modified platelets was ~ 70 in comparison to the pure polymer that presents 45 and the enhancement in permittivity is more significant with increasing BT platelets volume fraction.

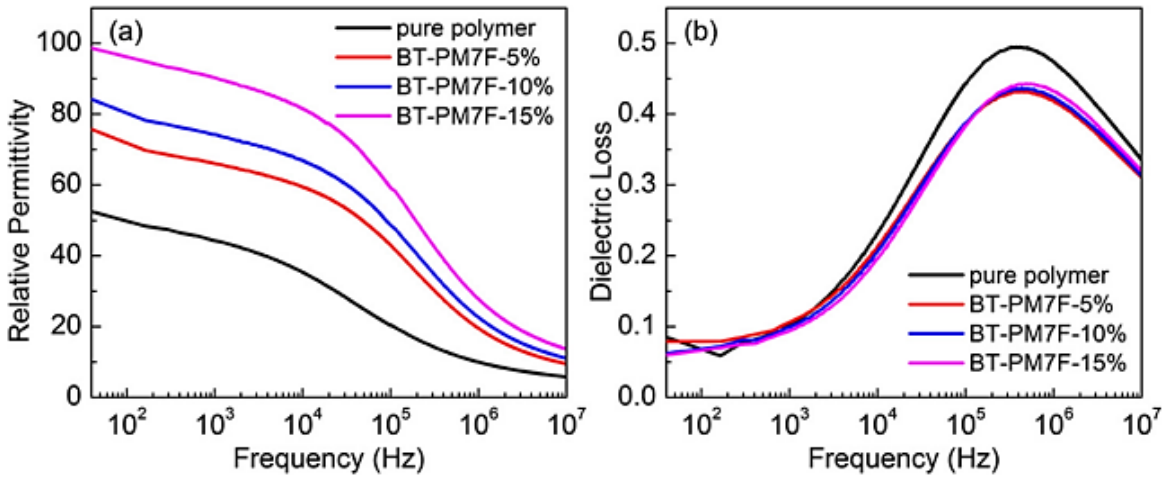

Fig. 33. Frequency dependence of (a) permittivities and (b) dielectric loss for $BaTiO_3$-PM7F/poly(VDF-*ter*-TrFE-*ter*-CTFE) nanocomposites. Reproduced with permission of [118]. Copyright 2018 Elsevier.

IV-3-8. P3F@BT or P5F@BT/ poly(VDF-*ter*-TrFE- *ter*-CTFE)

Qian *et al*. [117] prepared three kinds of nanocomposites consisting on BT nanoparticles and poly(VDF-*ter*-TrFE-*ter*-CTFE) polymer matrix. These nanoparticles were first modified with three types of fluoropolymers denoted as P-nF (n = 3, 5 or 7, is the number of terminal fluorinated groups), (Section IV-2-2-10). Fig. 34 exhibits the frequency dependence of permittivity of the poly(VDF-*ter*-TrFE-*ter*-CTFE)-based nanocomposites with different loading of functionalized BT nanoparticles. It can be seen that the permittivity of the nanocomposites increased by increasing the volume fraction of modified BT nanoparticles. For instance, in the case of P-3F@$BaTiO_3$/poly(VDF-*ter*-TrFE-*ter*-CTFE) nanocomposites, the permittivity increased from 55.4 to 88.5 at 1 kHz when the volume fraction of the modified BT nanoparticles was changed from 5% to 30%. On the other hand, when the BT surface was modified with P-7F polymers, the resulting nanocomposites exhibited the lowest permittivities (~ 67 at 30 % of modified BT). This was explained by the good dispersion of BT nanoparticles and the increase of interfacial adhesion between the modified nanoparticles and the polymer matrix, leading to limitation in the movement of molecular dipoles of the polymer matrix.

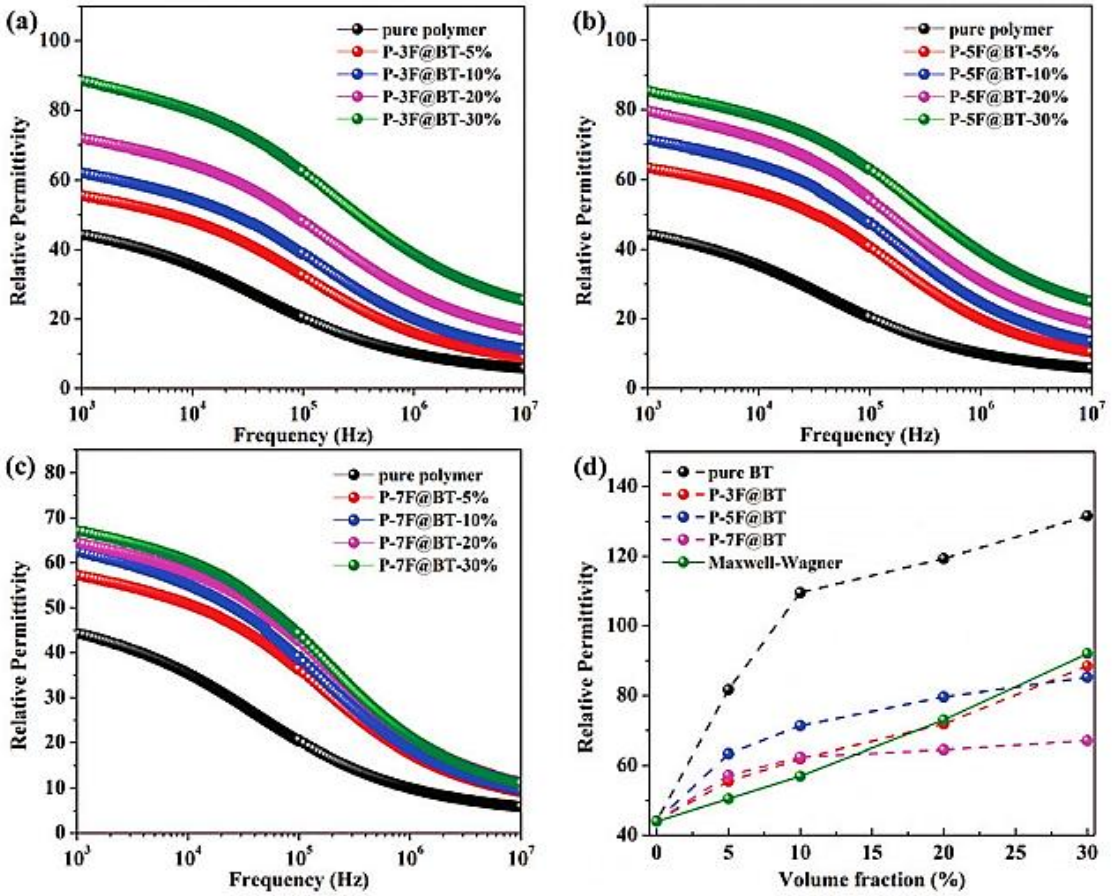

Fig. 34. Frequency dependence of permittivity of the P-nF@BT/P (VDF-TrFE-CTFE) nanocomposite films with (a) P-3F@$BaTiO_3$, (b) P-5F@$BaTiO_3$, and (c) P-7F@$BaTiO_3$. (d) Comparison of the relative permittivity (at 1 kHz) of the nanocomposite with the Maxwell–Wagner model. The permittivity of 100 nm $BaTiO_3$ particles is around 1700. Reproduced with permission of [117]. Copyright 2018 Royal Society of Chemistry.

IV-3-9. PVDF@BT or PS@BT/PVDF

Ma *et al.* [85] reported two kinds of polymer@BT nanoparticles used as composite fillers in PVDF matrix (Scheme 12). First, PS@BT and PVDF@BT were synthesized by thiol-ene reaction (Section IV-2-3-2). Then, a second shell of PVDF was introduced by simple casting and hot pressing. The dielectric properties and the electric breakdown strength of both PVDF@BT/PVDF and PS@BT/PVDF nanocomposites exhibit an enhancement compared to the pure polymer. For example, the permittivity of PS@BT/PVDF nanocomposites increased from 9.2 for the pure PVDF to 23.6 for

nanocomposites filled with 30 vol% of PS@BT. Moreover, the authors revealed that PVDF@BT had a better interfacial interaction with PVDF matrix than that of PS@BT fillers, and this is due to the fact that the shell of the fillers has the same structure as that of the polymer matrix.

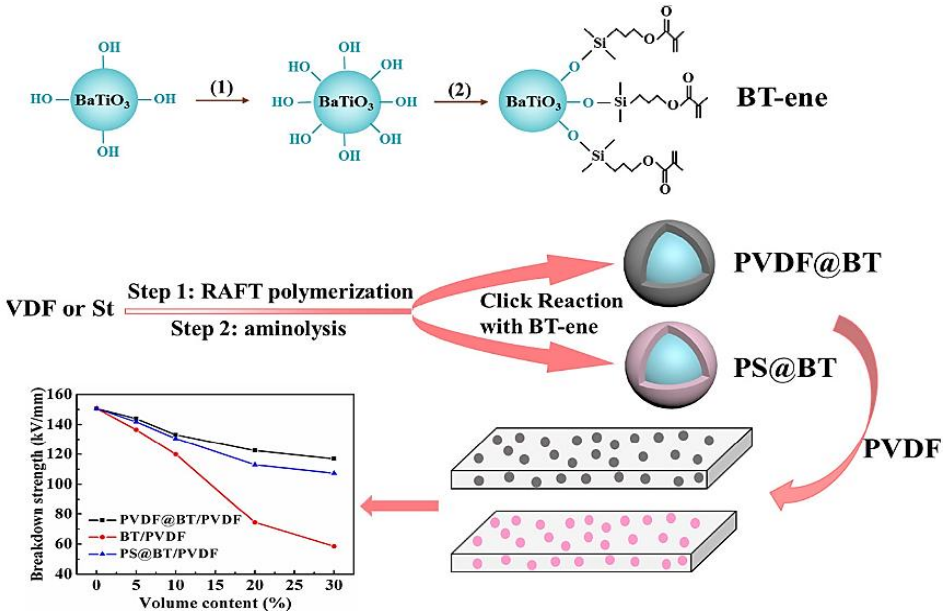

Scheme 12. Schematic illustration of the synthetic process of the core@double shell nanocomposites (PS@BT/PVDF or PVDF@BT/PVDF). Reproduced with permission of [85]. Copyright 2019 Elsevier.

IV-3-10. HBP@BT/poly(VDF-*ter*-TrFE-*ter*-CFE)

Xie *et al.* [122] used hyperbranched aromatic polyamide (HBP) to decorate BT surface using a polycondensation of 3,5-diaminobenzoic acid (Scheme 13), then, poly(VDF-*ter*-TrFE-*ter*-CFE) was introduced via a solution blending method.

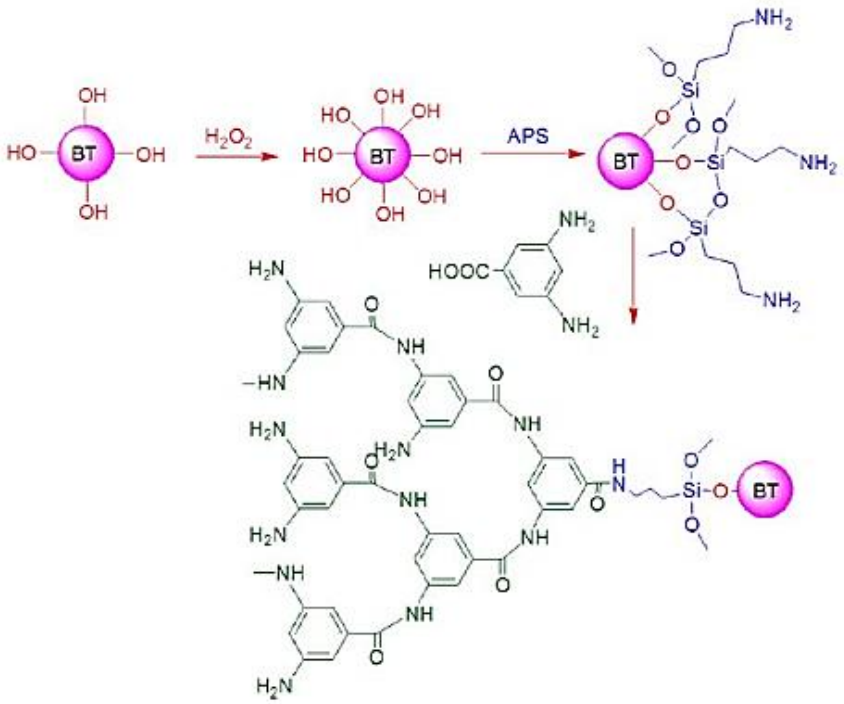

Scheme 13. Schematic Diagram Illustrating the Preparing Process of BT-HBP. Reproduced with permission of [122] . Copyright American Chemical Society 2013.

Results show that the as prepared nanocomposites exhibit enhanced dielectric permittivity compared to the pure polymer. Moreover, by increasing the loading of functionalized nanoparticles, high values were reached. As shown in Fig.35, at 1 kHz and with a loading of 40 vol% of HBP@BT, a high dielectric constant of 1485.5 was achieved for the nanocomposites compared to poly(VDF-*ter*-TrFE-*ter*-CFE) that exhibit only 206.3.

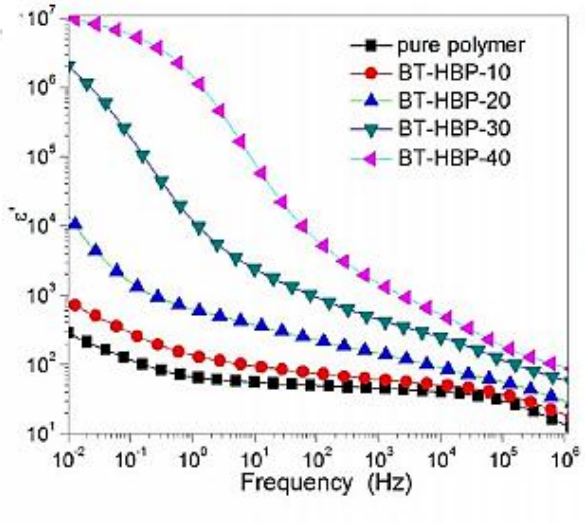

Fig. 35. Frequency dependence of dielectric constant for HBP@BT/ poly(VDF-*ter*-TrFE-*ter*-CFE) nanocomposites for different loading of functionalized nanoparticles. Reproduced with permission of [122] . Copyright American Chemical Society 2013.

Table 7 summarizes the permittivities obtained for core-shell systems discussed above. It can be seen that nanocomposites containing more fluorinated polymers exhibit high dielectric constants. For instance, in reference 85, when PVDF is used instead of PS, for the same filler loading, the dielectric permittivity increased from 23.6 to 27.9 at 1 kHz. Indeed, we can not increase the permittivity of fluorinated polymers compared to that of pure $BaTiO_3$, even when using high nanoparticle loading [123]. In fact, by adding higher concentration of ceramic nanoparticles inevitably induces aggregation and inhomogeneity in the fluorinated polymer shell giving rise to electron conduction with a high dielectric loss, very low breakdown strength and undesirable porosity and voids, resulting in deteriorated electrical properties in polymer nanocomposites (*i. e.* permittivity of the resulting nanocomposites). Thus, an appropriate surface modification and choice of the polymer shell would lead to the desired properties.

Table 7. Summary of permittivities obtained for core-shell $BaTiO_3$@polymer/Fluorinated polymer nanocomposites.

Core-shell Polymer@BT/Fluorinated polymer nanocomposites	Dielectric permittivity (at a given frequency and fillers loading)	References
PTFEA@BT/P(VDF-HFP)	42.5 (1 kHz, 50 %wt)	27
PS@BT/PVDF	23.6 (1 kHz, 30 vol%)	85
PVDF@BT/PVDF	27.9 (1 kHz, 30 vol%)	85
PTFMPCS@BT/poly(VDF-ter-TrFE- ter-CTFE)	80.6 (1 kHz, 30 vol%)	86
PMMA@BT/PVDF	30 (100 Hz, 80 wt%)	113
PTFEMA@BT/PVDF	36 (100 Hz, 80 wt%)	113
PtBA@BT/PVDF	15 (100 Hz, 30 wt%)	115
PHEMA@BT/PVDF	21 (100 Hz, 20 wt%)	73
PGMA@BT/PVDF	18 (100 Hz, 20 wt%)	73
PM7F@BT/P(VDF-ter-TrFE- ter-CTFE)	70 (1 kHz, 5 vol%)	118

V. Applications

Polymer nanocomposites present unique physicochemical properties that cannot be obtained with one component. Thus, the improvement in the properties of polymer nanocomposites have resulted in major interest for versatile fields including medicine, coatings and energy storage [124]. In medical applications, damaged tissues are often replaced with synthetic materials such as ceramics or metals, which are used for engineering hard tissues (*e,g,.* bones and teeth), or even polymers that can be used to manufacture a wide range of both hard and soft tissues, and in some cases, their composites could be also used [125–127]. Gopalakrishnan *et al.* [128] introduced silver nanoparticles into PMMA polymer matrix to reinforce its structure for dental prosthetic materials. The addition of silver nanoparticles was found to enhance the mechanical properties of the polymer and also retarded crack propagation and fracture behavior, and thus improved the durability of the denture base.

Another promising field of use of polymer nanocomposite materials is energy storage applications [71,129–133]. Kumar *et al*. [129] used nanocomposite materials consisting on BT nanoparticles and poly(VDF-*co*-HFP) polymer matrix to prepare a composite solid polymer electrolyte (CSPE) for Li-ion batteries. Since the ionic conductivity of the pure polymer poly(VDF-*co*-HFP) is not enough to be used as SPE, lithium triflate salt was added and the nanocomposites were synthesized by solution casting technique. Fig. 36-a exhibits the ionic conductivity of the CSPE with 10 wt% in lithium triflate salt for different BT loading. The ionic conductivity of the CSPE increases to reach 8.89×10^{-6} S cm^{-1} as the maximum value for 4 wt% of BT and decreases by further addition of BT. Fig. 36-b gives a comparison of conductivity (σ_{DC}) of pure polymer, SPE loaded with 10 wt% of lithium triflate and 4 wt% of BT. It can be observed that after introduction of BT into the system, the ionic conductivity increased by four orders of magnitude.

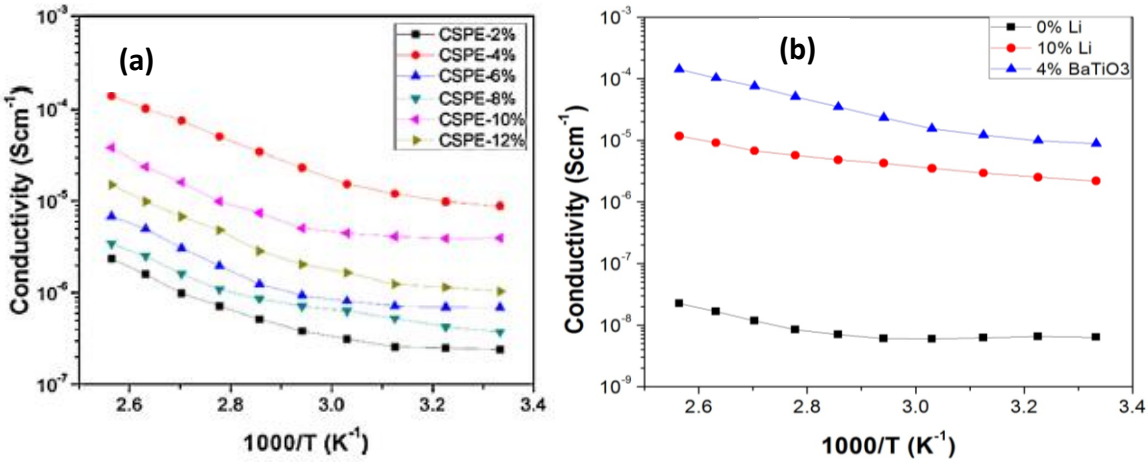

Fig. 36. (a) Direct current (DC) conductivity (σ_{DC}) of the CSPEs calculated from complex impedance plots and (b) DC ionic conductivity of pure polymer, SPE loaded with 10 wt. % lithium triflate salt and CSPE loaded with 10 wt. % lithium triflate salt and 4 wt. % $BaTiO_3$. Reproduced with permission of [129]. Copyright 2016 Elsevier.

A similar strategy for the same application was also reported by Sasikumar *et al.* [130] who prepared CSPE using BT, PVAc/poly(VDF-*co*-HFP) and lithium bis-trifluoromethanesulfonylimide (LiTFSI) as the salt (Fig. 37). Results show that compared with ceramic free SPE, the conductivity was increased to reach a value of 2 x 10^{-3} Scm^{-1} at ambient temperature. Moreover, it was found that in the case of CSPE

made by 7 wt% of BT, an enhancement in discharge capacity of 132 mAh g^{-1} at 0.1 C, cycling performance up to 40 cycles and 99 % Coulombic efficiency were noted.

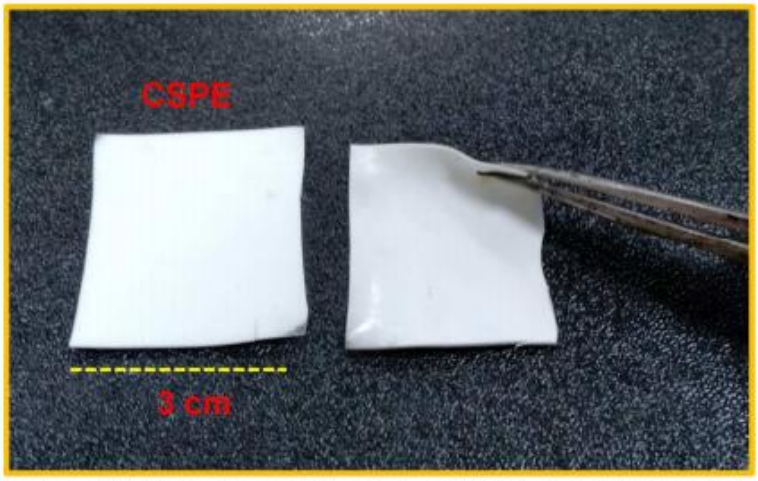

Fig. 37. Photograph of free-standing and flexible CSPE. Reproduced with permission of [130] Copyright 2018 American Chemical Society.

In addition to their application in Li-ion batteries, BT based fluoropolymer nanocomposites are also used in capacitors. For example, Tang *et al.* [71] prepared high energy density nanocomposite capacitors using BT nanowires and poly(VDF-*ter*-TrFE-*ter*-CFE) polymer (63/29/8 % mole ratio). Dielectric measurements revealed that the obtained nanocomposites exhibit increased dielectric permittivity at low volume fraction of the fillers and high electric field for energy storage (Fig. 38-a). Moreover, BT/poly(VDF-TrFE-CFE) nanocomposites showed an increase in energy density of 10.48 J/cc, which is higher than that of the neat poly(VDF-*ter*-TrFE-*ter*-CFE) polymer (7.21 J/cc) at 300 MV/m electric field (Fig. 38-b). This value is more than seven times larger than a high performance commercial polypropylene capacitor.

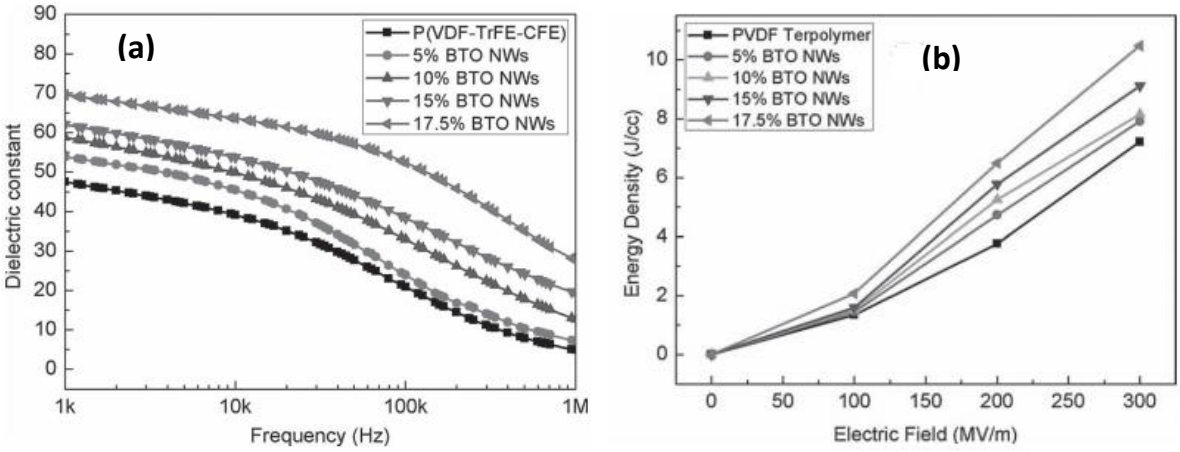

Fig. 38. (a) Dielectric permittivity constants of different BT NWs volume fractions in P(VDF-*ter*-TrFE-*ter*-CFE) from 1 kHz to 1 MHz and (b) Energy density of BT/ P(VDF-*ter*-TrFE-*ter*-CFE) nanocomposite with different volume fractions of BT as a function of the electric field. Reproduced with permission of [71] . Copyright 2013 Wiley.

Hao *et al*. [134] designed a parallel plate capacitance device. The multilayer nanocomposite film consists on a central layer composed of high volume fraction of BT, while the outer layers were predominately PVDF, with a small loading of BT nanoparticles. The obtained films (1.2-1.5 μm) were found to be mechanically flexible and could be removed from the substrate (Fig. 39). Moreover, a maximum breakdown strength as high as 495 KV/mm which is 50 % higher than that of the pure PVDF, and a discharge energy density of 19.37 J/cm^3 were obtained, leading to high energy density nanocomposites.

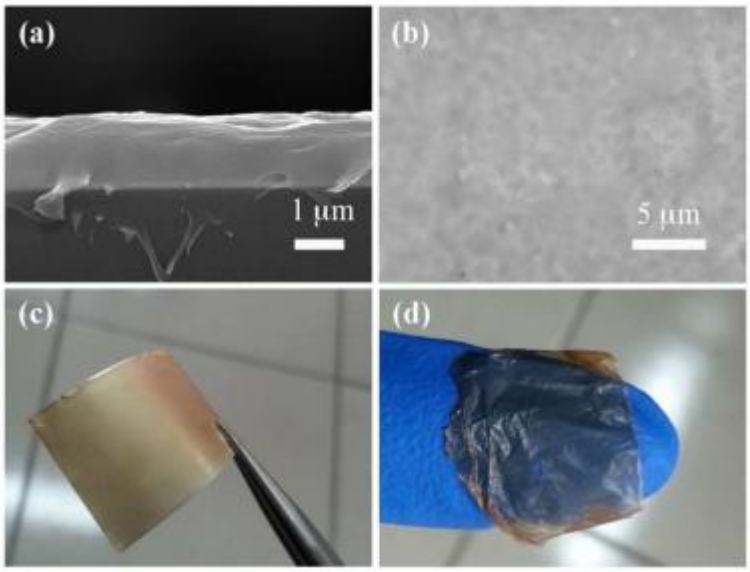

Fig. 39. (a) Cross-sectional and (b) Surface SEM image of the BTO/PVDF nanocomposite film, showing a rough interface between the transparent top PVDF layer and the bottom nanocomposite layer. (c) Photograph of the nanocomposite on a flexible aluminum foil substrate, and (d) delaminated from the substrate, showing its continuous polymer nature. Reproduced with permission of [134]. Copyright 2015 Royal Society of Chemistry.

Another promising application of polymer nanocomposites is piezoelectric nanogenerators (PNGs), which aims to convert the mechanical energy available in our daily life like vehicle motion or even in human body (artificial muscle actuators). In fact, PVDF and its copolymers are considered to be the most used polymeric materials in PNGs [135]. Dudem *et al*. [136] designed a PNGs using barium titanate nanoparticles embedded into PVDF. The nanoparticles were first dispersed with Ag nanowires; the resulted mixture was introduced into PVDF matrix. In order to fabricate the PNGs, the nanocomposite film was sandwiched between two Aluminum substrate and then sealed with a Kapton tape. The prepared PNGs were then tested to harvest the mechanical energy from bicycle, motorcycle, car and human hand. Fig. 40 exhibits the piezoelectric potential curves generated by the PNGs device at bending positions and on human hand. The results revealed that the resulting device is flexible enough to generate the electrical output under various bending conditions, and exhibits a hight output voltage of ~4.8 V under large bending conditions.

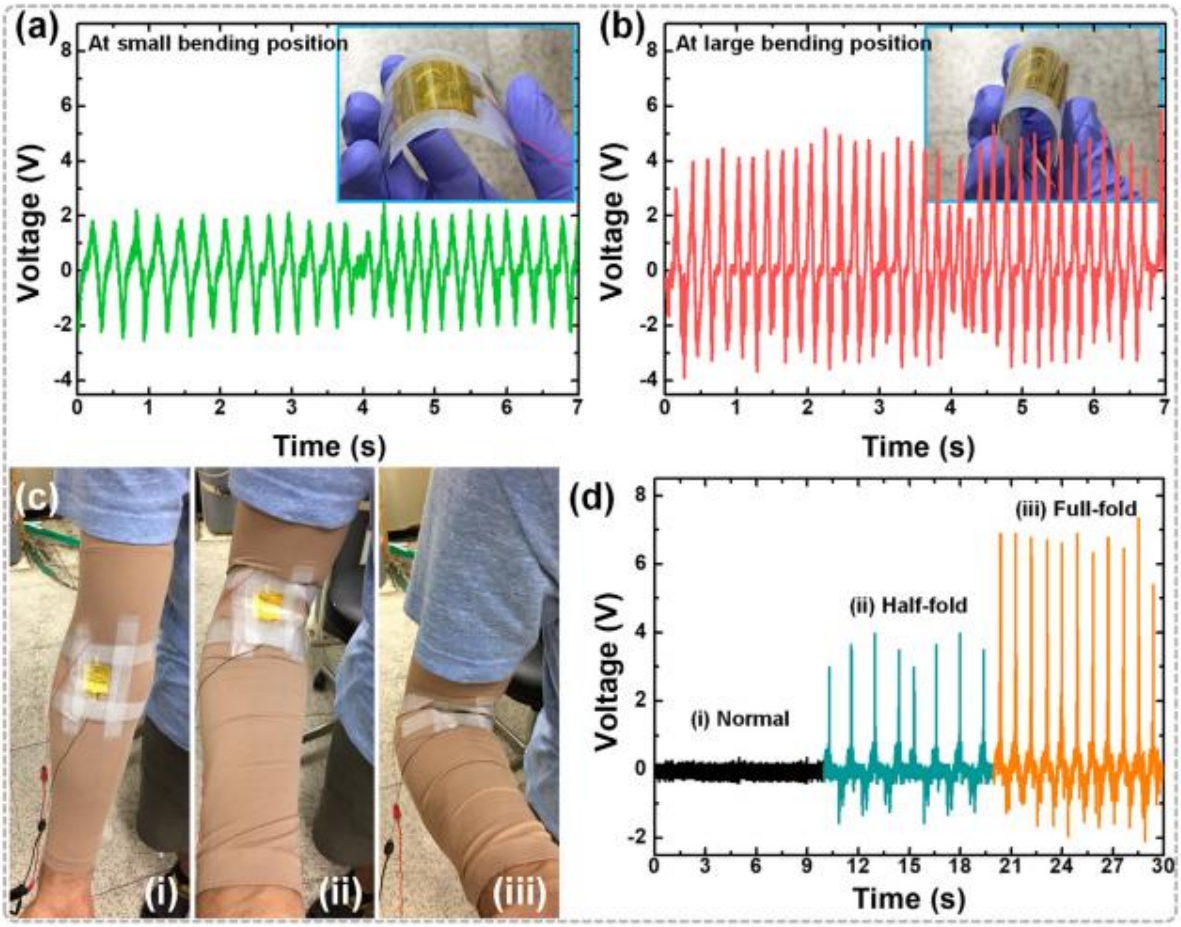

Fig. 40. Demonstration for the high-flexibility of the Ag/BTO-PNG device. Piezoelectric potential (i.e., VOC) generated by the Ag/BTO-PNG at (a) small and (b) large bending positions/conditions. Insets of (a) and (b) also depict the photographic images of Ag/BT O-PNG at the small and large bending conditions, respectively. (c) Photographic images and (d) piezoelectric potentials of the Ag/BTO-PNG device located on a human hand (i.e., in front part of the elbow) at (i) normal, (ii) half-, and (iii) full-fold conditions, respectively. Reproduced with permission of [136]. Copyright 2018 Elsevier.

VI. Conclusion and perspectives

Nanocomposites depicted in this review are composed of a barium titanate core embedded in a fluorinated polymeric shell. BT is as a ferroelectric ceramic mostly used in dielectric material due to its high dielectric constant. However, this ceramic suffer from low breakdown strength and processing difficulties. In the other hand, polymers generally exhibit high breakdown strength and low permittivities. Thus, by combining the advantages of both components, high dielectric constant materials could be achieved. Various fluoropolymers could be used as shells such as poly(fluoroolefins), poly[fluoro(meth)acrylates] of various fluoroalkyl lengths, PVDF and VDF-containing-copolymers. In certain cases, core-shell $BaTiO_3$@polymer/Fluorinated polymer nanocomposites have also been reported, in order to take advantages from the inner and outer polymer shell.

In fact, these nanocomposite materials could be obtained by different strategies ranging from "grafting from", "grafting onto" or blending. The first route requires to modify the BT surface by either a macroinitiator (for ATRP method) or macro chain transfer agent (xanthates or trithiocarbonates for RAFT technique), while the third strategy consists on a simple mixing of the pre-prepared polymer with the functionalized nanoparticles. Actually, the first two routes are efficient since they create covalent and thus strong bonds between the core and the shell. The blending technique has been possible when BT@PMMA has been prepared, followed by mixing it with PVDF, taking into account that PVDF and PMMA are miscible.

In the last decade, a growing interest from such nanocomposites has been highlighted by the wide range of applications, focusing on energy storage devices or piezoelectric systems and it can be expected that designing further materials with various sizes and efficiency for the searched applications will still be challenging and will attract the interest of many researchers.

Acknowledgements

The authors thank the French Government, the Centre National pour la Recherche Scientifique et Technique in Morocco (grant CNRST (7UCA2016)) and

Ministère de l'Enseignement Supérieur de la Recherche Scientifique et de la Formation des Cadres in Morocco (MESRSFC) for the financial supports.

References

[1] Raman N, Sudharsan S, Pothiraj K. Synthesis and structural reactivity of inorganic–organic hybrid nanocomposites – A review. J Saudi Chem Soc 2012;16:339–52. doi:10.1016/j.jscs.2011.01.012.

[2] Fu S-Y, Sun Z, Huang P, Li Y-Q, Hu N. Some basic aspects of polymer nanocomposites: A critical review. Nano Mater Sci 2019;1:2–30. doi:10.1016/j.nanoms.2019.02.006.

[3] Huang T-C, Yeh J-M, Lai C-Y. Polymer nanocomposite coatings. Adv. Polym. Nanocomposites, Elsevier; 2012, p. 605–38. doi:10.1533/9780857096241.3.605.

[4] Dang Z-M, Yuan J-K, Yao S-H, Liao R-J. Flexible Nanodielectric Materials with High Permittivity for Power Energy Storage. Adv Mater 2013;25:6334–65. doi:10.1002/adma.201301752.

[5] Chen Q, Shen Y, Zhang S, Zhang QM. Polymer-Based Dielectrics with High Energy Storage Density. Annu Rev Mater Res 2015;45:433–58. doi:10.1146/annurev-matsci-070214-021017.

[6] Chu B, Xin Z, Kailiang R, Bret N, Minren L, Qing W, et al. A Dielectric Polymer with High Electric Energy Density and Fast Discharge Speed. Science (80-) 2006;313:334–6. doi:10.1126/science.1127798.

[7] Huang X, Jiang P. Core-Shell Structured High-k Polymer Nanocomposites for Energy Storage and Dielectric Applications. Adv Mater 2015;27:546–54. doi:10.1002/adma.201401310.

[8] Terzić I, Meereboer NL, Mellema HH, Loos K. Polymer-based multiferroic nanocomposites via directed block copolymer self-assembly. J Mater Chem C 2019;7:968–76. doi:10.1039/C8TC05017A.

[9] Villa SM, Mazzola VM, Santaniello T, Locatelli E, Maturi M, Migliorini L, et al. Soft Piezoionic/Piezoelectric Nanocomposites Based on Ionogel/BaTiO3 Nanoparticles for Low Frequency and Directional Discriminative Pressure Sensing. ACS Macro Lett 2019;8:414–20. doi:10.1021/acsmacrolett.8b01011.

[10] Wang G, Huang X, Jiang P. Tailoring Dielectric Properties and Energy Density of Ferroelectric Polymer Nanocomposites by High-k Nanowires. ACS Appl Mater Interfaces 2015;7:18017–27. doi:10.1021/acsami.5b06480.

[11] Zhang X, Shen Y, Xu B, Zhang Q, Gu L, Jiang J, et al. Giant Energy Density and Improved Discharge Efficiency of Solution-Processed Polymer Nanocomposites for Dielectric Energy Storage. Adv Mater 2016;28:2055–61. doi:10.1002/adma.201503881.

[12] Qiao Y, Islam MS, Wang L, Yan Y, Zhang J, Benicewicz BC, et al. Thiophene

Polymer-Grafted Barium Titanate Nanoparticles toward Nanodielectric Composites. Chem Mater 2014;26:5319–26. doi:10.1021/cm502341n.

[13] Li J, Seok S Il, Chu B, Dogan F, Zhang Q, Wang Q. Nanocomposites of Ferroelectric Polymers with TiO2 Nanoparticles Exhibiting Significantly Enhanced Electrical Energy Density. Adv Mater 2009;21:217–21. doi:10.1002/adma.200801106.

[14] Xu N, Hu L, Zhang Q, Xiao X, Yang H, Yu E. Significantly Enhanced Dielectric Performance of Poly(vinylidene fluoride-co-hexafluoropylene)-based Composites Filled with Hierarchical Flower-like TiO2 Particles. ACS Appl Mater Interfaces 2015;7:27373–81. doi:10.1021/acsami.5b08987.

[15] Guo R, Roscow J, Bowen C, Luo H, Huang Y, Ma Y, et al. Significantly enhanced permittivity and energy density in dielectric composites with aligned BaTiO3 lamellar structures. J Mater Chem A 2020. doi:10.1039/C9TA11360F.

[16] Bai Y, Cheng Z-Y, Bharti V, Xu HS, Zhang QM. High-dielectric-constant ceramic-powder polymer composites. Appl Phys Lett 2000;76:3804–6. doi:10.1063/1.126787.

[17] Li W, Meng Q, Zheng Y, Zhang Z, Xia W, Zhuo X. Electric energy storage properties of poly(vinylidene fluoride). Appl Phys Lett 2010;96:192905. doi:10.1063/1.3428656.

[18] Claude J, Lu Y, Li K, Wang Q. Electrical Storage in Poly(vinylidene fluoride) based Ferroelectric Polymers: Correlating Polymer Structure to Electrical Breakdown Strength. Chem Mater 2008;20:2078–80. doi:10.1021/cm800160r.

[19] Yu K, Wang H, Zhou Y, Bai Y, Niu Y, Yu K, et al. Enhanced dielectric properties of BaTiO3 / poly (vinylidene fluoride) nanocomposites for energy storage applications. J Appl Phys 2013;113:34105. doi:10.1063/1.4776740.

[20] Bouharras FE, Raihane M, Silly G, Totee C, Ameduri B. Core shell structured Poly(Vinylidene Fluoride) -grafted- BaTiO3 nanocomposites prepared via Reversible Addition fragmentation chain transfer (RAFT) polymerization of VDF for high energy storage capacitors. Polym Chem 2019;10:891–904. doi:10.1039/C8PY01706A.

[21] Dang Z-M, Wang H-Y, Peng B, Nan C-W. Effect of BaTiO3 size on dielectric property of BaTiO3/PVDF composites. J Electroceramics 2008;21:381–4. doi:10.1007/s10832-007-9201-8.

[22] Li J, Claude J, Norena-Franco LE, Seok S Il, Wang Q. Electrical Energy Storage in Ferroelectric Polymer Nanocomposites Containing Surface-Functionalized BaTiO3 Nanoparticles. Chem Mater 2008;20:6304–6. doi:10.1021/cm8021648.

[23] Dai Z-H, Han J-R, Gao Y, Xu J, He J, Guo B-H. Increased dielectric permittivity of poly(vinylidene fluoride-co-chlorotrifluoroethylene) nanocomposites by coating BaTiO3 with functional groups owning high bond dipole moment. Colloids Surfaces A Physicochem Eng Asp 2017;529:560–70. doi:10.1016/J.COLSURFA.2017.05.065.

[24] Xie L, Huang X, Wu C, Jiang P. Core-shell structured poly(methyl methacrylate)/BaTiO3 nanocomposites prepared by in situ atom transfer radical polymerization: a route to high dielectric constant materials with the inherent low loss of the base polymer. J Mater Chem 2011;21:5897. doi:10.1039/c0jm04574h.

[25] Ejaz M, Puli VS, Elupula R, Adireddy S, Riggs BC, Chrisey DB, et al. Core-shell structured poly(glycidyl methacrylate)/BaTiO3 nanocomposites prepared by surface-initiated atom transfer radical polymerization: A novel material for high energy density dielectric storage. J Polym Sci Part A Polym Chem 2015;53:719–28. doi:10.1002/pola.27485.

[26] Ameduri B. From Vinylidene Fluoride (VDF) to the Applications of VDF-Containing Polymers and Copolymers: Recent Developments and Future Trends. Chem Rev 2009;109:6632–86. doi:10.1021/cr800187m.

[27] Yang K, Huang X, Huang Y, Xie L, Jiang P. Fluoro-Polymer@BaTiO3 Hybrid Nanoparticles Prepared via RAFT Polymerization: Toward Ferroelectric Polymer Nanocomposites with High Dielectric Constant and Low Dielectric Loss for Energy Storage Application. Chem Mater 2013;25:2327–38. doi:10.1021/cm4010486.

[28] Xie L, Huang X, Yang K, Li S, Jiang P. "Grafting to" route to PVDF-HFP-GMA/BaTiO3 nanocomposites with high dielectric constant and high thermal conductivity for energy storage and thermal management applications. J Mater Chem A 2014;2:5244. doi:10.1039/c3ta15156e.

[29] Barber P, Balasubramanian S, Anguchamy Y, Gong S, Wibowo A, Gao H, et al. Polymer Composite and Nanocomposite Dielectric Materials for Pulse Power Energy Storage. Materials (Basel) 2009;2:1697–733. doi:10.3390/ma2041697.

[30] Todd MG, Shi FG. Complex permittivity of composite systems: a comprehensive interphase approach. IEEE Trans Dielectr Electr Insul 2005;12:601–11. doi:10.1109/TDEI.2005.1453466.

[31] Tanaka T, Kozako M, Fuse N, Ohki Y. Proposal of a multi-core model for polymer nanocomposite dielectrics. IEEE Trans Dielectr Electr Insul 2005;12:669–81. doi:10.1109/TDEI.2005.1511092.

[32] Smith MB, Page K, Siegrist T, Redmond PL, Walter EC, Seshadri R, et al. Crystal Structure and the Paraelectric-to-Ferroelectric Phase Transition of Nanoscale BaTiO3. J Am Chem Soc 2008;130:6955–63. doi:10.1021/ja0758436.

[33] Huang K-C, Huang T-C, Hsieh W-F. Morphology-Controlled Synthesis of Barium Titanate Nanostructures. Inorg Chem 2009;48:9180–4. doi:10.1021/ic900854x.

[34] Helen DM. Crystal Structure of Barium Titanate. Nature 1945;155:484–5. doi:10.1038/155484b0.

[35] Vijatovic MM, Bobic JD, Stojanovic BD. History and challenges of barium titanate: Part I. Sci Sinter 2008;40:155–65. doi:10.2298/SOS0802155V.

[36] Kwei GH, Lawson AC, Billinge SJL, Cheong SW. Structures of the ferroelectric

phases of barium titanate. J Phys Chem 1993;97:2368–77. doi:10.1021/j100112a043.

[37] Pan M-J, Randall CA. A brief introduction to ceramic capacitors. IEEE Electr Insul Mag 2010;26:44–50. doi:10.1109/MEI.2010.5482787.

[38] Neagu AM, Curecheriu LP, Cazacu A, Mitoseriu L. Impedance analysis and tunability of BaTiO3–chitosan composites: Towards active dielectrics for flexible electronics. Compos Part B Eng 2014;66:109–16. doi:10.1016/J.COMPOSITESB.2014.04.020.

[39] Hirose N, West AR. Impedance Spectroscopy of Undoped BaTiO3 Ceramics. J Am Ceram Soc 1996;79:1633–41. doi:10.1111/j.1151-2916.1996.tb08775.x.

[40] Tian Z, Wang X, Shu L, Wang T, Song T-H, Gui Z, et al. Preparation of Nano BaTiO3-Based Ceramics for Multilayer Ceramic Capacitor Application by Chemical Coating Method. J Am Ceram Soc 2009;92:830–3. doi:10.1111/j.1551-2916.2009.02979.x.

[41] Feteira A, Sinclair DC, Reaney IM, Somiya Y, Lanagan MT. BaTiO3-Based Ceramics for Tunable Microwave Applications. J Am Ceram Soc 2004;87:1082–7. doi:10.1111/j.1551-2916.2004.01082.x.

[42] Dutta PK, Gregg JR. Hydrothermal synthesis of tetragonal barium titanate (BaTiO3). Chem Mater 1992;4:843–6. doi:10.1021/cm00022a019.

[43] Eckert JO, Hung-Houston CC, Gersten BL, Lencka MM, Riman RE. Kinetics and Mechanisms of Hydrothermal Synthesis of Barium Titanate. J Am Ceram Soc 1996;79:2929–39. doi:10.1111/j.1151-2916.1996.tb08728.x.

[44] Bouloo M, Guillemetfritsch S, Mathieu F, Durand B, Lebey T, Bley V. Hydrothermal synthesis of nanosized BaTiO3 powders and dielectric properties of corresponding ceramics. Solid State Ionics 2005;176:1301–9. doi:10.1016/j.ssi.2005.02.024.

[45] Hao Y, Wang X, Zhang H, Shen Z, Li L. Investigation on the synthesis procedure of ultrafine monodispersed BaTiO3 powders by solvothermal method. J Ceram Soc Japan 2013;121:506–11. doi:10.2109/jcersj2.121.506.

[46] Buscaglia MT, Bassoli M, Buscaglia V, Vormberg R. Solid-State Synthesis of Nanocrystalline BaTiO3 Reaction Kinetics and Powder Properties. J Am Ceram Soc 2008;91:2862–9. doi:10.1111/j.1551-2916.2008.02576.x.

[47] Ashiri R. On the solid-state formation of BaTiO3 nanocrystals from mechanically activated BaCO3 and TiO2 powders: innovative mechanochemical processing, the mechanism involved, and phase and nanostructure evolutions. RSC Adv 2016;6:17138–50. doi:10.1039/C5RA22942A.

[48] Simon-Seveyrat L, Hajjaji A, Emziane Y, Guiffard B, Guyomar D. Re-investigation of synthesis of BaTiO3 by conventional solid-state reaction and oxalate coprecipitation route for piezoelectric applications. Ceram Int 2007;33:35–40. doi:10.1016/J.CERAMINT.2005.07.019.

[49] Miot C, Proust C, Husson E. Dense ceramics of BaTiO3 produced from powders

prepared by a chemical process. J Eur Ceram Soc 1995;15:1163–70. doi:10.1016/0955-2219(95)00090-9.

[50] Stockenhuber M, Mayer H, Lercher JA. Preparation of Barium Titanates from Oxalates. J Am Ceram Soc 1993;76:1185–90. doi:10.1111/j.1151-2916.1993.tb03738.x.

[51] Veith M, Mathur S, Lecerf N, Huch V, Decker T. Sol-Gel Synthesis of Nano-Scaled BaTiO3, BaZrO3 and BaTi0.5Zr0.5O3 Oxides via Single-Source Alkoxide Precursors and Semi-Alkoxide Routes. J Sol-Gel Sci Technol 2000;15:145–58.

[52] Ritter JJ, Roth RS, Blendell JE. Alkoxide Precursor Synthesis and Characterization of Phases in the Barium-Titanium Oxide System. J Am Ceram Soc 1986;69:155–62. doi:10.1111/j.1151-2916.1986.tb04721.x.

[53] Lemoine C, Gilbert B, Michaux B, Pirard J-P, Lecloux A. Synthesis of barium titanate by the sol-gel process. J Non Cryst Solids 1994;175:1–13. doi:10.1016/0022-3093(94)90309-3.

[54] Cernea M. Sol-gel synthesis and characterization of BaTiO3 powder. J Opt Adv Mater 2005;7;3015-3022. doi:10.1.1.551.789&rep=rep1&type=pdf.

[55] K. S. Mazdiyasni. Fine particle perovskite processing. Am Ceram SOC Bull 1984;63:591–4.

[56] Flaschen SS. An Aqueous Synthesis of Barium Titanate. J Am Chem Soc 1955;77:6194–6194. doi:10.1021/ja01628a030.

[57] Phule PP, Risbud SH. Sol-Gel Synthesis of Barium Titanate Powders Using Barium Acetate and Titanium(IV) Isopropoxide. Adv Ceram Mater 1988;3:183–5. doi:10.1111/j.1551-2916.1988.tb00197.x.

[58] Buscaglia MT, Buscaglia V, Viviani M, Petzelt J, Savinov M, Mitoseriu L, et al. Ferroelectric properties of dense nanocrystalline BaTiO3 ceramics. Nanotechnology 2004;15:1113–7. doi:10.1088/0957-4484/15/9/001.

[59] Li B, Wang X, Li L, Zhou H, Liu X, Han X, et al. Dielectric properties of fine-grained BaTiO3 prepared by spark-plasma-sintering. Mater Chem Phys 2004;83:23–8. doi:10.1016/j.matchemphys.2003.08.009.

[60] Luan W, Gao L, Kawaoka H, Sekino T, Niihara K. Fabrication and characteristics of fine-grained BaTiO3 ceramics by spark plasma sintering. Ceram Int 2004;30:405–10. doi:10.1016/S0272-8842(03)00124-X.

[61] Zhao Z, Buscaglia V, Viviani M, Buscaglia MT, Mitoseriu L, Testino A, et al. Grain-size effects on the ferroelectric behavior of dense nanocrystalline BaTiO 3 ceramics. Phys Rev B 2004;70:24107. doi:10.1103/PhysRevB.70.024107.

[62] Hsiang H-I, Yen F-S, Huang C-Y. Effects of Porosity on Dielectric Properties of BaTiO3 Ceramics. Jpn J Appl Phys 1995;34:1922–5. doi:10.1143/JJAP.34.1922.

[63] Fang T-T, Hsieh H-L, Shiau F-S. Effects of Pore Morphology and Grain Size on the Dielectric Properties and Tetragonal-Cubic Phase Transition of High-Purity

Barium Titanate. J Am Ceram Soc 1993;76:1205–11. doi:10.1111/j.1151-2916.1993.tb03742.x.

[64] Kingery WD, Bowen HK, Uhlmann DR. Introduction to ceramics. Wiley. New York: 1976.

[65] Murugaraj P, Mainwaring D, Mora-Huertas N. Dielectric enhancement in polymer-nanoparticle composites through interphase polarizability. J Appl Phys 2005;98:54304. doi:10.1063/1.2034654.

[66] Tuncer E, Serdyuk YV, Gubanski SM. Dielectric mixtures: electrical properties and modeling. IEEE Trans Dielectr Electr Insul 2002;9:809–28. doi:10.1109/TDEI.2002.1038664.

[67] Yoon D-H, Zhang J, Lee BI. Dielectric constant and mixing model of BaTiO3 composite thick films. Mater Res Bull 2003;38:765–72. doi:10.1016/S0025-5408(03)00075-8.

[68] Vo HT, Todd M, Shi FG, Shapiro AA, Edwards M. Towards model-based engineering of underfill materials: CTE modeling. Microelectronics J 2001;32:331–8. doi:10.1016/S0026-2692(00)00152-X.

[69] Wang Q, Zhu L. Polymer nanocomposites for electrical energy storage. J Polym Sci Part B Polym Phys 2011;49:1421–9. doi:10.1002/polb.22337.

[70] Zhu L, Wang Q. Novel Ferroelectric Polymers for High Energy Density and Low Loss Dielectrics. Macromolecules 2012;45:2937–54. doi:10.1021/ma2024057.

[71] Tang H, Lin Y, Sodano HA. Synthesis of High Aspect Ratio BaTiO3 Nanowires for High Energy Density Nanocomposite Capacitors. Adv Energy Mater 2013;3:451–6. doi:10.1002/aenm.201200808.

[72] Soulestin T, Marcelino Dos Santos Filho P, Ladmiral V, Lannuzel T, Domingues Dos Santos F, Améduri B. Ferroelectric fluorinated copolymers with improved adhesion properties. Polym Chem 2017;8:1017–27. doi:10.1039/C6PY02063A.

[73] Zhu M, Huang X, Yang K, Zhai X, Zhang J, He J, et al. Energy Storage in Ferroelectric Polymer Nanocomposites Filled with Core–Shell Structured Polymer@BaTiO3 Nanoparticles: Understanding the Role of Polymer Shells in the Interfacial Regions. ACS Appl Mater Interfaces 2014;6:19644–54. doi:10.1021/am504428u.

[74] Kim P, Doss NM, Tillotson JP, Hotchkiss PJ, Pan M-J, Marder SR, et al. High Energy Density Nanocomposites Based on Surface-Modified BaTiO3 and a Ferroelectric Polymer. ACS Nano 2009;3:2581–92. doi:10.1021/nn9006412.

[75] Ferri A, Barrau S, Bourez R, Da Costa A, Chambrier MH, Marin A, et al. Probing the local piezoelectric behavior in stretched barium titanate/poly(vinylidene fluoride) nanocomposites. Compos Sci Technol 2020;186. doi:10.1016/j.compscitech.2019.107914.

[76] You Y, Tu L, Wang Y, Tong L, Wei R, Li X. Achieving secondary dispersion of modified nanoparticles by hot-stretching to enhance dielectric and mechanical properties of polyarylene ether nitrile composites. Nanomaterials 2019;9.

doi:10.3390/nano9071006.

[77] Ghallabi Z, Samet M, Arous M, Kallel A, Boiteux G, Royaud I, et al. Giant Permittivity and Low Dielectric Loss in Three Phases BaTiO3/Carbon Nanotube/Polyvinylidene Fluoride Composites. J Adv Phys 2014;3:87–91. doi:10.1166/jap.2014.1108.

[78] Prateek, Thakur VK, Gupta RK. Recent Progress on Ferroelectric Polymer-Based Nanocomposites for High Energy Density Capacitors: Synthesis, Dielectric Properties, and Future Aspects. Chem Rev 2016;116:4260–317. doi:10.1021/acs.chemrev.5b00495.

[79] Ullah A, ur Rahman A, Won Ahn C, Rahman M, Ullah A, Rehman Z, et al. Enhancement of dielectric and energy density properties in the PVDF-based copolymer/terpolymer blends. Polym Eng Sci 2015;55:1396–402. doi:10.1002/pen.24083.

[80] Capsal J-F, Galineau J, Lallart M, Cottinet P-J, Guyomar D. Plasticized relaxor ferroelectric terpolymer: Toward giant electrostriction, high mechanical energy and low electric field actuators. Sensors Actuators A Phys 2014;207:25–31. doi:10.1016/J.SNA.2013.12.008.

[81] Park IJ, Lee S-B, Choi CK. Surface properties for poly(perfluoroalkylethyl methacrylate)/poly(n-alkyl methacrylate)s mixtures. J Appl Polym Sci 1994;54:1449–54. doi:10.1002/app.1994.070541008.

[82] Liu M, Chen Y, Zhang C, Bo Z. Stable superhydrophobic fluorine containing polyfluorenes. Chinese J Polym Sci 2012;30:308–15. doi:10.1007/s10118-012-1127-1.

[83] Fu GD, Kang ET, Neoh KG, Lin CC, Liaw DJ. Rigid Fluorinated Polyimides with Well-Defined Polystyrene/Poly(pentafluorostyrene) Side Chains from Atom Transfer Radical Polymerization. Macromolecules 2005;38:7593–600. doi:10.1021/ma0506435.

[84] Ameduri B. Fluoropolymers: The Right Material for the Right Applications. Chem - A Eur J 2018;24:18830–41. doi:10.1002/chem.201802708.

[85] Ma J, Azhar U, Zong C, Zhang Y, Xu A, Zhai C, et al. Core-shell structured PVDF@BT nanoparticles for dielectric materials: A novel composite to prove the dependence of dielectric properties on ferroelectric shell. Mater Des 2019;164:107556. doi:10.1016/J.MATDES.2018.107556.

[86] Chen S, Lv X, Han X, Luo H, Bowen CR, Zhang D. Significantly improved energy density of BaTiO3 nanocomposites by accurate interfacial tailoring using a novel rigid-fluoro-polymer. Polym Chem 2018;9:548–57. doi:10.1039/C7PY01914A.

[87] Toor A, So H, Pisano AP. Improved Dielectric Properties of Polyvinylidene Fluoride Nanocomposite Embedded with Poly(vinylpyrrolidone)-Coated Gold Nanoparticles. ACS Appl Mater Interfaces 2017;9:6369–75. doi:10.1021/acsami.6b13900.

[88] Xie L, Huang X, Yang K, Li S, Jiang P. "Grafting to" route to PVDF-HFP-GMA/BaTiO3 nanocomposites with high dielectric constant and high thermal conductivity for energy storage and thermal management applications. J Mater Chem A 2014;2:5244. doi:10.1039/c3ta15156e.

[89] Capsal J-F, Dantras E, Dandurand J, Lacabanne C. Physical structure of P(VDF-TrFE)/barium titanate submicron composites. J Non Cryst Solids 2012;358:794–8. doi:10.1016/j.jnoncrysol.2011.12.028.

[90] Kim Y, Kim KH, Lee A, Kim M-S, Yoo B, Lee J-K. Highly Fluorinated Polymer-Inorganic Nanoparticle Composites Processable with Fluorous Solvents. J Nanosci Nanotechnol 2017;17:5510–4. doi:10.1166/jnn.2017.14179.

[91] Martins P, Lopes AC, Lanceros-Mendez S. Electroactive phases of poly(vinylidene fluoride): Determination, processing and applications. Prog Polym Sci 2014;39:683–706. doi:10.1016/J.PROGPOLYMSCI.2013.07.006.

[92] Soulestin T, Ladmiral V, Dos Santos FD, Améduri B. Vinylidene fluoride- and trifluoroethylene-containing fluorinated electroactive copolymers. How does chemistry impact properties? Prog Polym Sci 2017;72:16–60. doi:10.1016/j.progpolymsci.2017.04.004.

[93] Costa CM, Firmino Mendes S, Sencadas V, Ferreira A, Gregorio R, Gómez Ribelles JL, et al. Influence of processing parameters on the polymer phase, microstructure and macroscopic properties of poly(vinilidene fluoride)/Pb(Zr0.53Ti0.47)O3 composites. J Non Cryst Solids 2010;356:2127–33. doi:10.1016/J.JNONCRYSOL.2010.07.037.

[94] Jiang B, Pang X, Li B, Lin Z. Organic–Inorganic Nanocomposites via Placing Monodisperse Ferroelectric Nanocrystals in Direct and Permanent Contact with Ferroelectric Polymers. J Am Chem Soc 2015;137:11760–7. doi:10.1021/jacs.5b06736.

[95] Qiao S, Mingxin Y, Xiao Z, Yushun Y, Chunrong W. Structure and performance of porous polymer electrolytes based P(VDF-HFP) for lithium ion batteries. J Power Sources 2002;103:286–92. doi:https://doi.org/10.1016/S0378-7753(01)00868-0.

[96] Li GC, Zhang P, Zhang HP, Yang LC, Wu YP. A porous polymer electrolyte based on P(VDF-HFP) prepared by a simple phase separation process. Electrochem Commun 2008;10:1883–5. doi:10.1016/j.elecom.2008.09.035.

[97] Soresi B, Quartarone E, Mustarelli P, Magistris A, Chiodelli G. PVDF and P(VDF-HFP)-based proton exchange membranes. Solid State Ionics 2004;166:383–9. doi:10.1016/J.SSI.2003.11.027.

[98] Neese B, Wang Y, Chu B, Ren K, Liu S, Zhang QM, et al. Piezoelectric responses in poly(vinylidene fluoride/hexafluoropropylene) copolymers. Appl Phys Lett 2007;90:242917. doi:10.1063/1.2748076.

[99] Cho Y, Ahn D, Park JB, Pak S, Lee S, Jun BO, et al. Enhanced Ferroelectric Property of P(VDF-TrFE-CTFE) Film Using Room-Temperature Crystallization for High-Performance Ferroelectric Device Applications. Adv Electron Mater

2016;2:1600225. doi:10.1002/aelm.201600225.

[100] Zhou T, Zha J-W, Cui R-Y, Fan B-H, Yuan J-K, Dang Z-M. Improving Dielectric Properties of BaTiO3/Ferroelectric Polymer Composites by Employing Surface Hydroxylated BaTiO3 Nanoparticles. ACS Appl Mater Interfaces 2011;3:2184–8. doi:10.1021/am200492q.

[101] Kim BP, Jones SC, Hotchkiss PJ, Haddock JN, Kippelen B, Marder SR, et al. Phosphonic Acid-Modified Barium Titanate Polymer Nanocomposites with High Permittivity and Dielectric Strength. Adv Mater 2007;19:1001–5. doi:10.1002/adma.200602422.

[102] Song Y, Shen Y, Liu H, Lin Y, Li M, Nan C-W. Improving the dielectric constants and breakdown strength of polymer composites: effects of the shape of the BaTiO3 nanoinclusions, surface modification and polymer matrix. J Mater Chem 2012;22:16491. doi:10.1039/c2jm32579a.

[103] Defebvin J, Barrau S, Lyskawa J, Woisel P, Lefebvre J-M. Influence of nitrodopamine-functionalized barium titanate content on the piezoelectric response of poly(vinylidene fluoride) based polymer-ceramic composites. Compos Sci Technol 2017;147:16–21. doi:10.1016/j.compscitech.2017.05.001.

[104] Guo C, Fuji M. Effect of silicone coupling agent on dielectric properties of barium titanate/silicone elastomer composites. Adv Powder Technol 2016;27:1162–72. doi:10.1016/J.APT.2016.03.028.

[105] Liu S, Xue S, Zhang W, Zhai J. Enhanced dielectric and energy storage density induced by surface-modified BaTiO3 nanofibers in poly(vinylidene fluoride) nanocomposites. Ceram Int 2014;40:15633–40. doi:10.1016/J.CERAMINT.2014.07.083.

[106] Dalle Vacche S, Oliveira F, Leterrier Y, Michaud V, Damjanovic D, Månson J-AE. Effect of silane coupling agent on the morphology, structure, and properties of poly(vinylidene fluoride–trifluoroethylene)/BaTiO3 composites. J Mater Sci 2014;49:4552–64. doi:10.1007/s10853-014-8155-x.

[107] Kim P, Jones SC, Hotchkiss PJ, Haddock JN, Kippelen B, Marder SR, et al. Phosphonic Acid-Modified Barium Titanate Polymer Nanocomposites with High Permittivity and Dielectric Strength. Adv Mater 2007;19:1001–5. doi:10.1002/adma.200602422.

[108] Ehrhardt C, Fettkenhauer C, Glenneberg J, Münchgesang W, Pientschke C, Großmann T, et al. BaTiO3–P(VDF-HFP) nanocomposite dielectrics—Influence of surface modification and dispersion additives. Mater Sci Eng B 2013;178:881–8. doi:10.1016/j.mseb.2013.04.013.

[109] Zhang X, Ma Y, Zhao C, Yang W. High dielectric constant and low dielectric loss hybrid nanocomposites fabricated with ferroelectric polymer matrix and BaTiO3 nanofibers modified with perfluoroalkylsilane. Appl Surf Sci 2014;305:531–8. doi:10.1016/J.APSUSC.2014.03.131.

[110] Yu K, Niu Y, Xiang F, Zhou Y, Bai Y, Wang H. Enhanced electric breakdown strength and high energy density of barium titanate filled polymer

nanocomposites. J Appl Phys 2013;114:174107. doi:10.1063/1.4829671.

[111] Wang G, Huang X, Jiang P. Bio-Inspired Fluoro-polydopamine Meets Barium Titanate Nanowires: A Perfect Combination to Enhance Energy Storage Capability of Polymer Nanocomposites. ACS Appl Mater Interfaces 2017;9:7547–55. doi:10.1021/acsami.6b14454.

[112] Wang J, Guan F, Cui L, Pan J, Wang Q, Zhu L. Achieving high electric energy storage in a polymer nanocomposite at low filling ratios using a highly polarizable phthalocyanine interphase. J Polym Sci Part B Polym Phys 2014;52:1669–80. doi:10.1002/polb.23554.

[113] Zhang X, Zhao S, Wang F, Ma Y, Wang L, Chen D, et al. Improving dielectric properties of BaTiO3/poly(vinylidene fluoride) composites by employing core-shell structured BaTiO3@Poly(methylmethacrylate) and BaTiO3@Poly(trifluoroethyl methacrylate) nanoparticles. Appl Surf Sci 2017;403:71–9. doi:10.1016/j.apsusc.2017.01.121.

[114] Zhang X, Chen H, Ma Y, Zhao C, Yang W. Preparation and dielectric properties of core–shell structural composites of poly(1H,1H,2H,2H-perfluorooctyl methacrylate)@BaTiO3 nanoparticles. Appl Surf Sci 2013;277:121–7. doi:10.1016/J.APSUSC.2013.03.178.

[115] Du X, Liu Y, Wang J, Niu H, Yuan Z, Zhao S, et al. Improved Triboelectric Nanogenerator Output Performance through Polymer Nanocomposites Filled with Core–shell-Structured Particles. ACS Appl Mater Interfaces 2018;10:25683–8. doi:10.1021/acsami.8b05966.

[116] Huang Y, Huang X, Schadler LS, He J, Jiang P. Core@Double-Shell Structured Nanocomposites: A Route to High Dielectric Constant and Low Loss Material. ACS Appl Mater Interfaces 2016;8:25496–507. doi:10.1021/acsami.6b06650.

[117] Qian K, Lv X, Chen S, Luo H, Zhang D. Interfacial engineering tailoring the dielectric behavior and energy density of BaTiO3/P(VDF-TrFE-CTFE) nanocomposites by regulating a liquid-crystalline polymer modifier structure. Dalt Trans 2018;47:12759–68. doi:10.1039/C8DT02626B.

[118] Lv X, Luo H, Chen S, Han X, Ma C, Zhou X, et al. BaTiO3 platelets and poly(vinylidene fluoride-trifluoroethylene-chlorofluoroethylene) hybrid composites for energy storage application. Mech Syst Signal Process 2018;108:48–57. doi:10.1016/j.ymssp.2018.02.011.

[119] Yang K, Huang X, Zhu M, Xie L, Tanaka T, Jiang P. Combining RAFT Polymerization and Thiol–Ene Click Reaction for Core–Shell Structured Polymer@BaTiO3 Nanodielectrics with High Dielectric Constant, Low Dielectric Loss, and High Energy Storage Capability. ACS Appl Mater Interfaces 2014;6:1812–22. doi:10.1021/am4048267.

[120] Su J, Zhang J. Recent development on modification of synthesized barium titanate (BaTiO3) and polymer/BaTiO3 dielectric composites. J Mater Sci Mater Electron 2018;30:1–19. doi:10.1007/s10854-018-0494-y.

[121] Niu Y, Wang H. Dielectric Nanomaterials for Power Energy Storage: Surface

Modification and Characterization. ACS Appl Nano Mater 2019;2:627–42. doi:10.1021/acsanm.8b01846.

[122] Xie L, Huang X, Huang Y, Yang K, Jiang P. Core-shell Structured Hyperbranched Aromatic Polyamide/BaTiO3 Hybrid Filler for Poly(vinylidene fluoride-trifluoroethylene-chlorofluoroethylene) Nanocomposites with the Dielectric Constant Comparable to That of Percolative Composites. ACS Appl Mater Interfaces 2013;5:1747–56. doi:10.1021/am302959n.

[123] Guo N, DiBenedetto SA, Tewari P, Lanagan MT, Ratner MA, Marks TJ. Nanoparticle, Size, Shape, and Interfacial Effects on Leakage Current Density, Permittivity, and Breakdown Strength of Metal Oxide−Polyolefin Nanocomposites: Experiment and Theory. Chem Mater 2010;22:1567–78. doi:10.1021/cm902852h.

[124] Luo H, Zhou X, Ellingford C, Zhang Y, Chen S, Zhou K, et al. Interface design for high energy density polymer nanocomposites. Chem Soc Rev 2019;48:4424–65. doi:10.1039/c9cs00043g.

[125] Dasgupta Q, Madras G, Chatterjee K. Biodegradable polyol-based polymers for biomedical applications. Int Mater Rev 2019;64:288–309. doi:10.1080/09506608.2018.1505066.

[126] Liu T, Huang K, Li L, Gu Z, Liu X, Peng X, et al. High performance high-density polyethylene/hydroxyapatite nanocomposites for load-bearing bone substitute: fabrication, in vitro and in vivo biocompatibility evaluation. Compos Sci Technol 2019;175:100–10. doi:10.1016/j.compscitech.2019.03.012.

[127] Salari M, Mohseni Taromsari S, Bagheri R, Faghihi Sani MA. Improved wear, mechanical, and biological behavior of UHMWPE-HAp-zirconia hybrid nanocomposites with a prospective application in total hip joint replacement. J Mater Sci 2019;54:4259–76. doi:10.1007/s10853-018-3146-y.

[128] Gopalakrishnan S, Raj I, Mathew T. A, Abraham J, Maria HJ, Mozetič M, et al. Development of oral- fluid- impervious and fracture- resistant silver–poly(methyl methacrylate) nanoformulations for intra- oral/extra- oral rehabilitation. J Appl Polym Sci 2019;136:47669. doi:10.1002/app.47669.

[129] Kumar A, Sharma R, Das MK, Gajbhiye P, Kar KK. Impacts of ceramic filler and the crystallite size of polymer matrix on the ionic transport properties of lithium triflate/poly (vinylidene fluoride-co-hexafluoropropene) based polymer electrolytes. Electrochim Acta 2016;215:1–11. doi:10.1016/J.ELECTACTA.2016.08.087.

[130] Sasikumar M, Raja M, Krishna RH, Jagadeesan A, Sivakumar P, Rajendran S. Influence of Hydrothermally Synthesized Cubic-Structured BaTiO3 Ceramic Fillers on Ionic Conductivity, Mechanical Integrity, and Thermal Behavior of P(VDF–HFP)/PVAc-Based Composite Solid Polymer Electrolytes for Lithium-Ion Batteries. J Phys Chem C 2018;122:25741–52. doi:10.1021/acs.jpcc.8b03952.

[131] Prabakaran P, Manimuthu RP, Gurusamy S. Influence of barium titanate

nanofiller on PEO/PVdF-HFP blend-based polymer electrolyte membrane for Li-battery applications. J Solid State Electrochem 2017;21:1273–85. doi:10.1007/s10008-016-3477-z.

[132] Chen J, Xiong X, Shui L, Zhang Q, Yang H, Zhang F. Enhanced dielectric constant and hydrophobicity of P(VDF–TrFE)-based composites. J Mater Sci Mater Electron 2018;29:17612–21. doi:10.1007/s10854-018-9864-8.

[133] Wang Y, Wang L, Yuan Q, Chen J, Niu Y, Xu X, et al. Ultrahigh energy density and greatly enhanced discharged efficiency of sandwich-structured polymer nanocomposites with optimized spatial organization. Nano Energy 2018;44:364–70. doi:10.1016/j.nanoen.2017.12.018.

[134] Hao YN, Wang XH, O'Brien S, Lombardi J, Li LT. Flexible BaTiO3/PVDF gradated multilayer nanocomposite film with enhanced dielectric strength and high energy density. J Mater Chem C 2015;3:9740–7. doi:10.1039/C5TC01903F.

[135] Shepelin NA, Glushenkov AM, Lussini VC, Fox PJ, Dicinoski GW, Shapter JG, et al. New developments in composites, copolymer technologies and processing techniques for flexible fluoropolymer piezoelectric generators for efficient energy harvesting. Energy Environ Sci 2019;12:1143–76. doi:10.1039/C8EE03006E.

[136] Dudem B, Kim DH, Bharat LK, Yu JS. Highly-flexible piezoelectric nanogenerators with silver nanowires and barium titanate embedded composite films for mechanical energy harvesting. Appl Energy 2018;230:865–74. doi:10.1016/j.apenergy.2018.09.009.

Figure captions

Schemes

Tables